



Australian Government
Bureau of Meteorology

The Centre for Australian Weather and Climate Research
A partnership between CSIRO and the Bureau of Meteorology



Extending atmospheric CO₂ and tracer capabilities in ACCESS

Katherine D. Corbin and Rachel M. Law

CAWCR Technical Report No. 035

April 2011



www.cawcr.gov.au



Extending atmospheric CO₂ and tracer capabilities in ACCESS

Katherine D. Corbin and Rachel M. Law

*The Centre for Australian Weather and Climate Research
- a partnership between CSIRO and the Bureau of Meteorology*

CAWCR Technical Report No. 035

April 2011

ISSN: 1836-19X

National Library of Australia Cataloguing-in-Publication entry

Author: Corbin, Katherine D.

Title: Extending atmospheric CO₂ and tracer capabilities in ACCESS / Katherine D. Corbin and Rachel M. Law

ISBN: 978-1-921826-177 [Electronic Resource – PDF]

Series: CAWCR technical report, 35

Notes: Includes bibliographical references and index.

Subjects: Access (Computer program)
Atmospheric carbon dioxide--Measurement.
Greenhouse gases--Measurement.

Other Authors/Contributors: Law, Rachel M.
Centre for Australian Weather and Climate Research

Dewey Number: 551.5112

Enquiries should be addressed to:
Dr. Rachel Law
Centre for Australian Weather and Climate Research
A partnership between the Bureau of Meteorology and CSIRO
Private Bag No. 1
Aspendale, VIC 3195
AUSTRALIA

Rachel.Law@csiro.au

Copyright and Disclaimer

© 2011 CSIRO and the Bureau of Meteorology. To the extent permitted by law, all rights are reserved and no part of this publication covered by copyright may be reproduced or copied in any form or by any means except with the written permission of CSIRO and the Bureau of Meteorology.

CSIRO and the Bureau of Meteorology advise that the information contained in this publication comprises general statements based on scientific research. The reader is advised and needs to be aware that such information may be incomplete or unable to be used in any specific situation. No reliance or actions must therefore be made on that information without seeking prior expert professional, scientific and technical advice. To the extent permitted by law, CSIRO and the Bureau of Meteorology (including each of its employees and consultants) excludes all liability to any person for any consequences, including but not limited to all losses, damages, costs, expenses and any other compensation, arising directly or indirectly from using this publication (in part or in whole) and any information or material contained in it.

CONTENTS

ABSTRACT	1
1. Introduction	2
2. Model modifications	5
2.1 General description	5
2.2 Model implementation.....	6
2.2.1 CO ₂	6
2.2.2 Atmospheric tracers and associated surface fluxes	6
2.2.3 CO ₂ and atmospheric tracer mass conservation	8
2.2.4 CH ₄ , Radon and MCF chemistry.....	9
2.3 Utilizing the model modifications.....	10
2.3.1 CO ₂	10
2.3.2 Atmospheric tracers	10
3. Atmospheric mass conservation	13
3.1 Model simulations.....	13
3.2 Simple tracer mass fix results.....	14
3.3 Mass conservation conclusions	17
4. Assessing the impact of model setup and boundary layer parameterization on atmospheric transport in ACCESS	18
4.1 Model simulations.....	18
4.2 Annual mean CO ₂ concentrations.....	18
4.3 Seasonal cycle	22
4.4 Diurnal cycle.....	27
4.5 CABLE vs. MOSES transport conclusions.....	31
5. Assessing stratospheric transport in ACCESS	32
5.1 TransCom CH ₄ model simulation.....	32
5.2 ACCESS CH ₄ results.....	33
5.3 Methane test case simulations and results	34
5.4 Advection scheme tests.....	38
5.5 Discussion	40
5.6 Conclusions.....	42
6. Assessing atmospheric methane in ACCESS	43
6.1 Global spatial and vertical methane distributions	44
6.2 Simulated vs. GLOBALVIEW CH ₄ concentrations	45
6.3 Simulated vs. GLOBALVIEW CH ₄ vertical distributions	48
6.4 Conclusions.....	50
7. Future work	51
Acknowledgments	52
References.....	53
Appendix A – Modified routines in ACCESS.....	59
Appendix B – New routines in ACCESS	62
Appendix C – Mass conservation subroutine	63

Appendix D – Methodology to utilize the atmospheric CO₂ tracer	68
D.1 UMUI checklist to turn on the atmospheric CO ₂ tracer	68
D.2 CO ₂ concentration hand edit file (CO2.ed).....	69
D.3 CO ₂ flux hand edit file (CO2_emits.ed).....	70
Appendix E – Methodology to utilize atmospheric tracers	71
E.1 UMUI checklist to use atmospheric tracers with prescribed CO ₂ /SF ₆ fluxes	71
E.2 UMUI checklist to use atmospheric tracers with prescribed fluxes of CH ₄ , MCF, Radon and SF ₆	72
E.3 CO ₂ tracer hand edit file (CO2_tracers.ed).....	73
E.4 CH ₄ , MCF, and Radon hand edit file (all_tracers.ed).....	76
E.5 Tracer flux STASH-master file (tracer_fluxes.stash).....	80
E.6 OH, Cl and O ¹ D, photolysis and ocean deposition STASH-master file (methane_loss.stash)	81

LIST OF FIGURES

- Fig. 3.1:** (Top Left) Global atmospheric CO₂ mixing ratio for the CASA 3-hour tracer in the UM (black line) and the expected atmospheric CO₂ mixing ratio from the surface fluxes (red line). (Bottom Left) The difference between modelled and expected CO₂ mixing ratio for the CASA 3-hour tracer. (Top Right) Modelled and expected CO₂ mixing ratio from the fossil fuel tracer. (Bottom Right) Corresponding difference for the fossil fuel tracer.....14
- Fig. 3.2:** (Top Left) Global atmospheric CO₂ mixing ratio for the CASA 3-hour tracer in the UM with the mass fixer (black line) and the expected atmospheric CO₂ mixing ratio from the surface fluxes (red line). (Bottom Left) The difference between modelled and expected CO₂ mixing ratio for the CASA 3-hour tracer. (Top Right) Modelled and expected CO₂ mixing ratio with the mass fixer for the fossil fuel tracer. (Bottom Right) Corresponding difference for the fossil fuel tracer.....15
- Fig. 3.3:** (Top Left) Annual mean biospheric CO₂ tracer concentrations in the mass conserving simulation. The background concentration of 380 ppm has been removed. (Top Right) Annual mean biospheric CO₂ tracer differences between the simulation with the mass fixer and the original simulation (mass fixer simulation minus original). Bottom Left) Annual mean fossil fuel tracer concentrations in the mass conserving simulation. Bottom Right) Annual mean fossil fuel tracer differences between the simulation with the mass fixer and the original simulation.16
- Fig. 3.4:** (Left) Annual mean zonally-averaged biospheric CO₂ concentrations for the mass conserving (black) and the original (red) simulation. Right) Annual mean zonally averaged fossil fuel concentrations.....16
- Fig. 3.5:** Seasonal cycle of the inter-hemispheric difference in fossil CO₂, calculated by subtracting monthly hemispheric concentrations using a spline fit to marine boundary layer sites. The gray lines indicate results from the fossil flux in other model simulations (from the TransCom-continuous experiment, Law et al. 2008).....17
- Fig. 4.1:** Annual mean total CO₂ concentrations at 20 m, using the hybrid stable boundary layer scheme. The mean concentrations are calculated by adding the biospheric (diurnally varying), ocean and fossil contributions and averaging the concentrations over the last three years. (Top Left) UM version 6.3 with MOSES. Top Centre) UM version 7.3 with MOSES. (Top Right) UM version 7.3 with CABLE. Bottom Left) Difference due to changing the model version (UM 7.3 MOSES minus UM 6.3 MOSES). (Bottom Right) Difference due to changing the land surface model (UM 7.3 CABLE minus UM 7.3 MOSES).....19
- Fig. 4.2:** Maps of mean CO₂ concentrations at 20 m from the N48 simulation (left four panels) and the N96 simulation (right four panels). The CO₂ concentrations are the sum of the biospheric fluxes (monthly varying), ocean fluxes and fossil fuel emissions. The results shown use the LT boundary layer scheme. Far left column) Mean total CO₂ concentrations from the N48 simulation with CABLE for January (top) and July (bottom). (Middle left column) Zonal mean vertical distribution of the total CO₂ concentrations from the N48 CABLE simulation during January (top) and July (bottom). (Middle right column) Mean total CO₂ concentrations from the N96 CABLE simulation. Far right column) Zonal mean vertical distribution of the total CO₂ concentrations from the N96 CABLE simulation.....20
- Fig. 4.3:** Fossil CO₂ concentrations from 20 m sampled at marine boundary layer (MBL) sites. Grey lines indicate TransCom results. Coloured lines indicate UM results. Red is UM 6.3 MOSES, green is UM 7.3 MOSES, blue is UM 7.3 CABLE, with all simulations using N48 resolution. Different line styles indicate different boundary layer schemes. Solid is sharpest scheme, dashed is long-tailed scheme, and dotted is hybrid long-tails over land. Top) Annual mean inter-hemispheric gradient, from splines fit to annual mean MBL concentrations. Bottom) Monthly inter-hemispheric gradients, from splines fit to the monthly-mean MBL concentrations.21

Fig. 4.4:	Fossil CO ₂ concentrations at 20 m sampled at MBL sites for the UM 7.3 CABLE N48 simulations (blue), same as in Fig 4.3) and UM 7.3 CABLE N96 simulations (purple).....	22
Fig. 4.5:	Total CO ₂ seasonal cycles at selected observation sites. All the data were de-trended to remove the growth over time. Model concentrations include the contributions from biospheric (diurnally varying), fossil and ocean fluxes. The model is sampled at the grid cell that includes the observation location and at the closest vertical level to the sampling height. Black lines indicate the observations, which are from GLOBALVIEW-CO ₂ (2009) and are based on quasi-continuous samples.	23
Fig. 4.6:	Total CO ₂ seasonal cycles at selected observation sites for the UM 7.3 CABLE N48 simulations (blue, same as Fig. 4.5) and UM 7.3 CABLE N96 simulations (purple).....	24
Fig. 4.7:	Zonally averaged peak-to-peak amplitude of the seasonal cycle from the biospheric CO ₂ fluxes (monthly) for all the N48 configurations.....	25
Fig. 4.8:	Zonally averaged peak-to-peak amplitude of the seasonal cycle from the biospheric CO ₂ fluxes (monthly) for the UM 7.3 CABLE N48 simulations (blue, same as Fig. 4.7) and UM 7.3 CABLE N96 simulations (purple).....	25
Fig. 4.9:	Vertical profiles of monthly-mean CO ₂ concentrations at two tall towers in the USA. The monthly mean concentration has been removed from all plots to highlight the vertical gradients. The LEF tower (left) extends up to 396 m and the WKT tower (right) extends up to 500 m. The model is sampled from the grid cell including the tower and at the bottom five vertical levels. Top Left) January profiles at LEF. Bottom Left) July profiles at LEF. (Top Right) January profiles at WKT. (Bottom Right) July profiles at WKT. The black lines indicate the observations and the coloured lines show the model results (same colours/styles as Fig. 4.4).....	25
Fig. 4.10:	Vertical profiles of monthly-mean CO ₂ concentrations at two tall towers in the USA for the UM 7.3 CABLE N48 simulations (blue, same as Fig. 4.9) and UM 7.3 CABLE N96 simulations (purple).....	26
Fig. 4.11:	Peak-to-peak amplitude of the mean JJA (June, July, August) diurnal cycle for observed 2002 CO ₂ (black dot), TransCom models for 2002 (error bar shows minimum, maximum and median model) and the UM N48 cases. The model amplitudes are calculated from the sum of concentrations from biospheric (diurnally varying), fossil and ocean emissions. Sites are listed on the x-axis and their locations are shown in Table 4.1. CBW, LEF, HUN, and TPJ are sampled at various vertical levels, which are specified in meters. The asterisk indicates coastal sites. Output for LJO and KIS were not saved for the UM cases.....	27
Fig. 4.12:	Vertical profiles of the peak-to-peak diurnal cycle amplitudes for JJA at two tower sites in the northern hemisphere. The model is sampled from the grid cell including the tower and at the vertical levels most closely matching the observations levels, and all N48 cases are displayed. (Left) Vertical profiles at Cabauw. (Right) Vertical profiles at LEF.....	29
Fig. 4.13:	Ratio of peak-to-peak mean JJA diurnal concentration amplitude to diurnal JJA flux amplitude, using the diurnally varying biospheric tracer and flux for the models. Each site is indicated by a letter and identified in the key, with the model listed along the x-axis. The UM results are in colour, while the TransCom models are gray. Observed ratios shown in the last column are only currently available at LEF, BOB, HVF, and TPJ, where both fluxes and concentrations are measured.....	30
Fig. 5.1:	(Left) Area-weighted global mean methane concentrations from the top three levels in the model (L38: solid, L37: dashed, L36: dot-dash). (Right) Global mean methane concentrations from the bottom model level (nearest the surface).....	34

Fig. 5.2:	Vertical profile of zonal mean concentrations for January and December from the first test case, with 1700 ppb in the top level only.....	35
Fig. 5.3:	Top of the atmosphere area-weighted global mean concentrations for each of the test simulations. (Top) L38; (Middle) L37; (Bottom) L36.....	36
Fig. 5.4:	Area-weighted global mean concentrations at the bottom of the atmosphere.....	37
Fig. 5.5:	Daily top of the atmosphere area-weighted global mean concentrations from the advection tests: (Higher 1) Cubic Lagrange interpolation, (Higher 2) Quintic Lagrange interpolation, (Higher 3) ECMWF quasi-cubic interpolation, (Higher 4) ECMWF monotone quasi-cubic interpolation, (Higher 5) Bi-cubic Lagrange interpolation in the horizontal and linear interpolation in the vertical, (Higher 6) ECMWF quasi-cubic interpolation in the horizontal and quintic in the vertical, and (Higher 7) Cubic Lagrange interpolation in the horizontal and quintic in the vertical.....	39
Fig. 5.6:	Top of the atmosphere CH ₄ concentrations for the CTL tracer from three simulations following the TransCom CH ₄ protocol. Red indicates the original set-up, orange shows results from removing the loss from the top level, and blue indicates results from setting the top level equal to the neighbouring lower level.....	41
Fig. 5.7:	Monthly mean methane concentrations from the three simulations over the northern hemisphere (NH; top), tropics (middle, 20 S through 20 N), and southern hemisphere (SH; bottom). The concentrations are for the CTL tracer and are the mean values from the sites sampled in GLOBALVIEW-CH ₄ (GV; 2009), which has weekly temporal resolution. The majority of the sites are located near the surface in the lowest model level. The model is sampled hourly at the grid cell and level that most closely matches the observation location. The black lines indicate the GV results, and the coloured lines show the model results from the three simulations in Fig. 5.6	42
Fig. 6.1:	(Top left) Mean near-surface January methane concentrations. (Bottom left) Mean near-surface July methane concentrations. (Top right) Mean zonally averaged vertical profile for January. (Bottom right) Mean zonally averaged vertical profile for July.....	44
Fig. 6.2:	Monthly mean methane concentrations in the northern hemisphere (NH; top), tropics (middle, 20 S through 20 N), and southern hemisphere (SH; bottom). The concentrations are the mean values from the sites sampled in GLOBALVIEW-CH ₄ (GV; 2009), which has weekly temporal resolution. The model is sampled hourly at the grid cell and level that most closely matches the observation location. The black lines indicate the GV results, and the coloured lines show the model results from each of the six different methane tracers.....	45
Fig. 6.3:	Methane mean seasonal cycle for sites in the NH (top), tropics (middle), and SH (bottom). Black lines show the GV results and coloured lines indicate the model results.....	46
Fig. 6.4:	(Left) Annual mean methane inter-hemispheric differences, calculated by subtracting the monthly mean SH concentrations from the NH concentrations. (Right) Methane monthly mean inter-hemispheric difference.....	47
Fig. 6.5:	The annual growth rate of methane for both the GV dataset (black) and the UM (colours), calculated by subtracting the annual mean concentrations.....	47
Fig. 6.6:	Vertical profiles of monthly mean methane concentrations at the five GV sites sampled by aircraft. Rather than using the full extended record, the comparisons only include times when there are actual data. Solid lines show the profiles in January, and dashed lines show the profiles in July. The sites are ordered by decreasing latitude.....	48
Fig. 6.7:	Vertical profiles of the methane mean seasonal cycle amplitude.....	49

LIST OF TABLES

Table 4.1:	Latitude, longitude and reference for the CO ₂ observations sites used in Fig. 4.11.	28
Table 5.1:	Methane passive tracer tests defined by the initial condition used in level 38, level 37 and the rest of the atmosphere and whether tracer conservation is used. Also given are the labels and line colours used in Figs 5.3 and 5.4.	35
Table 6.1:	List of the six CH ₄ tracers simulated in the TransCom-CH ₄ inter-comparison project. Fluxes either have inter-annual variations (IAV) or are annual repeating (CYC).	43

ABSTRACT

The Australian Community Climate and Earth System Simulator (ACCESS) is a coupled land-ocean-atmosphere model being developed for a wide variety of applications. One key area of research with ACCESS is the carbon cycle, in particular atmospheric carbon dioxide (CO₂) and methane (CH₄) concentrations resulting from prescribed surface fluxes. ACCESS derives its atmospheric model from the UK Met Office Unified model (UM), which included both a specific atmospheric CO₂ tracer (used for climate-carbon feedback studies) as well as other generic atmospheric tracers, developed for stratospheric transport studies. For our applications, the CO₂ and generic tracers within the UM required several modifications. The use of the CO₂ tracer was made more flexible, with less assumed coupling with other model components (e.g. radiation). For atmospheric tracers, associated surface fluxes were added for the first twenty tracers, and a methodology to more easily initialize the tracers was implemented. To participate in a model inter-comparison, new routines were added to simulate the atmospheric loss of CH₄ and methyl chloroform (MCF) without explicitly modelling chemistry, as well as radioactive decay of radon. Investigations of the tracers revealed that the atmospheric mass was not being conserved, and a simple mass mixing ratio fixer has been developed to ensure tracer conservation, taking into account any global mixing ratio change resulting from surface fluxes. The new capabilities in ACCESS are used to investigate the model transport using atmospheric CO₂ concentrations, indicating that the inter-hemispheric mixing may be too slow and that the night-time and winter stable boundary layers apparently mix too slowly, particularly using the “sharpest” stable boundary layer parameterization. Analysis of resulting CH₄ concentrations for the model inter-comparison, revealed a problem with the transport in the top level of the model, which impacted the atmospheric concentrations throughout the atmosphere. Case studies using various model set-ups indicated that a simple fix is to set the top level equal to the neighbouring lower level; however, further investigation into the mixing at the top of the atmosphere should be conducted to fully diagnose the problem.

1. INTRODUCTION

Over recent decades, the modelled transport of atmospheric tracers (variables representing the mass-mixing ratio of species that are advected throughout the atmosphere) has become important for a variety of applications. Global, climate-scale simulations use atmospheric tracer transport to investigate potential climatic feedbacks and possible scenarios for future climate. Atmospheric tracers can be used to investigate transport processes, leading to further understanding of both the atmospheric circulation and the distributions of simulated elements and compounds. Tracer transport modelling is used in atmospheric inversion studies to determine the sources and sinks of various species, such as carbon dioxide (CO₂), carbon monoxide (CO), and methane (CH₄). Finally, the analysis of atmospheric tracers has been used to evaluate model transport, resulting in further understanding of transport processes and mechanisms.

The atmospheric transport of CO₂ forms one component of the carbon cycle. Modelling atmospheric CO₂ concentrations and accounting for the interactions between the Earth's surface and the atmosphere alters the feedback between CO₂ concentrations and climate warming. A model inter-comparison conducted with eleven different climate models including full carbon cycles unanimously showed that future climate change will reduce the efficiency of the earth system to absorb the anthropogenic-carbon perturbation, causing a larger fraction of the anthropogenic CO₂ to stay air-borne than that predicted by climate models that do not include the carbon cycle (Friedlingstein et al. 2006).

Atmospheric transport influences tracer distributions at various scales: from long-range global-scale inter-annual processes to seasonal inter-hemispheric transport to large-scale eddies to convection to small-scale transport via vertical diffusion (Miyazaki et al. 2008). The circulation processes acting at these scales have been investigated using various tracers (e.g. Plumb and Mahlman 1987; Bratseth 2003; Bowman and Erukhimova 2004; Hess 2005). Focusing on the carbon cycle, distinct variations in the atmospheric CO₂ concentration can provide useful information about atmospheric transport processes (Lintner et al. 2006; Miyazaki et al. 2009). At the same time, atmospheric transport models have been used to investigate the relative importance of various transport processes to the CO₂ distribution (e.g. Strahan et al. 1998; Kawa et al. 2004; Tiwari et al. 2006; Miyazaka et al. 2008; Miyazaki et al. 2009). Understanding CO₂ transport processes advances the knowledge of the carbon cycle and provides important information to improve transport models (Miyazaki et al. 2008).

Atmospheric concentration measurements provide critical information about sources and sinks of CO₂, CO, CH₄ and other important trace gases. To interpret atmospheric measurements in terms of surface fluxes, atmospheric transport must be taken into account. Atmospheric inversions provide a method to estimate surface fluxes utilizing atmospheric concentration information. In inversions, tracer transport models simulate the atmospheric tracer concentrations resulting from surface fluxes. The magnitude of the fluxes is then adjusted to create concentration distributions that match observations. Atmospheric inversions have provided valuable information regarding surface fluxes of CO₂ (e.g. Gurney et al. 2002; Rödenbeck et al. 2003; Baker et al. 2006), CO (e.g. Palmer et al. 2003; Heald et al. 2004; Kopacz et al. 2009), and CH₄ (e.g. Bousquet et al. 2006; Bergamaschi et al. 2009; Villani et al. 2010).

Due to improvements in the quality and quantity of observational data, enhancements in computer resources, and developments in both climate model complexity and the inversion methodology, one of the largest sources of uncertainty in carbon budget studies is the atmospheric transport (Law et al. 1996; Denning et al. 1999). The Atmospheric Tracer Transport Model Inter-comparison Project (TransCom) was established to systematically evaluate transport models. In the first phase, TransCom examined the atmospheric concentration response to surface emissions of fossil fuel CO₂ and biospheric CO₂ (Rayner and Law 1995;

Law et al. 1996). Since the models showed significant differences, modellers participated in a second phase of TransCom designed to understand the mechanisms by which the models diverged (Denning et al. 1999). In that study, participants modelled sulphur hexafluoride (SF₆) concentration, which is useful in assessing model transport since it has a long atmospheric lifetime, a relatively well-known source, and more than twenty years of observations around the globe. Following the work investigating model transport in forward simulations, TransCom assessed the sensitivity of CO₂ inverse flux estimates to the transport model used (e.g. Gurney et al. 2002; Gurney et al. 2004; Baker et al. 2006). More recently, a new set of forward simulations (TransCom continuous or TC-cont) compared models on synoptic and diurnal timescales (Law et al. 2008; Patra et al. 2008).

In order to contribute to atmospheric research as well as provide reliable weather forecasts, the Centre for Australian Weather and Climate Research (CAWCR) is developing a coupled land-ocean-atmosphere model, the Australian Community Climate and Earth System Simulator (ACCESS). The atmospheric component of ACCESS is the UK Met Office Unified Model (UM). For the ocean, the UM is coupled to the Australian Climate Ocean Model (AusCOM). Over land, the existing land surface module (UK Met Office Surface Exchange Scheme; MOSES) is replaced by CSIRO's Community Atmosphere-Biosphere Land Exchange (CABLE) model. All the simulations in this report use a setup similar to the HadGEM2 model (Collins et al. 2008) with the new Met Office prognostic cloud scheme PC2 (Wilson and Bushell 2007; Wilson et al. 2008). ACCESS will be used for a variety of applications, including weather forecasting, climate change investigations, tracer transport analyses, and carbon cycle studies.

Designed for simple atmospheric chemistry studies, the UM contains the facility to advect a number of atmospheric tracers, focusing on stratospheric applications (UM User Guide). The tracers are advected using the standard semi-Lagrangian advection scheme with the same selections as for the moisture variables, with additional mixing through sub-grid scale processes such as convection and boundary layer mixing. Atmospheric tracer advection is done as accurately as possible while conserving mass, and the tracer concentrations are forced to remain greater than zero. The tracers can be initialized either from an input start file or from an ancillary tracer file; however, all atmospheric tracers must be included in the same initial file.

One area of focus with the ACCESS model will be the carbon cycle. The UM already has a specified CO₂ tracer, which was set-up to include fluxes from both their land and ocean carbon-cycle modules, as well as an additional input flux file, generally used for fossil emissions. In order to utilize this field, the existing interactive carbon cycle must be turned on. The interactive carbon cycle requires interactive vegetation, which is simulated with the TRIFFID dynamic global vegetation model (Cox 2001). For ACCESS, dynamic vegetation is currently not included, and the land surface model CABLE receives land cover information from vegetation maps. The interactive carbon cycle also requires both the land surface model (MOSES) and the ocean carbon cycle model (Hadley Centre Ocean Carbon Cycle; HADOCC) to be active, which is not a requirement for many ACCESS studies. Finally, the interactive carbon cycle requires the modelled atmospheric CO₂ concentrations to interact with the radiation scheme. This requirement is not optimal for case studies of CO₂; for example, test simulations may not initialize CO₂ to realistic atmospheric concentrations in order to study transport, and this would have serious unintended consequences on the atmospheric radiation and hence on the climate. To utilize the atmospheric CO₂ tracer with ACCESS, it is necessary to modify the UM to not require interactive vegetation and to have the option to use a global constant CO₂ value to feed back into the radiation scheme even when the CO₂ tracer is being used.

In addition to the specified CO₂ tracer, the atmospheric tracers in ACCESS can be set up to transport additional CO₂ fluxes, as well as other species useful in investigating the carbon cycle and atmospheric transport, such as CH₄, SF₆ and radon; however, the atmospheric tracers have several limitations that need to be addressed. Currently, the atmospheric tracers do not have any interaction with the surface, and tracer flux variables are included only as diagnostic output. Many trace gases have sources and sinks at the surface, making it necessary to include surface fluxes for the tracers, with separate files for each tracer species to allow fluxes with different temporal resolution. For species such as CH₄, the ability to prescribe chemical loss terms is also required. For carbon budget and inter-comparison studies, it is essential that the tracer atmospheric mean mass mixing ratio is conserved. Although a conservative advection scheme for atmospheric tracers exists, it needs to be evaluated with species that have surface fluxes to ensure that mass is conserved both during the surface exchange as well as during transport. Finally, since the land surface may act as a sink for some species, requiring the tracer concentrations to remain above zero is an unnecessary limitation for ACCESS applications.

To simulate more complex chemistry and atmospheric aerosols, work is on going to include a chemistry and aerosol model in the UM. The United Kingdom Chemistry and Aerosol (UKCA) module (Morgenstern et al. 2008) is being coupled to ACCESS. The UKCA supports three tropospheric chemistry schemes to simulate a variety of species, including NO_x, HO_x, CO, CH₄, and O₃. To accurately predict these species, the model includes over thirty species with more than 150 reactions. The UKCA also simulates photolysis, wet deposition, dry deposition, and surface emissions for a variety of chemical species. The UKCA uses the same tracer transport algorithms as used by the generic atmospheric tracers; hence, our work to simulate CH₄ and MCF using prescribed loss terms provides a useful tool for comparison and model evaluation.

This document describes the modifications in the UM necessary for using atmospheric CO₂ and tracers in tropospheric and near-surface studies. In addition to providing a description of the changes to the model, this report outlines the methodology to use the tracer modifications. The new atmospheric tracer capabilities are then utilized to investigate modelled atmospheric transport, using simulated CO₂, SF₆, and CH₄ from various simulations.

2. MODEL MODIFICATIONS

2.1 General description

Since ACCESS is being developed for a variety of climate and carbon cycle applications, several modifications to the UM are necessary in order to simulate CO₂ and atmospheric tracers with an emphasis on surface concentrations. Code changes in UM versions 6.3 and 7.3 have been made to extend the CO₂ tracer options, to more easily initialize tracer concentrations, and to utilize tracer flux fields for atmospheric tracers. In order to specify whether the CO₂ tracer or a global constant concentration is used for the radiation calculations, a flag has been added. To simplify the initialization of tracers, the UM was modified to have the capability to initialize each tracer from separate files or to set the tracer field to zero. Since the land surface may act as a sink for some species, the tracers are allowed to be negative.

The tracer flux fields were originally set-up in the UM as diagnostic output from the tracer fields. In order to provide flux information to each atmospheric tracer, the code has been modified to use twenty of these tracer flux fields to store the fluxes for atmospheric tracers. To specify the fluxes, each tracer flux field has an accompanying ancillary file. Similar to other ancillary files in the UM, the tracer flux files can be set-up with various temporal resolutions for changing and updating the fluxes throughout a simulation; and the tracer flux fields can be output with the other model variables.

In order to ensure conservation for CO₂ and atmospheric tracers, a simple mass fixing routine has been added. The mass fixing routine requires the global mean mass mixing ratio of each field to equal the mean from the previous time-step in addition to the change in mixing ratio resulting from the surface trace gas fluxes. Two flags have been set-up to easily turn on and off the mass fix routine: one flag for the CO₂ tracer and one flag for the atmospheric tracers. In order to conserve the mass for only a selection of the tracers, the user can set the number of the tracer in which to begin mass conservation. Starting at the specified tracer, the mass fixer routine is called for all subsequent tracers being used in the simulation.

The opportunity to participate in a model inter-comparison focussed on atmospheric transport aspects of methane has required further adaptation of the tracer code. The inter-comparison required simulations of six methane tracers with different surface fluxes, methyl chloroform (MCF), and radon, with atmospheric loss of methane and MCF through prescribed hydroxyl radical (OH) concentrations. A subroutine has been added to calculate the atmospheric loss of methane due to oxidation by reaction with the hydroxyl radical (OH), as well as stratospheric loss from chlorine (Cl) and oxygen (O¹D), provided as loss rates. A flag has been added to turn on methane loss. The methane tracers must be included first, as the atmospheric loss is calculated for the tracers up to the user-specified tracer number. To calculate the atmospheric loss due to oxidation at each model level, a three-dimensional OH field is read in from an ancillary file with expected concentration units of molecules per cubic centimetre, and a temperature-dependent rate constant for the reaction is specified in the subroutine. The stratospheric loss due to Cl and O¹D is combined into a single ancillary file, with loss rate units (s⁻¹). These fields are included in the same ancillary file, which has the option of updating throughout the run, and they can also be included in the model output.

Similar to CH₄, a subroutine to calculate the atmospheric loss of MCF has also been added, including loss contributions from reaction with OH, photolysis in the stratosphere, and ocean deposition. The loss for MCF is calculated for the tracer number specified by the user, and the routine is only called if the user turns on the associated MCF loss flag. For atmospheric oxidation, the MCF field uses the same OH field as methane and a specified temperature dependent rate constant is calculated. Photolysis rates due to solar ultra-violet

radiation, in units of s^{-1} , and ocean deposition velocities, in m s^{-1} , are both specified in the same ancillary file as OH and the stratospheric CH_4 loss, and also have temporal updating capabilities. Both of these variables can also be included in the model output.

Radon can also be simulated in an atmospheric tracer. A subroutine to calculate the exponential decay of radon has been added, using a half-life of 3.8 days. The decay is calculated for the specified radon tracer number if the decay flag is turned on.

2.2 Model implementation

Numerous subroutines were modified and added in order to update the CO_2 and tracer capabilities. A list of all the routines altered, along with a brief description of the changes, is included in Appendix A. A list of all the routines added is included in Appendix B. This section provides a description of the code changes.

2.2.1 CO_2

Although atmospheric CO_2 concentrations are already modelled in the UM, a few changes have been made for ACCESS. All CO_2 calculations in the UM require the CO_2 interactive switch (L_CO2_INTERACTIVE) to be set to true. For atmospheric radiation calculations, a specified global CO_2 constant (CO2_MMR, in mass mixing ratio of kg kg^{-1}) is used if the interactive CO_2 tracer is not defined; however, if the CO_2 interactive switch is turned on, then the radiation scheme automatically uses the CO_2 tracer concentrations. To provide the option of using the global constant CO_2 value even when the CO_2 tracer is being used, a switch to control the radiation (L_CO2_RADIATION; defined in cntlatm.h) was added. The switch is used in the main radiation routine (glue_rad-rad_ctl2.F90) and the short-wave radiation routine (glue_rad-rad_ctl3c.F90) to set the CO_2 concentration used in the radiation calculations. To be defined in the short-wave radiation routine, three routines were modified to pass the CO_2 radiation switch (atm_step.F90, atmos_physics1.F90, and ni_rad_ctl.F90).

The flux input into the CO_2 array is set in a boundary layer mixing routine (bl_trmix_dd.F90). Since the version of ACCESS currently being used does not include an ocean carbon module, the flux contribution from the ocean is not used, and the atmospheric CO_2 concentration only has contributions from the land fluxes simulated by CABLE (LAND_CO2) and from the fluxes specified from a file (CO2_EMIT). If a file with flux values is provided, the UM expects flux units of $\text{kg CO}_2 \text{ m}^{-2} \text{ s}^{-1}$.

2.2.2 Atmospheric tracers and associated surface fluxes

The atmospheric tracers in the UM have been modified to provide the capabilities required for various ACCESS studies. To simplify the initialization of tracers, the UM was modified to have the capability to initialize each tracer from separate files (rather than from the ATRACER file) or to set the tracer field to zero or to a specified constant value. The units for the atmospheric tracers are kg kg^{-1} . Variable initialization in the UM occurs in the reconfiguration, which is a separate executable from the main model. All of the reconfiguration routines are in the qxreconf folder. In order to initialize the tracers to concentration distributions from individual user-specified files, the expected file name and file format for the tracers was changed in three routines responsible for reading and processing the initial conditions (replanca-rcf_replanca.F90, rcf_aux_file_mod.F90, and rcf_create_dump_mod.F90). In order to use these changes, a new reconfiguration executable needs to be created, which can be done by performing a compile job using the UMUI.

In order to provide flux information to each atmospheric tracer, the code was modified to use twenty tracer flux fields to store fluxes for the first twenty atmospheric tracers. The tracer fluxes are variables in the boundary layer section (section 3, items 100-119). In order to initialize, update, and output the tracer fluxes, they are set-up as ancillary fields, and each tracer flux has an associated ancillary file, with expected flux units of $\text{kg (species) m}^{-2} \text{ s}^{-1}$. To process the fluxes, they must be included in the UM script containing user-defined ancillary fields (UAFIELDS_A), and the associated files must be included in the UM job script containing user-defined ancillary files (UAFILES_A). Similar to other ancillary files in the UM, the tracer flux files can have various temporal resolutions for updating them throughout the simulation. Each ancillary file must contain the variable code (numbers 3100-3119) that corresponds to the tracer flux number. As a note, the user defined ancillary fields and files (UAFIELDS_A and UAFILES_A) are not the same as the user-defined single-level ancillaries and multi-level ancillaries that can be declared in the UMUI. The single-level and multi-level ancillaries have the capability to simulate twenty different species each and are stored in the user defined single-level and multi-level variables; however, the single-level ancillaries are currently being used to store CABLE variables. The single and multi level ancillaries are also more difficult to utilize for individual atmospheric tracers, as all the fields are read in from a single file for the single-level and a single file for the multi-level ancillaries. In contrast, the user defined ancillary fields and files lists provide a method to make any variable that needs to be updated, such as the tracer fluxes, into an ancillary field with an associated ancillary file, making it easy to change the number of tracers being simulated and to use various temporal resolutions for the tracer fluxes.

To initialize the tracer fluxes, several reconfiguration routines were modified. Since the flux variables are in the boundary layer section rather than with other prognostic variables, the boundary layer section has been added to the list of sections processed in the reconfiguration (rcf_stashcodes_mod.F90 and rcf_address_mod.F90). The user-defined ancillary fields and files have been added to the lists of variables processed in the reconfiguration (rcf_ancil_atmos_mod.F90). If the tracer fluxes exist in the user-defined ancillary field list, then the tracer fluxes are automatically initialized to 0 (rcf_set_data_source_mod.F90). To use user-specified filenames, the routine that handles reading the user ancillary files was changed (calc_nlookups_mod.F90). Since the tracer fluxes can be updated, the reconfiguration routine that handles updating was modified to use individual file names specified for each tracer (inancila-rcf_inancila.F90). Similar to the changes made to the model reconfiguration for CO_2 , these changes need to be included in the reconfiguration executable.

All the global variables used in the UM are defined in the include folder. To include variables and associated file information for the tracer fluxes, several files were changed. Twenty tracer fluxes are added in four routines (arg_atm_fields.h, s_mainn.h, typ_atm_fields.h, and s_maina.h), and integer pointers to the flux variables are also added (typptra.h). Since the tracer fluxes have associated ancillary files, the maximum number of ancillary fields and files was increased (cancmaxa.h and conanc.h), and ancillary item codes and names are assigned to the tracer flux variables (cancflda.h and canctita.h). To read in the ancillary files, Fortran file unit numbers are assigned to the tracer flux files (cancftna.h), and variables were added to store file names for the tracer fluxes (cancila.h). Finally, the tracer fluxes were added to the list of ancillary fields (canclsta.h).

To initialize and store the tracer fluxes during a simulation, numerous control and atmospheric routines were modified. In ACCESS, all the model variables used in a simulation are saved in a single main storage array. To allocate space for the tracer fluxes in this main array, the boundary layer section was added to the list of prognostic variables processed during model initialization (adres.F90). The model routine used to initialize

prognostic variables and to copy these variables to the main storage array was modified to include initialization of the tracer fluxes (replanca-rpanca1a.F90). In order to more easily pass and reference the tracer fluxes, individual flux arrays are allocated (atm_fields_mod.F90). To use the flux arrays, the atmospheric routine that sets pointers for prognostic variables back to the main storage array is modified to set the tracer flux pointers (set_atm_pointers.F90), and the routine that actually sets the new variables to point to the main storage array is changed to include the tracer fluxes (set_atm_fields.F90).

To update the tracer fluxes, two routines are modified. An ancillary routine is changed to include tracer fluxes in the list of variables that may need updating and to then allow the flux to be updated from a user-specified file (inancila-inanca1a.F90). In order to provide the additional information required by the tracer fluxes to the updating ancillary routine, a control routine was modified to pass the necessary variables and arrays (inancctl.F90).

The tracer fluxes interact with the atmospheric tracers in a boundary layer routine (bl_trmix_dd.F90). In order to provide the tracer fluxes to this routine, several routines were modified to pass along the fluxes (atm_step.F90, atmos_physics2.F90, ni_imp_ctl.F90, bl_tracer_intctl.F90). Each flux is mixed into the lowest model level of the associated atmospheric tracer using an atmospheric mixing routine (tr_mix.F90). Following the emission of the fluxes into the atmosphere, the fluxes were originally copied back to the flux variables for diagnostic output; however, since the fluxes are specified from input files, this step is no longer performed.

Since the atmospheric tracers can be initialized to zero and can be used to simulate species that have surface sinks, it is necessary that they can contain and transport negative values. The tracer advection routine that forced the tracer concentrations to be greater than zero was changed to allow the concentrations to contain negative values (sl_tracer2-sltrac2_2a.F90). Initializing an atmospheric tracer to zero rather than specifying an atmospheric background concentration may be useful for various studies, as it allows easier tracking of the sign of concentration anomalies and it also may provide more computer accuracy by removing excess digits. However, running with a background concentration of zero may cause problems when using the mass fixer with fluxes that change sign from positive to negative, such as biospheric CO₂ fluxes. When the global flux contribution approaches the magnitude of the atmospheric concentration, the simple scaling used in the mass fixer breaks down and causes spurious changes in concentrations. Therefore it is not advised to use a background of zero for tracers that have fluxes of alternating sign.

2.2.3 CO₂ and atmospheric tracer mass conservation

For tracers that are chemically inert in the atmosphere, it is essential to conserve atmospheric mass, particularly for climate studies over long time periods where changes in mass can accumulate and result in biases in the concentrations. The atmospheric mass of both the CO₂ tracer and the free atmospheric tracers in the UM is investigated in depth in Chapter 3. To ensure that mass is conserved, including the surface flux contribution, a simple mass fix routine was implemented. Details of the mass fixer are provided in Appendix C, which also provides the code for the subroutine. Note that the mass fixer actually constrains the total tracer mass relative to the total mass of the atmosphere, conserving the global atmospheric mean mixing ratio of the trace gas. This is done because the global mass of the atmosphere is not perfectly conserved.

To save various properties that are required by the mass fixer, several variables were added to the UM. Switches to turn on the mass fixer for CO₂ (L_CO2_MASS) and the atmospheric tracers (L_TRACER_MASS) were incorporated, as well as an integer to store the tracer at which to start using the mass fixer (I_TRACERMASS_START). To store the atmospheric mass and the flux of CO₂ and the mass of

the twenty tracers with associated surface fluxes, three global variables were required (CO2MASS, CO2EMITMASS, TMASS). All these variables are stored in a common data file (cntlatm.h).

Implementing the mass fixing routine required both top level and atmospheric subroutines to be modified. To calculate the initial mass of CO₂ and the tracers, a new subroutine was created (tracer_massinit.F90). This routine is called from the main atmospheric time-step routine (atm_step.F90) and is only called on the very first time-step. This routine uses the existing tracer routine to calculate the global atmospheric mass (tracer_mass.F90). A few modifications were made to the tracer mass routine, primarily to output the calculated atmospheric masses and to alter the print statements. To calculate the mass of the flux emissions, another new routine was created (tracer_fluxemit.F90). This routine calculates the global total mass of the emissions per time-step, accounting for the changing grid cell sizes. The mass of the CO₂ emissions is calculated in the routine that controls the boundary layer interactions (ni_imp_ctl.F90), and the mass of the tracer emissions is calculated in the mass fixing routine itself (tracer_massfix.F90). Once the variables have been set-up, the mass fixer is called after the fluxes are mixed into the atmosphere (atm_step.F90). The mass fixing routine ensures that the global mass mixing ratio of the current time-step equals the global mass mixing ratio of the previous time-step combined with the surface emissions, printing the original and fixed mass mixing ratios and the fixing factor to the standard output.

2.2.4 CH₄, Radon and MCF chemistry

The atmospheric tracers can be used to simulate a variety of species. Three specific species that were required to participate in a transport model inter-comparison are CH₄, MCF, and radon. In addition to having surface fluxes, all three of these species experience atmospheric loss. In order to model these compounds, subroutines have been added to calculate the dominant atmospheric loss terms for each species.

To model CH₄, a new subroutine was added to calculate the loss of methane due to the oxidation from reaction with OH and due to the reactions with both Cl and O¹D in the stratosphere (tracer_methaneloss.F90). To use the methane routine, a switch was added to call the loss routine (L_METHANE_LOSS) and an integer was added to specify how many methane tracers are being simulated (I_METHANE_TRACERS). Both of these variables are stored with other user specifications in a data file (cntlatm.h). The methane loss routine is called from the main time-step routine (ATM_STEP.F90) after the tracer fluxes are mixed into the atmosphere.

To model MCF, a new subroutine was added to calculate the loss of MCF due to the reaction with OH, to photolysis in the stratosphere, and to ocean deposition (tracer_mcfloss.F90). Two variables were added in a data file (cntlatm.h) to store the options for MCF: a switch was added to determine whether to call the loss routine (L_MCF_LOSS) and an integer was added to specify the number of the tracer that is MCF (I_MCF_TRACERNUMBER). The MCF loss routine is called from the main time-step routine (ATM_STEP.F90) immediately after the call to the methane loss routine, after the fluxes have been mixed into the atmosphere.

To model radon, a new subroutine was added to calculate the exponential decay (L_RADON_DECAY). Similar to MCF, two variables were added in data file (cntlatm.h): a switch to determine whether to call the radon decay routine and an integer was added to specify the number of the tracer that is radon (I_RADON_TRACERNUMBER). The radon loss routine is called from the main time-step routine (ATM_STEP.F90) immediately after the call to the MCF loss routine.

Since CH₄, MCF, and radon all have atmospheric loss terms, the global loss in the atmosphere would be a useful quantity for various applications. A new routine was added (tracer_massprint.F90) to print out the atmospheric mass, flux and loss for every tracer every time-step. At the end of every month, the routine prints out the instantaneous global mass and loss for every level.

2.3 Utilizing the model modifications

In order to utilize the changes to ACCESS, some settings for the model must be changed and various flags and user specifications must be added. The Unified Model user interface (UMUI) controls the settings required for each simulation. To perform a simulation, the UMUI is processed and creates job scripts with all the settings. To change the setting manually, the user can use a hand-edit. A hand-edit is a file that contains user-specified changes to the job script files for the UM. To use the hand-edit, it must be included in the user hand-edit files list in the UMUI, which is located in the sub-model independent folder. Each entry in a hand-edit must contain the script that is to be changed followed by the requested changes. This section describes how to set-up and use the changes in ACCESS.

2.3.1 CO₂

To simulate atmospheric CO₂ concentrations, the interactive carbon cycle flag must be active; however, using the UMUI to turn on the carbon cycle requires interactive vegetation and an active ocean model. To override the UMUI, the CO₂ interactive flag (L_CO2_INTERACTIVE) can be turned on using a hand-edit. Once the CO₂ interactive flag is set, the model will automatically use a global constant CO₂ concentration in the radiation scheme, unless the CO₂ radiation flag (L_CO2_RADIATION) is set to true. The radiation flag must be added to a UM job script using a hand edit; however, the value of the constant CO₂ concentration for the radiation scheme can be set in the UMUI. To conserve the mass of the atmospheric CO₂ tracer, the flag controlling the CO₂ mass calculation (L_CO2_MASS) must be defined and set to true in a hand edit.

A list of the specific steps required to use the atmospheric CO₂ tracer in the UMUI is provided in Appendix D. Appendix D also contains a sample hand edit file (co2.ed), which includes the necessary UM job script changes required to turn on the CO₂ interactive cycle and to simulate the CO₂ concentrations resulting from the land surface model CABLE. A second hand edit file in Appendix D (co2_emits.ed) contains the commands required to add CO₂ fluxes from a file into the CO₂ atmospheric tracer. The hand edit files can also be found on cherax in the directory /cs/home/csdar/law181/CorbinLaw_Techrep35/hand_edits.

2.3.2 Atmospheric tracers

Since the tracer options in the UMUI are limited, hand edits are required to utilize the changes to atmospheric tracers. Atmospheric tracers can be turned on using the UMUI; however, to initialize the tracers to values other than the dump concentrations or the concentrations in the environmental tracer file (ATRACER, set in INITHIS), a hand edit is required to modify the reconfiguration job script (RECONA). At the bottom of the job script, each variable that needs to be initialized is added as an individual item entry. For atmospheric tracers with associated surface fluxes, the section is 33 and the items are 1-20. In order to initialize tracers to a concentration distribution from a single ancillary file, the source should be set to five and the USER_PROG_ANCIL_FILE variable should be added and set to the filename. To initialize to zero, the source should be set to three; and to initialize to a constant value, the source should be six and the USER_PROG_RCONST variable should be added and set to the requested concentration.

In order to include tracer fluxes in the model and output, the fluxes need modified information entries to the model output system, which is controlled by the Storage Handling and Diagnostic System (STASH). The STASH system is designed to handle versatile and optional model diagnostic fields for a range of model configurations and applications and to output a variety of requested model variables in a standard format (Barnes, 2008). Although the tracer fluxes are already included in the STASH, they are currently only defined for certain model set-ups. To include the tracer flux variables, a user-defined STASH-master file was created (tracer_fluxes.stash; Appendix E). The file defines each tracer flux (section 3, items 100-119) and provides codes to simulate these fluxes regardless of the model set-up. This STASH file presides over the original STASH-master, and removes the limitations on defining and using tracer fluxes. The STASH-master file can also be found on cherax in the directory /cs/home/csdlaw/law181/CorbinLaw_Techrep35/stash.

To use ancillary files to initialize and update the tracer fluxes, they must be considered user-defined ancillary fields and must have associated user-defined ancillary files. A hand edit is required to add the tracer flux information to the appropriate ancillary lists. The tracer fluxes are added to the list of ancillary fields by adding entries for each flux in the user-defined field job script (UAFIELDS_A), and the associated files are added to the file list by adding entries for every file in the user-defined file job script (UAFIELDS_A). All ancillary fields have reference numbers separate from the model output codes, and all ancillary files have specific file unit numbers. The ancillary reference numbers for the tracer fluxes are 188 through 207, and the file numbers for the flux files are 48 through 67.

Since the tracer fluxes are boundary layer variables rather than prognostic variables, they require being initialized and updated with a hand edit. The fluxes can be initialized to any one of the standard data initialization options for the UM: 1) Input dump, 2) Ancillary file 3) Zero, 4) Missing Data Indicator (MDI) 5) Tracer file 6) Constant 7) External dump and 8) Field Calculations. To initialize the fluxes to a file, in the reconfiguration script (RECONA) add items for each of the fluxes, set the source for each flux item to two, and specify the filename with USER_PROG_ANCIL_FILE. To update the fluxes, the atmospheric control script (CNTLATM) needs to be modified with a hand edit. In the ancillary update list (UPANCA), entries must be added for the tracer fluxes, using their associated ancillary reference number (188-207). In order to update the fluxes from file values, the flux entries must contain the variable FINPUT set to 1 and the variable FNAME set to the file name.

To use the new mass fixer, the atmospheric control script (CNTLATM) needs to be changed to include the new options. In the atmospheric name-list (NLSTCATM), the tracer mass flag must be added and set to true and the tracer number to start using the mass fixer at should also be added and specified. The mass fixer routine will only run on the tracers greater than or equal to this parameter.

To simulate CH₄, MCF, and radon, the options for these tracers must be added to the atmospheric name-list section (NLSTCATM) in the atmospheric control script (CNTLATM). To simulate the atmospheric loss of CH₄, the methane loss flag (L_METHANE_LOSS) must be added and set to true and the number of methane tracers must also be specified (I_METHANE_TRACERS). Methane tracers are assumed to be the first tracers, and the loss is only calculated for the tracers equal to or below the specified methane tracer number. To simulate the atmospheric loss of MCF, the MCF loss flag (L_MCF_LOSS) must be added and set to true and the number of the MCF tracer must also be specified (I_MCF_TRACERNUMBER). Finally, to simulate radon, the radon decay flag (L_RADON_DECAY) must be added and set to true and the number of the radon tracer must be specified (I_RADON_TRACERNUMBER).

To include atmospheric losses, atmospheric files of OH, stratospheric loss rates due to Cl and O¹D, photolysis rates, and ocean loss rates must be specified. All of these variables are combined into a single ancillary file, which is specified in the initial history script (INITHIS) in the variable CHEMOXID. In the STASH, these variables are in section 0, items 122-125. These variables must be included in a user-defined STASH-master file to allow them to be used when the sulphur cycle is not activated (methane_loss.stash; Appendix E). To update these variables, additional entries for these fields must be added to the ancillary update list (UPANCA) in the atmospheric control script (CNTLATM). The fields have ancillary reference numbers of 73-76.

A list of the specific steps required to use the tracers to simulate various CO₂ fluxes as well as CH₄, MCF, and radon is provided in Appendix E. Appendix E also contains sample hand edits files for both simulating tracers with prescribed CO₂ fluxes and with CH₄, radon, MCF, SF₆ and CO₂. The appendix also includes the STASH-master files required for both the tracer fluxes and the chemistry variables (OH, Cl and O¹D loss rates, photolysis loss rates, and ocean deposition rates). All the hand edit and STASH-master files are also available on cherax in the directory /cs/home/csdar/law181/CorbinLaw_Techrep35.

3. ATMOSPHERIC MASS CONSERVATION

Since the carbon cycle and chemistry are key components of ACCESS, it is essential to accurately model atmospheric transport while conserving mass. Investigating the mass of the CO₂ tracer in test simulations indicated that there could be discrepancies between the modelled mass of CO₂ and that expected from prescribed emissions of ten to twenty per cent (Chris Jones, personal communication). Additional simple tests using other atmospheric tracers also indicated that the mass was not being conserved compared with the input fluxes. This section further explores mass conservation of the atmospheric tracers.

3.1 Model simulations

To investigate the mass conservation of atmospheric tracers, the UM model, coupled to MOSES, is run at 3.75° longitude by 2.5° latitude (N48) with 38 levels in an AMIP-style configuration. The simulations start January 1990 and integrate forward for five years. This study focuses on 3-hourly biospheric CO₂ fluxes from CASA (Carnegie-Ames-Stanford Approach biogeochemical model) and fossil fuel CO₂ with constant emissions. Both tracers start from a globally uniform field, with the initial biosphere tracer concentration set to 380 ppm and the fossil tracer concentration set to 0 ppm. The global total mass of the atmosphere, the global total mass of each tracer, and the global mass of the surface fluxes added to the atmosphere was calculated at every time-step.

Results from the simulation indicate that the dry mass of the atmosphere varies on diurnal and longer timescales, causing the CO₂ tracer mass to vary in the same manner. Since the primary focus is to conserve the global mean tracer concentrations relative to the atmospheric dry mass, the tracer mass is divided by the total dry mass to convert the tracers into standard CO₂ mixing ratio units of parts-per-million (ppm).

The global average atmospheric mixing ratios of the two tracers in the UM do not match the change in mixing ratio expected from the surface fluxes (Fig. 3.1). Over the five-year period, both tracer concentrations increase more rapidly than expected from the prescribed fluxes. The biospheric mixing ratio accumulates more than 0.5 ppm in the five years (Fig. 3.1, left). Rather than being constant, the difference between the actual and expected mixing ratio of the biospheric tracer has a seasonal cycle, with the largest differences during the northern hemisphere summer. The fossil tracer has smaller differences between the actual and expected atmospheric mixing ratio, accumulating just over 0.3 ppm after five years (Fig. 3.1, right). The accumulation rate in the UM is more constant in the fossil tracer, with only small seasonalities in the differences.

To determine where the UM is not conserving mass, the CO₂ mass was calculated at various stages in the time-step from four week-long simulations starting on March 1, June 1, September 1, and December 1. It should be noted that this analysis is complicated because the tracer mass calculation requires the moisture fields, which are updated at different points in the time-step than the atmospheric tracers. The convection processes and the emission of the flux into the atmosphere caused approximately half of the mass discrepancies, with the relative contributions varying throughout the year. In May, September, and December 20-40 per cent of the mass accumulation occurred when the flux was emitted into the atmosphere, while 10-30 per cent occurred during convection; however, in June convection caused tracer mass loss and the emissions accounted for 70 per cent of the mass gain. The remaining half of the mass gain occurred from other subroutines, including the semi-Lagrangian tracer advection (despite using any available UM options to promote tracer conservation).

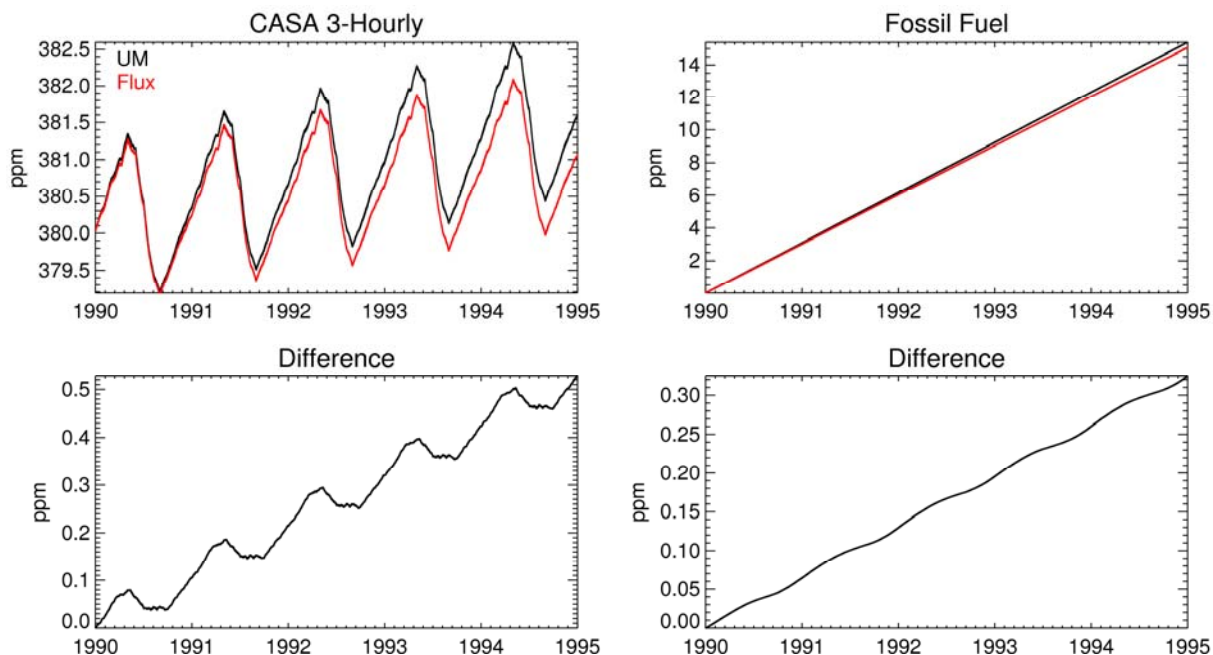


Fig. 3.1 (Top Left) Global atmospheric CO₂ mixing ratio for the CASA 3-hour tracer in the UM (black line) and the expected atmospheric CO₂ mixing ratio from the surface fluxes (red line). (Bottom Left) The difference between modelled and expected CO₂ mixing ratio for the CASA 3-hour tracer. (Top Right) Modelled and expected CO₂ mixing ratio from the fossil fuel tracer. (Bottom Right) Corresponding difference for the fossil fuel tracer.

Since there were several causes of error to the mass conservation that seasonally varied, we put in a simple mass fixer subroutine. The routine determines the tracer mass and the expected mass from the emissions, converts these to mixing ratios by dividing by the dry atmospheric mass, and calculates a scaling factor equal to the ratio of the expected and actual mixing ratios. To conserve mass, the routine rescales the atmospheric tracer mixing ratios to match the expected mixing ratios from the emissions. The code for the mass fixer subroutine is included in Appendix C. To evaluate the mass fixer, we perform the five-year simulation using the mass fixer and analyse the results from the last three years.

3.2 Simple tracer mass fix results

Using the simple mass fixer significantly improves the mass conservation in both the biospheric and fossil tracers, with small differences (< 0.002 ppm) between the actual and expected mixing ratios (Fig. 3.2). The biospheric tracer has some temporal variability in the mass differences; however, the errors remain small and unbiased. The difference between actual and expected mixing ratio in the fossil tracer increases with time, but remains two orders of magnitude smaller than the biospheric tracer differences. The mixing ratio errors may be smaller in the fossil tracer due to the initial background of 0 ppm, rather than 380 ppm and due to constant emissions, rather than diurnally varying fluxes. Both tracers conserve mass reasonably well, with minimal errors that may be due to computational precision.

Forcing mass conservation alters the atmospheric tracer CO₂ fields. Figure 3.3 shows the annual mean tracer concentrations and the differences due to mass conservation. The majority of the biospheric tracer CO₂ differences from conserving mass are small (< 0.5 ppm); however, differences of more than 2 ppm occur in some individual grid cells where the concentrations are high. The background biospheric CO₂ concentration

is lower in the mass fix run, due to the elimination of the spurious additional mass. Tropical land has higher annual mean concentrations when mass is conserved, while the subtropics and mid-latitudes have lower annual mean concentrations.

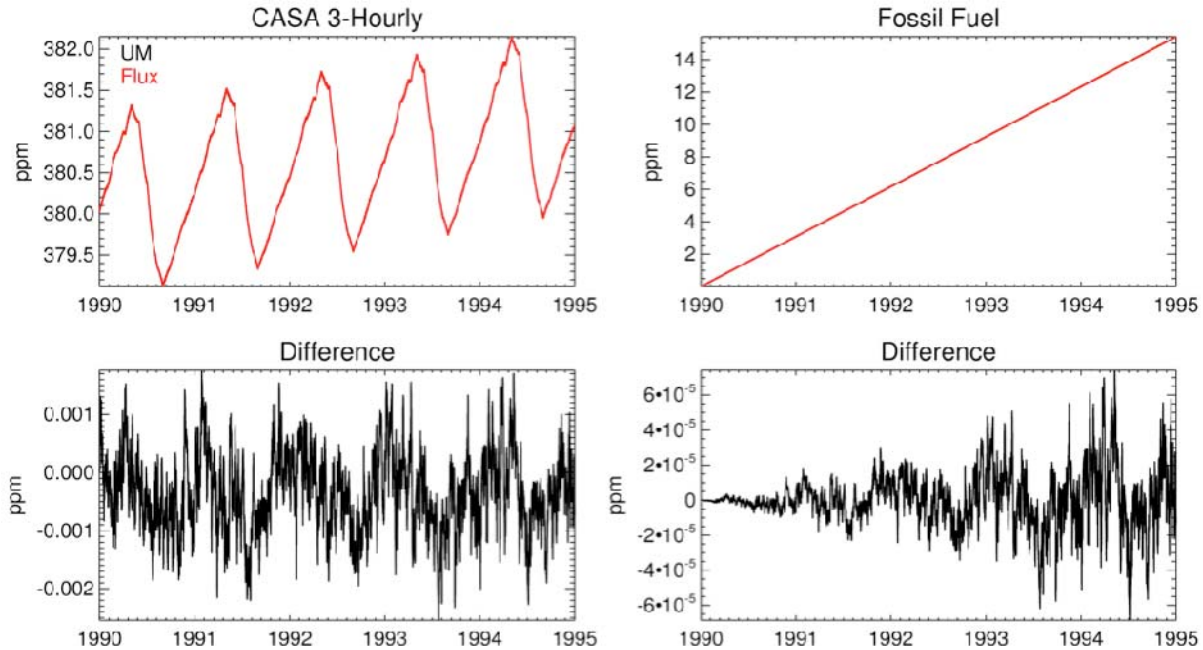


Fig. 3.2 (Top Left) Global atmospheric CO₂ mixing ratio for the CASA 3-hour tracer in the UM with the mass fixer (black line) and the expected atmospheric CO₂ mixing ratio from the surface fluxes (red line). (Bottom Left) The difference between modelled and expected CO₂ mixing ratio for the CASA 3-hour tracer. (Top Right) Modelled and expected CO₂ mixing ratio with the mass fixer for the fossil fuel tracer. (Bottom Right) Corresponding difference for the fossil fuel tracer.

The lower background concentrations can clearly be seen in the zonal-mean biospheric CO₂ concentrations (Fig. 3.4, left). Conserving mass lowers the concentrations by ~ 0.4 ppm, which is consistent with the amount of mass spuriously added in the original simulation. Despite the concentration shift, the zonal distribution remains similar between the two simulations, indicating that the spatial differences have minimal impact on the overall behaviour of the tracer.

The fossil tracer CO₂ differences due to mass conservation are minimal except near cities with high fossil fuel emissions, which is expected since the changes are scaled by the concentrations (Fig. 3.3, bottom). Over Europe and North America the CO₂ concentrations are lower when the mass is conserved, while the concentrations are higher over China and Japan. Similar to the biospheric flux, conserving mass has a minimal impact on the annual mean zonally averaged concentrations (Fig. 3.4, right).

To investigate the seasonality of the mass conservation impact, Fig. 3.5 shows the inter-hemispheric difference in fossil CO₂ sampled at marine boundary layer sites. Both simulations have inter-hemispheric differences similar to other model simulations. Conserving mass slightly increases the fossil inter-hemispheric difference in February and decreases it in July through September. While the monthly inter-hemispheric difference changes slightly, conserving mass does not significantly impact the global distribution of the fossil tracer.

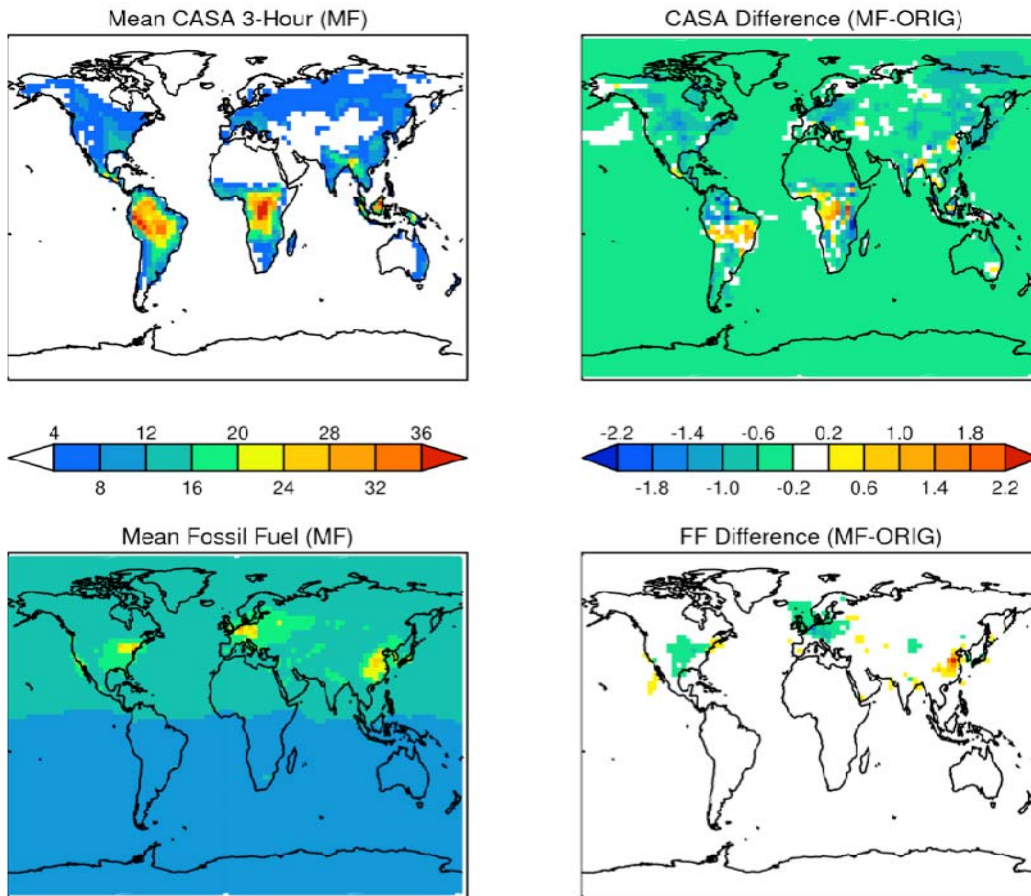


Fig. 3.3 Top Left) Annual mean biospheric CO₂ tracer concentrations in the mass conserving simulation. The background concentration of 380 ppm has been removed. Top Right) Annual mean biospheric CO₂ tracer differences between the simulation with the mass fixer and the original simulation (mass fixer simulation minus original). Bottom Left) Annual mean fossil fuel tracer concentrations in the mass conserving simulation. Bottom Right) Annual mean fossil fuel tracer differences between the simulation with the mass fixer and the original simulation.

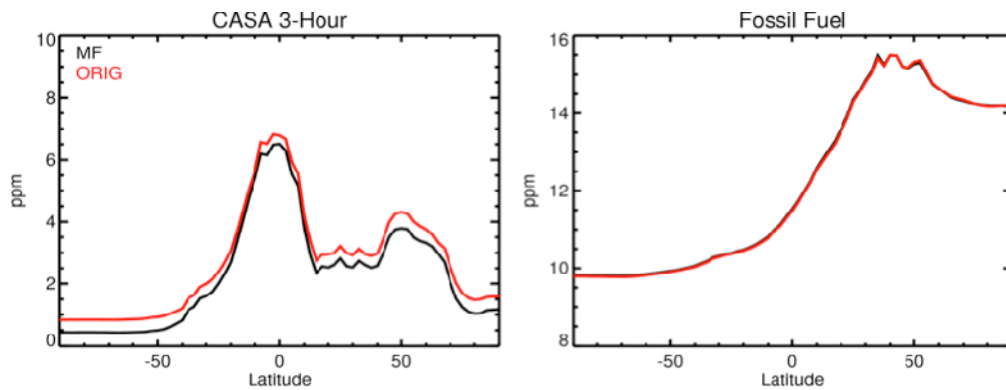


Fig. 3.4 Left) Annual mean zonal-averaged biospheric CO₂ concentrations for the mass conserving (black) and the original (red) simulation. Right) Annual mean zonal-averaged fossil fuel.

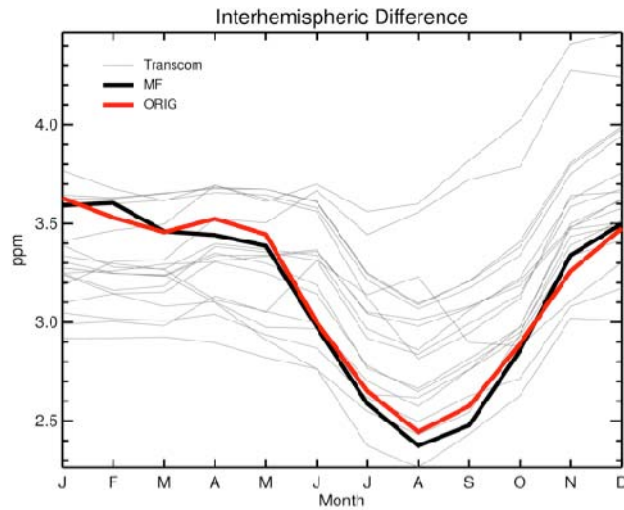


Fig. 3.5 Seasonal cycle of the inter-hemispheric difference in fossil CO₂, calculated by subtracting monthly hemispheric concentrations using a spline fit to marine boundary layer sites. The gray lines indicate results from the fossil flux in other model simulations (from the TransCom-continuous experiment, Law et al. 2008).

3.3 Mass conservation conclusions

Without a mass fixing routine, the UM was not conserving mass in the atmospheric tracers. Errors between actual and expected atmospheric mass occurred from emitting the tracer fluxes into the atmosphere, convection, and various other subroutines. To conserve mass, a simple mass fixer was implemented, which re-scales the tracer concentrations to the expected mixing ratios. Despite differences at individual grid cells, conserving mass did not alter the overall global distribution of the tracers.

A major application of ACCESS is to run coupled climate-carbon simulations. In these cases CO₂ fluxes are calculated by the land-surface scheme (CABLE) and the ocean carbon model and will vary at the temporal resolution of the simulation. With no mass fixer, this implies that substantial mass gain (or loss) could occur over century time-scales, with consequent implications for global mean CO₂ concentration and the radiative forcing associated with that CO₂.

Further work could be undertaken to investigate the tracer mass conservation of different sections of the code in more detail, but we do not see this as a high priority. Implementing an explicit mass fixer, at least for optional use, does appear to be necessary. Whether the simple scheme tested here is sufficient or a more sophisticated fixer is needed, may require further investigation and discussion with other potential users.

4. ASSESSING THE IMPACT OF MODEL SETUP AND BOUNDARY LAYER PARAMETERIZATION ON ATMOSPHERIC TRANSPORT IN ACCESS

The TransCom model comparisons provide a useful set of standard experiments that can be used to evaluate model transport and compare with results from other models. Since the UM had not participated in TransCom, Law and Corbin (2010, L10) used prescribed carbon and SF₆ fluxes from the most recent TransCom experiment to understand the characteristics of CO₂ and SF₆ transport in the UM model before MOSES was replaced by CABLE. The results from L10 suggest that inter-hemispheric mixing is slower in the UM than for other models; and simulations with various stable boundary layer parameterizations showed that near-surface mixing at continental sites is very sensitive to the choice of boundary layer scheme.

This chapter expands the work of L10 by using atmospheric CO₂ concentrations to evaluate the UK Met Office Unified Model (UM) version 7.3 coupled to CABLE. The following sections outline the model simulations and results. The near-surface concentration differences caused from the two different land surface models and from two different horizontal resolutions are assessed, and the sensitivity of atmospheric concentrations to the stable boundary layer scheme is investigated.

4.1 Model simulations

The original simulations in L10 use the UM version 6.3 coupled to MOSES. To investigate the impact of upgrading the atmospheric model version, switching land surface models, and increasing horizontal resolution, the experiments performed in L10 are repeated with various model configurations. Since CABLE is coupled to the UM version 7.3, simulations with two different configurations are performed to separately diagnose the impacts of changing model version and changing the land surface scheme. The first configuration uses the UM version 7.3 coupled to MOSES, and the second configuration couples the UM (7.3) to CABLE. Both of these configurations are run at N48 resolution (3.75° longitude by 2.5° latitude). To test the sensitivity to the model grid spacing, the second configuration (UM coupled to CABLE) is also run at N96 horizontal resolution (1.8° longitude x 1.25° latitude). All the simulations use 38 levels with prescribed sea surface temperatures (SSTs), similar to the AMIP simulations. Since ACCESS is only forced with monthly mean sea surface temperatures, the comparisons focus on annual, seasonal and diurnal time-scales. Comparisons of synoptic variations would require the model to be nudged to analysed meteorological fields or run in a forecast mode.

For each model configuration, five-year simulations are performed starting January 1990, and the results presented in this chapter are means from the last three years. Five trace gases are simulated: biospheric CO₂ using CASA monthly mean and diurnally varying fluxes, ocean CO₂, fossil CO₂ and SF₆. The input flux fields are those used in the TC-cont experiment and are described in L08. To test the sensitivity to the stable boundary layer parameterization, three different schemes are used: sharpest (S), long-tailed (LT), and a hybrid (LT land) scheme with the sharpest function over the ocean and the long-tailed function over the land. L10 discusses these functions in more detail.

4.2 Annual mean CO₂ concentrations

The near-surface annual mean CO₂ concentrations from all the model configurations at N48 resolution are displayed in Fig. 4.1. The total CO₂ concentrations shown are the sum of the contributions from the diurnally varying land fluxes, the ocean fluxes and the fossil fuel emissions. In all cases, the concentrations are higher

over land, due to both the fossil emissions and the biospheric fluxes. The highest concentrations occur in the tropics and over heavily populated regions. The concentrations over the ocean are lower, with differences of more than forty ppm between the ocean and the largest land concentrations.

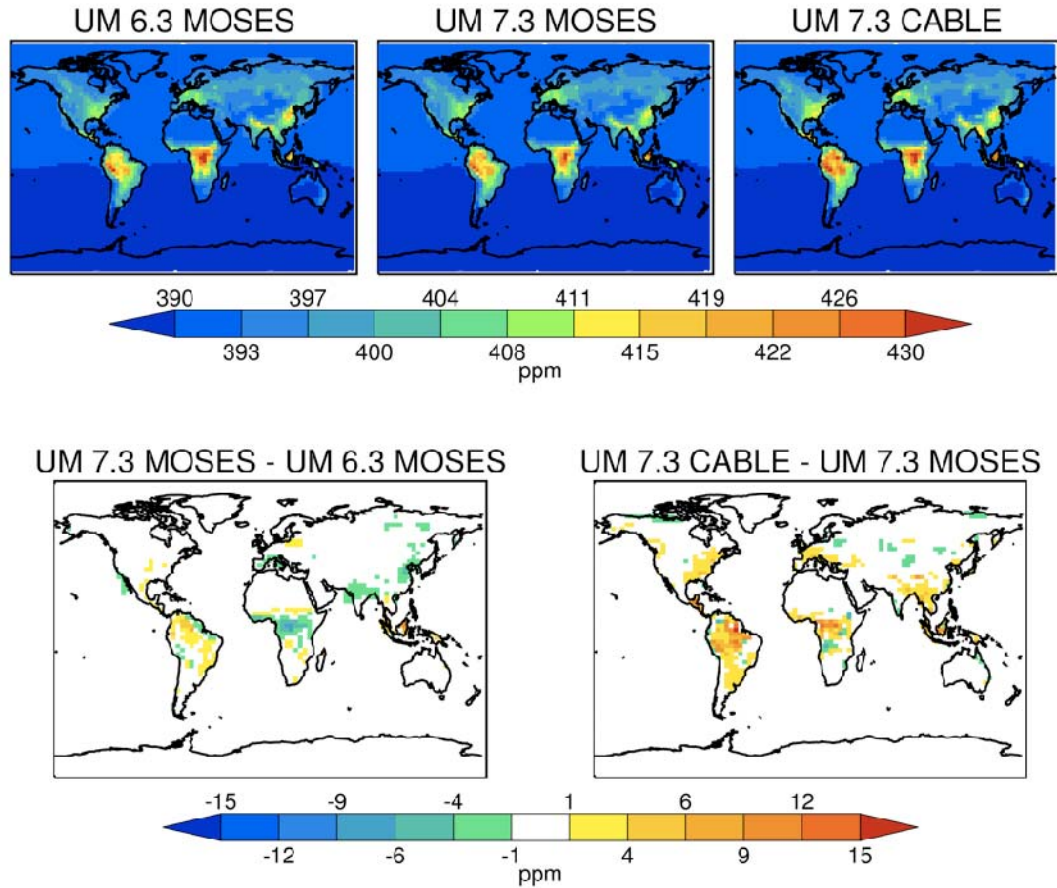


Fig. 4.1 Annual mean total CO₂ concentrations at 20 m, using the hybrid stable boundary layer scheme. The mean concentrations are calculated by adding the biospheric (diurnally varying), ocean and fossil contributions and averaging the concentrations over the last three years. Top Left) UM version 6.3 with MOSES. Top Centre) UM version 7.3 with MOSES. Top Right) UM version 7.3 with CABLE. Bottom Left) Difference due to changing the model version (UM 7.3 MOSES minus UM 6.3 MOSES). Bottom Right) Difference due to changing the land surface model (UM 7.3 CABLE minus UM 7.3 MOSES).

The differences due to changing model version are smaller than the differences due to changing the land surface model, as switching from MOSES to CABLE alters the concentrations more than 10 ppm in some individual grid cells. Updating the model version increases the concentrations in South America but decreases the concentrations in tropical Africa and Asia. Switching from MOSES to CABLE primarily increases the concentrations over land, particularly in the tropics and in the northern latitudes where the biospheric fluxes are larger. Over the oceans, changes in concentration due to the model version upgrade or land surface model switch are negligible.

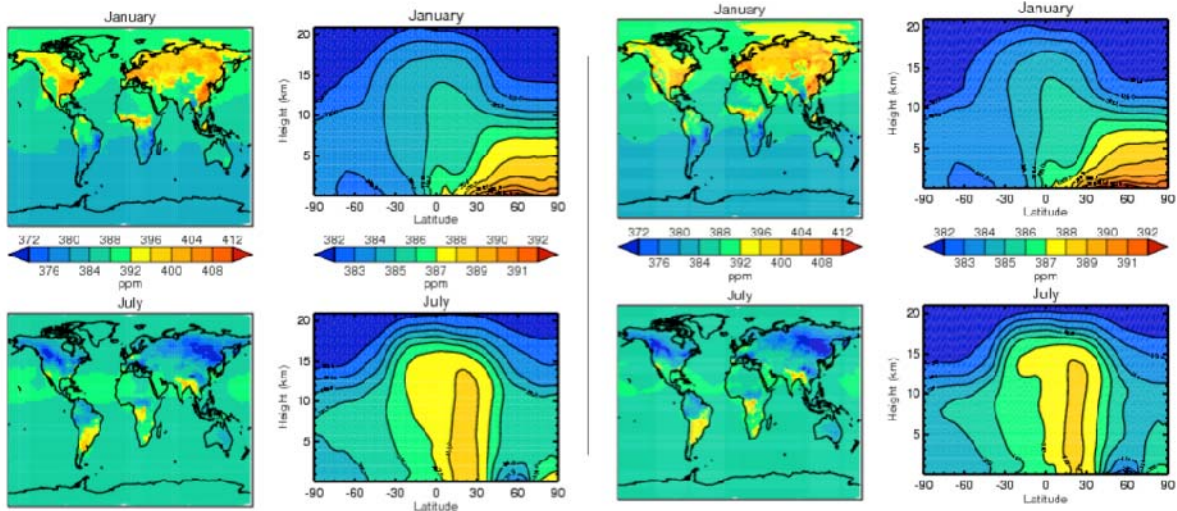


Fig. 4.2 Maps of mean CO₂ concentrations at 20 m from the N48 simulation (left four panels) and the N96 simulation (right four panels). The CO₂ concentrations are the sum of the biospheric fluxes (monthly varying), ocean fluxes and fossil fuel emissions. The results shown use the LT boundary layer scheme. Far left column) Mean total CO₂ concentrations from the N48 simulation with CABLE for January (top) and July (bottom). Middle left column) Zonal mean vertical distribution of the total CO₂ concentrations from the N48 CABLE simulation during January (top) and July (bottom). Middle right column) Mean total CO₂ concentrations from the N96 CABLE simulation. Far right column) Zonal mean vertical distribution of the total CO₂ concentrations from the N96 CABLE simulation.

To investigate the impact of using a higher spatial resolution, Fig. 4.2 shows the mean January and July CO₂ distributions and zonal mean vertical profiles using N48 (left) and N96 (right) horizontal resolutions. In January, the CO₂ concentrations in the NH are high, particularly over the land, and the concentrations are lower in the SH. Both resolutions show these dominant features. The differences between the N48 and N96 simulations are minimal, with perhaps slightly lower concentrations in the N48 simulation over western North America and central Asia. In July, the concentrations over the NH are low, particularly over the land due to the photosynthetic drawdown during the summer. The concentrations using N48 resolution are slightly lower in the tropics compared with the N96 results; however, the differences between the two simulations are small. The zonal mean CO₂ vertical profiles from both N48 and N96 are quite similar as well. In January, the high near-surface concentrations in the NH and the north-south gradient are clearly visible in both simulations. In July, the concentrations are higher in the tropics and lower in the higher latitudes. The near-surface concentrations in the NH are slightly higher in the N48 simulation and the profile over the tropics differs slightly between the two simulations.

Isolating the fossil concentrations, Fig. 4.3 shows annual mean near-surface fossil concentrations for all three model configurations at N48 resolution. Following L08, to calculate the annual mean inter-hemispheric gradient (Fig. 4.3, top), the model is sampled at a select number of marine boundary layer (MBL) sites and the annual mean concentrations at the sites are fit with a spline function. As expected, the fossil concentrations are higher in the northern hemisphere, where the majority of the fossil fuel CO₂ is emitted. The model simulations all have inter-hemispheric gradients of ~5-6 ppm, which falls within the range seen in the TransCom models. The UM version 6.3 with MOSES has the largest inter-hemispheric gradient, while the UM version 7.3 with CABLE has the smallest gradient.

The inter-hemispheric gradient is calculated separately for each month, and the resulting monthly gradients are displayed in Fig. 4.3 (bottom). All UM simulations have high inter-hemispheric gradients January

through April compared to the TransCom range. The larger gradients suggest that the inter-hemispheric transport in the UM is too slow and that the boundary layers are too shallow, leading to too much trapping of the high CO₂ near the surface in the northern hemisphere winter.

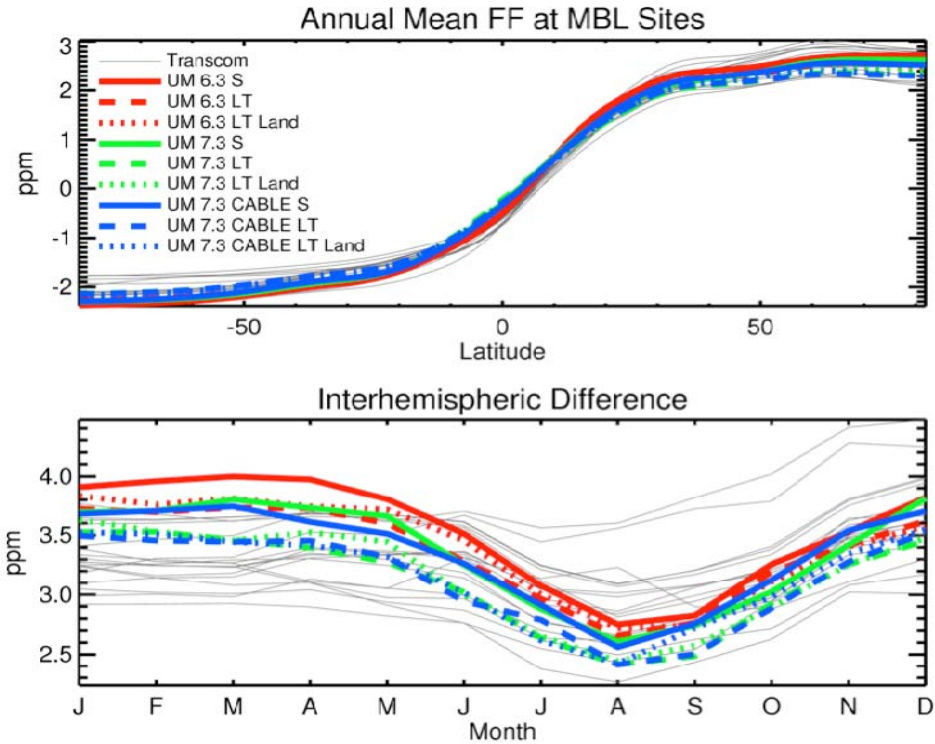


Fig. 4.3 Fossil CO₂ concentrations from 20 m sampled at marine boundary layer (MBL) sites. Grey lines indicate TransCom results. Coloured lines indicate UM results. Red is UM 6.3 MOSES, green is UM 7.3 MOSES, blue is UM 7.3 CABLE, with all simulations using N48 resolution. Different line styles indicate different boundary layer schemes. Solid is sharpest scheme, dashed is long-tailed scheme, and dotted is hybrid long-tails over land. Top) Annual mean inter-hemispheric gradient, from splines fit to annual mean MBL concentrations. Bottom) Monthly inter-hemispheric gradients, from splines fit to the monthly-mean MBL concentrations.

The gradients are lower with the new UM version 7.3 than the UM version 6.3, falling closer to the TransCom range in DJF and within the TransCom range in JJA. Using the UM version 7.3 decreases the north-south gradient, and using CABLE further lowers the inter-hemispheric difference. The gradient is sensitive to the stable boundary layer scheme for all model setups, with the highest gradients occurring with the sharpest scheme and the lowest concentrations occurring with the long tails scheme. Since the long tails scheme lowers the inter-hemispheric difference, it more closely matches the TransCom results.

Using a higher spatial resolution increases the inter-hemispheric difference (Fig. 4.4). The annual mean north-south gradient is larger when N96 resolution is used, with lower concentrations in the southern hemisphere (SH). It should be noted that only a select number of sites are being sampled, so a single site could have a significant impact, and these sites are expected to reflect base-line concentrations. The increased concentration in the SH seen in the N96 simulations is caused by the grid-point selected for Cape Grim being influenced by land rather than reflecting base-line concentrations; however, a comparison of zonal mean concentrations using all grid cells yields the same overall results: the inter-hemispheric gradient is larger in the N96 simulation than using N48 resolution. Looking at the monthly mean inter-hemispheric

differences, the N96 simulations have larger gradients all months, but are particularly higher during the NH winter (DJF). The N96 simulation shows the same sensitivity to the boundary layer scheme, with the highest gradients resulting from the sharpest scheme and the long-tail scheme most closely matching the TransCom models.

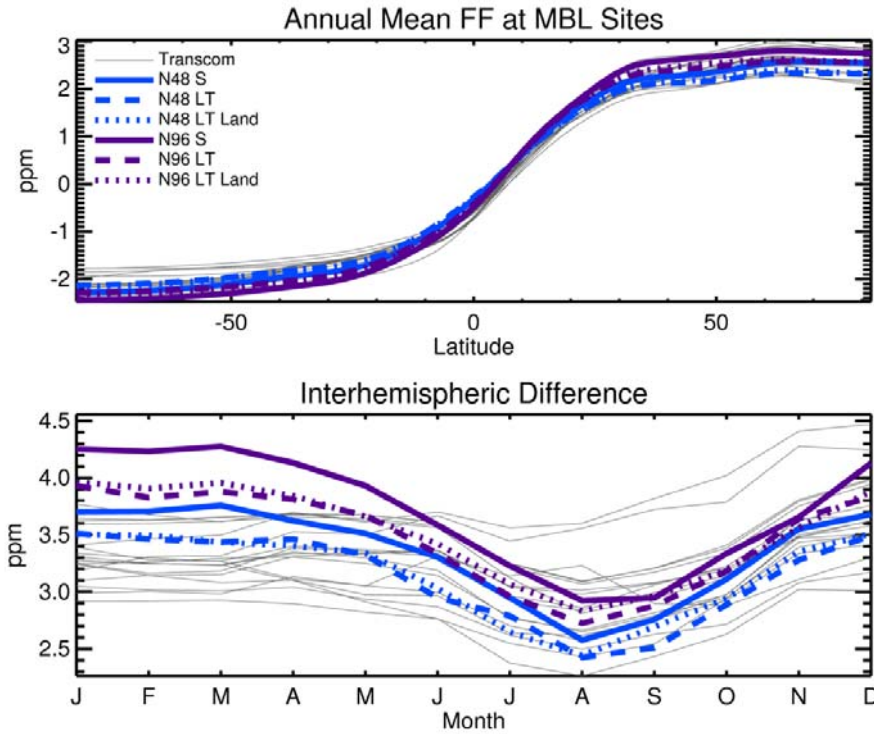


Fig. 4.4 Fossil CO₂ concentrations at 20 m sampled at MBL sites for the UM 7.3 CABLE N48 simulations (blue, same as in Fig 4.3) and UM 7.3 CABLE N96 simulations (purple). Three sites (CPTOCN, BHDOCN, and MHDOCN) are not included in this figure because the N96 time-series does not reflect base-line conditions at these locations.

4.3 Seasonal cycle

Since the seasonal cycle of atmospheric CO₂ concentrations is well understood, it is a useful metric to evaluate model transport. Seasonal cycles of CO₂ at select locations are displayed in Fig. 4.5. The seasonal cycle is large at the northern hemisphere sites (Fig. 4.5, top), with high concentrations in the winter due to a net biospheric source from respiration and low concentrations in the summer from photosynthesis. All N48 simulations with the UM model capture the amplitude of the seasonal cycle in the northern hemisphere relatively well, with minimal differences between all the cases. At Barrow, the UM more closely matches the timing of the low summertime concentrations than the majority of the TransCom models; however, all three setups of the UM tend to underestimate the summer drawdown during August and September. At LEF, ACCESS underestimates the amplitude of the seasonal cycle, underestimating both the winter flux and the summer drawdown at this site; however, it captures the timing of the seasonal cycle and lies within the range of the other TransCom models.

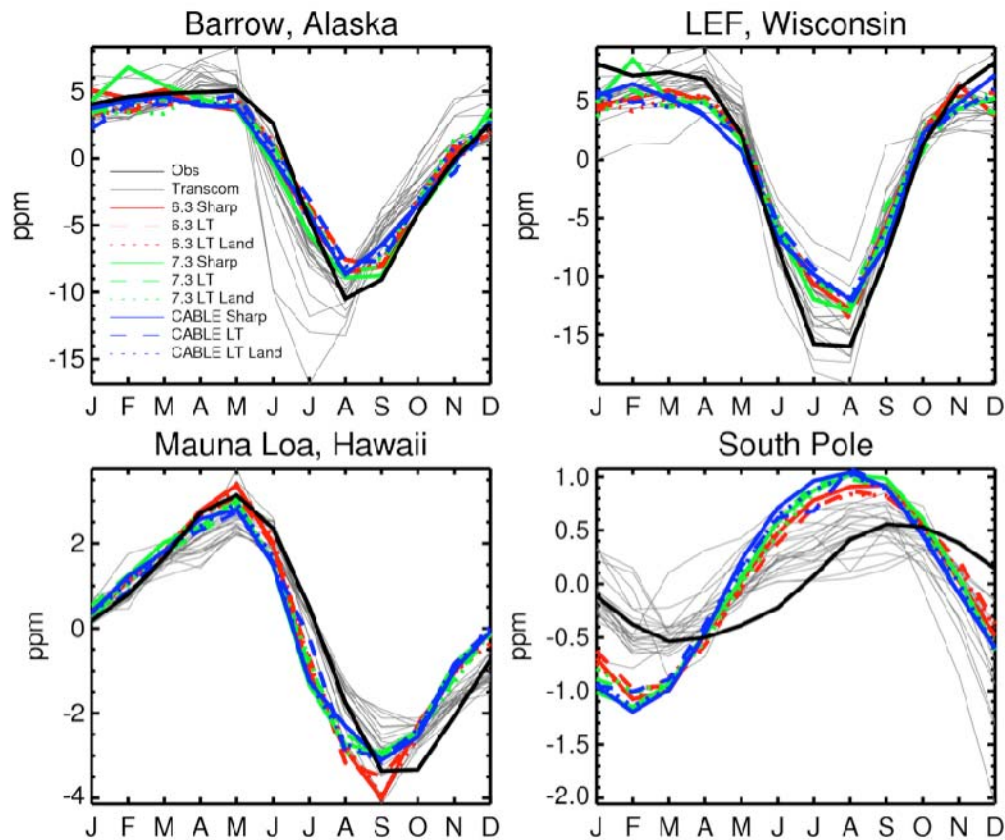


Fig. 4.5 Total CO₂ seasonal cycles at selected observation sites. All the data were de-trended to remove the growth over time. Model concentrations include the contributions from biospheric (diurnally varying), fossil and ocean fluxes. The model is sampled at the grid cell that includes the observation location and at the closest vertical level to the sampling height. Black lines indicate the observations, which are from GLOBALVIEW-CO₂ (2009) and are based on quasi-continuous samples.

Both the amplitude and timing of the seasonal cycle change at lower latitudes (Fig. 4.5, bottom). At the remote ocean site over Mauna Loa, ACCESS does a reasonable job matching the observed seasonal cycle, accurately simulating the amplitude and the maximum concentrations, but shifting the timing of the minimum concentrations slightly. Over the South Pole, both the TransCom models and ACCESS overestimate the amplitude of the seasonal cycle. ACCESS also shifts the timing of the minimum and maximum concentrations earlier in the year than observed.

Looking at the results using N96 resolution (Fig. 4.6), the seasonal cycles at all four selected sites are very similar to the results using N48. The northern NH sites both show minimal changes between the N48 and N96 simulations. The changes are slightly larger for the tropical and SH site. At Mauna Loa, the N96 simulations produce slightly larger amplitudes in the seasonal cycle and shift the timing of the minimum slightly earlier. At the South Pole, the amplitude of the seasonal cycle remains the same between the two cases, but the maximum concentrations are shifted slightly later in the N96 simulations. As with all the N48 cases, at the four remote sites the boundary layer scheme has a minimal impact on the mean seasonal cycle.

To further investigate the seasonal cycle, the zonal mean of the peak-to-peak amplitudes (maximum minus minimum monthly concentration) are displayed in Fig. 4.7. As expected, the amplitude of the seasonal cycle is large in the mid and high northern hemisphere latitudes and decreases to minimal seasonality at the South Pole.

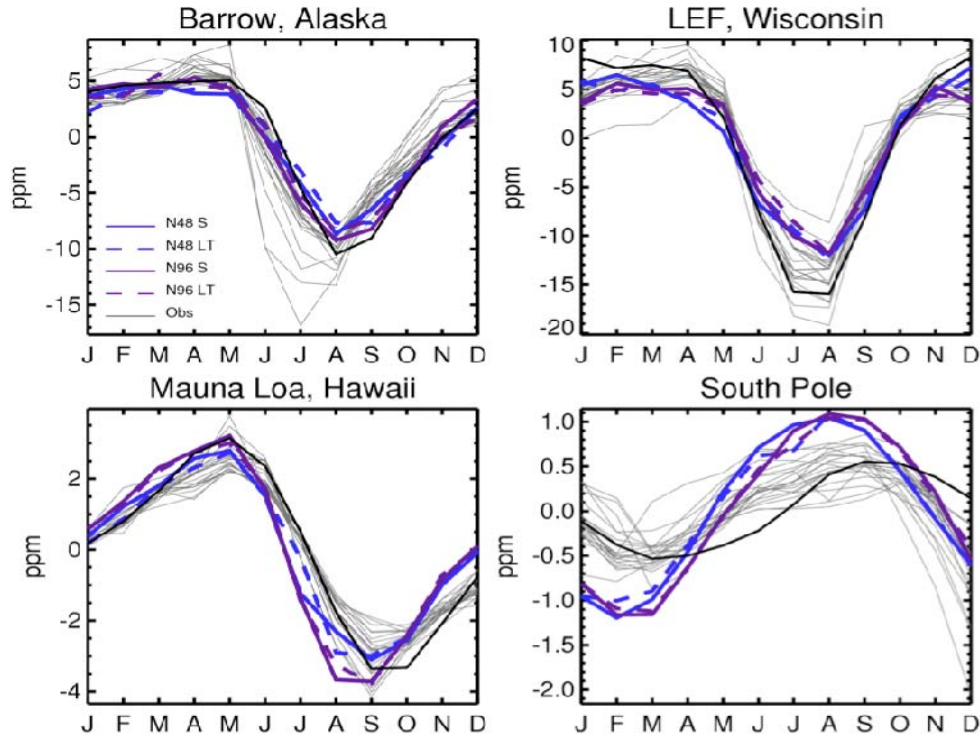


Fig. 4.6 Total CO₂ seasonal cycles at selected observation sites for the UM 7.3 CABLE N48 simulations (blue, same as Fig. 4.5) and UM 7.3 CABLE N96 simulations (purple).

Updating the UM version to 7.3 slightly lowers the amplitudes, particularly in the northern hemisphere, and coupling CABLE to the UM causes an additional slight lowering in the seasonal cycle amplitudes. All model setups are sensitive to choice of stable boundary layer, with the sharpest scheme overestimating the amplitude of the seasonal cycle in the northern hemisphere compared with the TransCom models. Using the long tail scheme over land significantly lowers the amplitude, and the concentrations lie within the spread of TransCom models. Using the long tail scheme everywhere, rather than just over land, further lowers the amplitude of the seasonal cycle in the mid and high northern latitudes in the UM coupled to CABLE. All UM cases overestimate the seasonal cycle amplitudes over the tropics compared to other models, but it is difficult to judge which better represents reality, since tropical CO₂ observations are sparse, especially for land regions.

Using higher spatial resolution does not significantly alter the mean seasonal cycle amplitudes (Fig. 4.8). With the sharpest scheme, the amplitudes in the NH are slightly lower using N96 rather than N48. Rather than model configuration altering the seasonal cycle amplitudes, the largest changes in seasonal cycle amplitude between the different simulations are due to the stable boundary layer parameterization. Similar to the N48 cases, using the long tail scheme with N96 horizontal resolution reduces the seasonal cycle amplitude in the NH; however, the reduction in amplitude is less with N96 than for N48.

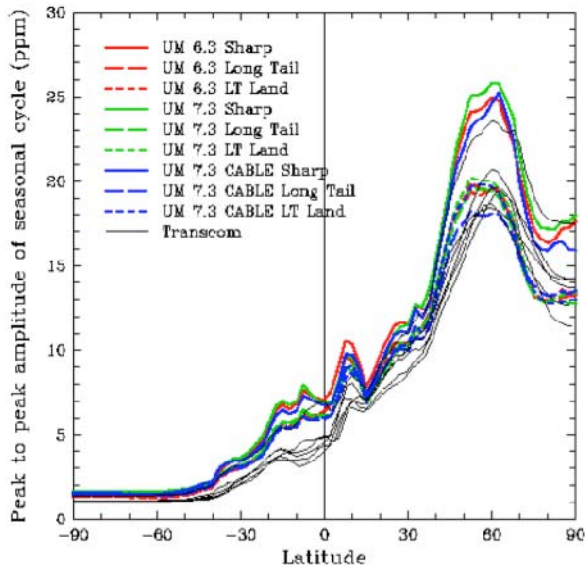


Fig. 4.7 Zonally averaged peak-to-peak amplitude of the seasonal cycle from the biospheric CO₂ fluxes (monthly) for all the N48 configurations.

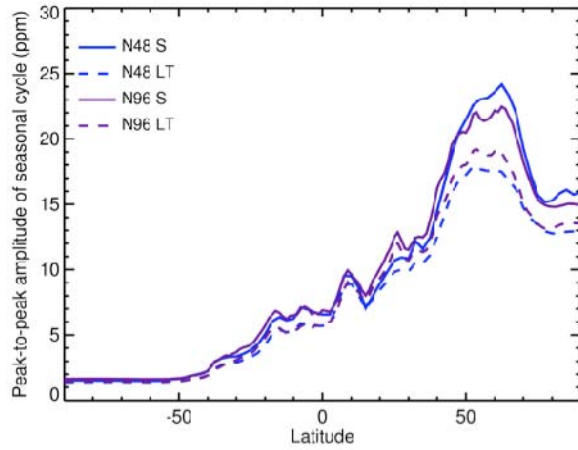


Fig. 4.8 Zonally averaged peak-to-peak amplitude of the seasonal cycle from the biospheric CO₂ fluxes (monthly) for the UM 7.3 CABLE N48 simulations (blue, same as Figure 4.7) and UM 7.3 CABLE N96 simulations (purple).

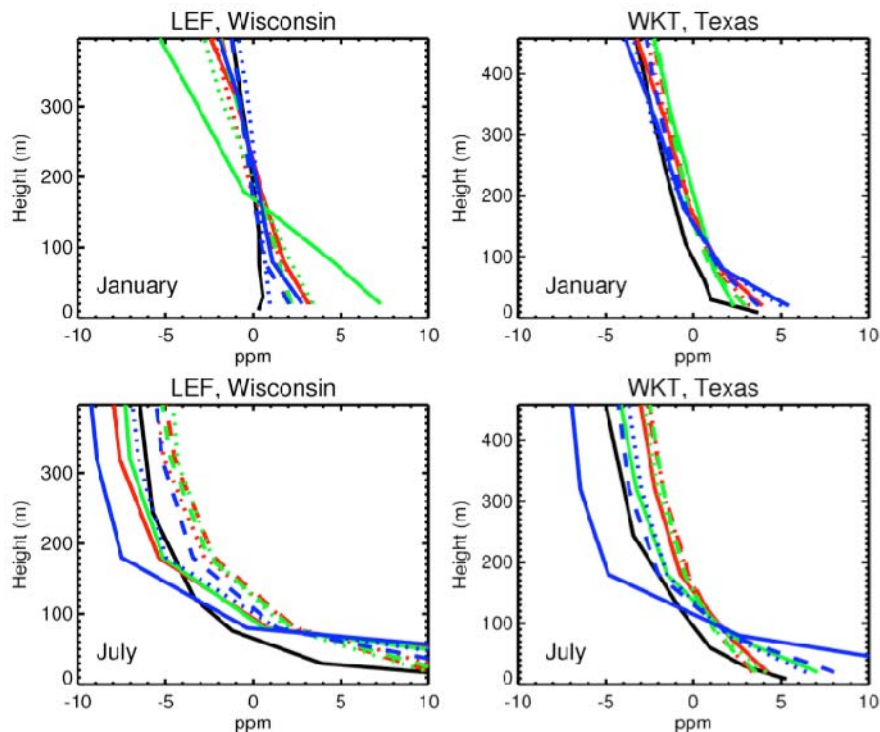


Fig. 4.9 Vertical profiles of monthly-mean CO₂ concentrations at two tall towers in the USA. The monthly mean concentration has been removed from all plots to highlight the vertical gradients. The LEF tower (left) extends up to 396 m and the WKT tower (right) extends up to 500 m. The model is sampled from the grid cell including the tower and at the bottom five vertical levels. Top Left) January profiles at LEF. Bottom Left) July profiles at LEF. Top Right) January profiles at WKT. Bottom Right) July profiles at WKT. The black lines indicate the observations and the coloured lines show the model results (same colours/styles as Fig. 4.4).

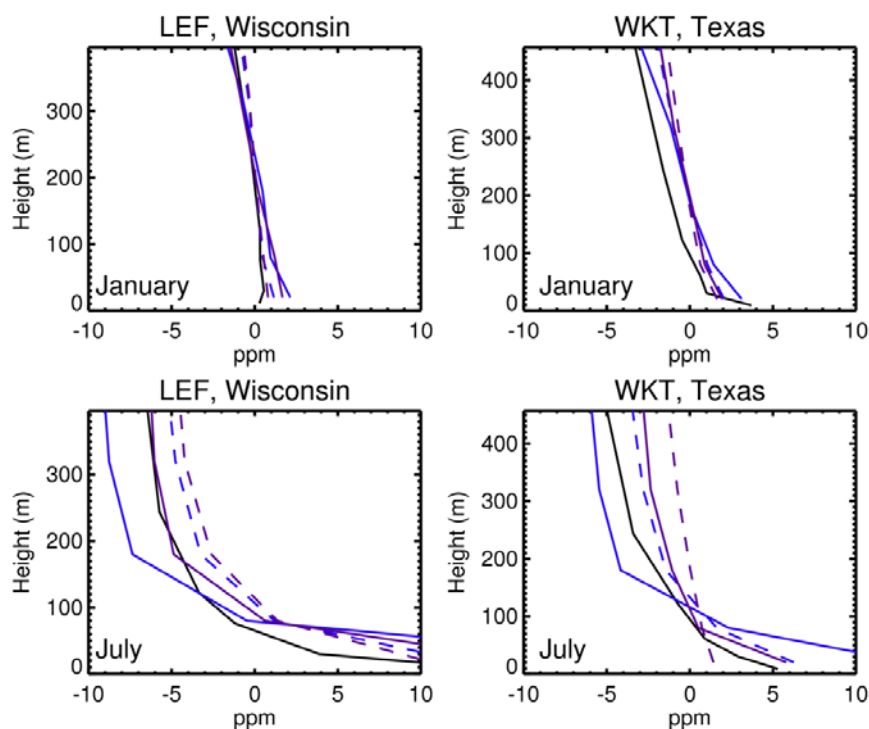


Fig. 4.10 Vertical profiles of monthly-mean CO₂ concentrations at two tall towers in the USA for the UM 7.3 CABLE N48 simulations (blue, same as Fig. 4.9) and UM 7.3 CABLE N96 simulations (purple).

In addition to varying with latitude, the seasonal cycle varies with height from the surface, particularly over continental sites with high surface fluxes. Monthly-mean total CO₂ profiles (with contributions from diurnally varying biospheric fluxes, fossil fluxes and ocean fluxes) at two tall towers in the USA are displayed in Fig. 4.9. At LEF, the UM overestimates the winter vertical gradient, particularly with the UM version 7.3 coupled to MOSES with the sharpest scheme. In the simulation with MOSES using the sharpest scheme, the concentrations in the lowest model level are more than 4 ppm greater than the near-surface concentrations from the other simulations, causing the large vertical gradient. In all model setups, the long tail scheme decreases the vertical gradient, with the UM coupled to CABLE using the long tails scheme most closely matching the tower observations. In the summer, the mean vertical gradient is much larger, with high concentrations near the surface and lower, relatively stable concentrations above approximately 100 m. The near-surface concentrations are high due to the diurnal rectifier effect, which describes the interaction between boundary layer depth and the surface fluxes. CO₂ sources at night typically mix into a much shallower boundary layer than do the CO₂ sinks during the day. This leads to a daily mean concentration that is higher at the surface than aloft despite the net CO₂ flux in summer being a sink. All cases capture the overall shape of the gradient; however, the gradient is sensitive to both model setup and the stable boundary layer parameterization. Using CABLE has the largest vertical gradient, with higher concentrations near the surface and lower concentrations above 100 m. Both versions of the UM with MOSES behave similarly, more closely matching the gradient than the UM coupled to CABLE. Switching to the long tail scheme decreases the vertical gradient. Using the long tail scheme with CABLE more closely matches the observations; however, using the long tail schemes with MOSES overestimates the concentrations above 100 m, with the observations lying between the long tail and sharpest results with MOSES. At the WKT tower in

Texas, which is an agricultural/grassland site, the concentrations are high near the surface and decrease with height during both the winter and summer. All cases perform similarly in January. In July, using CABLE with the sharpest scheme overestimates the vertical gradient, while using CABLE with the long tail scheme over land most closely matches the observations.

The vertical profiles for the N48 and N96 cases with CABLE are displayed in Fig. 4.10. In January the simulations are very similar, with a minimal vertical gradient at both sites. In July, the vertical gradients using N96 resolution are less than the N48 simulations. As with the N48 cases, N96 using the long tail scheme reduces the vertical gradient, resulting in an underestimation of the decrease in concentration with height compared to the observations in July.

4.4 Diurnal cycle

Continental atmospheric CO₂ concentrations near the surface have a strong diurnal cycle. Since photosynthesis requires sunlight but respiration does not, the biosphere is a source of CO₂ to the atmosphere at night and a sink of CO₂ during the day. This diurnal cycle of fluxes, combined with diurnal variations in atmospheric mixing, leads to significant diurnal cycles in atmospheric CO₂ over land. Modelled diurnal cycles can be compared against continuous observations at a variety of sites and atmospheric heights, but it should be noted that these comparisons assume that the input fluxes are correct and that the differences are primarily due to model transport.

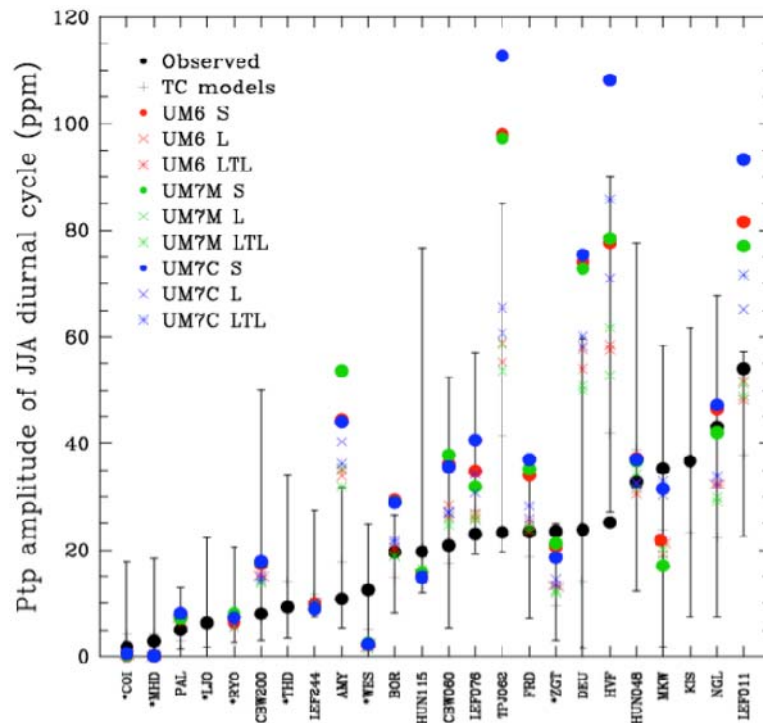


Fig. 4.11 Peak-to-peak amplitude of the mean JJA (June, July, August) diurnal cycle for observed 2002 CO₂ (black dot), TransCom models for 2002 (error bar shows minimum, maximum and median model) and the UM N48 cases. The model amplitudes are calculated from the sum of concentrations from biospheric (diurnally varying), fossil and ocean emissions. Sites are listed on the x-axis and their locations are shown in Table 4.1. CBW, LEF, HUN, and TPJ are sampled at various vertical levels, which are specified in meters. The asterisk indicates coastal sites. Output for LJO and KIS were not saved for the UM cases.

To investigate the diurnal cycle, half hourly tracer concentrations are output for specific locations where continuous CO₂ measurements are available. Using the total CO₂ concentrations from summing the biosphere (diurnally varying), fossil, and ocean contributions, the mean June through August (JJA) diurnal cycle amplitude at continental sites is displayed in Fig. 4.11. Overall, modelled amplitudes increase as observed amplitudes increase; however, as discussed in L10, there is a large model spread reflecting the limitations of representing an observing location with a large model grid cell. The UM captures the diurnal amplitude at coastal sites reasonably well, lying within the TransCom range. At in-land sites, the UM generally overestimates the amplitude of the diurnal cycle. As seen previously, the model version and land surface module do not alter the amplitudes as much as the stable boundary layer scheme. The over-estimation is greatest for the sharpest scheme, while the long tail scheme has lower amplitudes closer to the observations and generally within the variability seen in the TransCom models.

Table 4.1 Latitude, longitude and reference for the CO₂ observation sites used in Fig. 4.11.

Site	Lat	Lon	Reference
AMY	36.53	126.32	Kim and Park (2006)
BOR	55.87	98.46	Dunn et al. (2007)
CBW	52.00	90.20	A. Vermeulen (pers. comm., 2006)
COI	43.15	145.50	Tohjima et al. (2006)
DEU	49.77	7.05	Uhse and Meinhardt (2006)
FRD	49.88	-81.57	Higuchi et al. (2003)
HVF	42.53	-72.17	Urbanski et al. (2007)
HUN	46.95	16.65	Haszpra (2006)
KIS	36.08	139.55	Muto (2006)
LJO	32.90	-117.30	R. Keeling (pers. Comm. 2006)
MHD	53.33	-9.90	Biraud et al. (2002)
MKW	34.85	137.43	Iwata (2006)
NGL	53.15	13.03	Uhse and Meinhardt (2006)
PAL	67.97	24.12	Hatakka (2006)
LEF	45.93	-90.27	Bakwin et al. (1998)
RYO	39.03	141.83	Sasaki (2006)
TPJ	-2.86	-54.96	Hutyra et al. (2007)
THD	41.05	-124.15	Lueker et al. (2003)
WES	55.00	8.00	Uhse and Meinhardt (2006)
ZGT	54.43	12.73	Uhse and Meinhardt (2006)

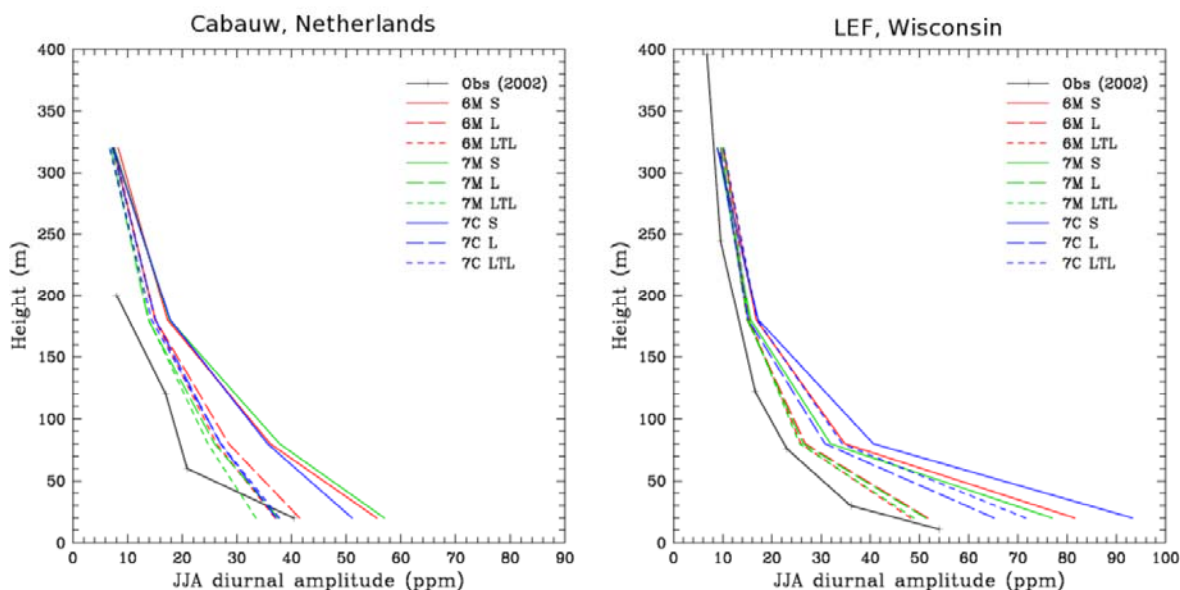


Fig. 4.12 Vertical profiles of the peak-to-peak diurnal cycle amplitudes for JJA at two tower sites in the northern hemisphere. The model is sampled from the grid cell including the tower and at the vertical levels most closely matching the observations levels, and all N48 cases are displayed. Left) Vertical profiles at Cabauw. Right) Vertical profiles at LEF.

The amplitude of the diurnal cycle varies with height, decreasing in amplitude with distance from the surface (Fig. 4.12). Although the UM overestimates the diurnal cycle amplitudes, it captures the decrease in amplitude with height at both locations. The sharpest scheme has the highest amplitudes, while the long tail scheme most closely matches the observations. The overestimation at the surface, particularly with the sharpest scheme, suggests that the model underestimates the nighttime boundary layer mixing, causing surface concentrations to build-up to higher concentrations than observed.

Following L10, the ratio of the diurnal peak-to-peak amplitude concentration to the flux amplitude is calculated at seven continental, low-altitude sites (Fig. 4.13). This metric reveals information regarding the vertical mixing strength. In general, the TransCom models tend to underestimate the ratio and have too little of a difference between sites, except for a few models that produce a very high ratio in the tropics. Using the UM, the concentration-to-flux ratio results are relatively similar between all three configurations and between the two horizontal resolutions, with a greater sensitivity to the stable boundary layer parameterization rather than model version, land surface scheme, or horizontal resolution. The UM has higher ratios using the sharpest scheme and lower ratios using the long tail scheme. Using the sharpest scheme results in very high ratios at the tropical site, TPJ. The high ratios further suggest that the sharpest scheme underestimates the vertical mixing. Using the long tail scheme more closely match the observations, with both the modelled and observed range falling between 1.2 and 2.8 ppm / $\mu\text{-mol m}^{-2} \text{s}^{-1}$.

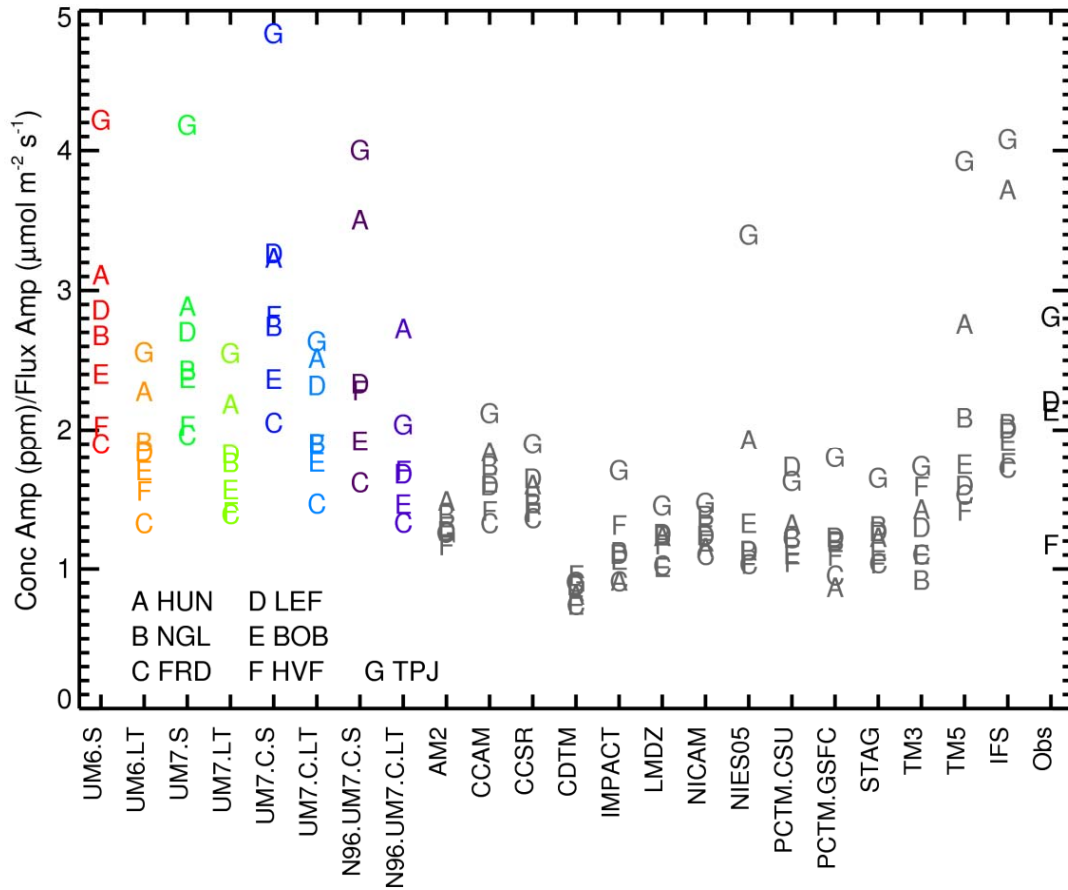


Fig. 4.13 Ratio of peak-to-peak mean JJA diurnal concentration amplitude to diurnal JJA flux amplitude, using the diurnally varying biospheric tracer and flux for the models. Each site is indicated by a letter and identified in the key, with the model listed along the x-axis. The UM results are in colour, while the TransCom models are gray. Observed ratios shown in the last column are only currently available at LEF, BOB, HVF, and TPJ, where both fluxes and concentrations are measured.

4.5 CABLE vs. MOSES transport conclusions

Atmospheric CO₂ concentrations can be a useful, independent metric to evaluate climate models. The changes due to different model configurations (UM 6.3 vs. UM 7.3, MOSES vs. CABLE) or different horizontal resolutions (N48 vs. N96) are minimal compared to the differences from using various boundary layer parameterizations. Although the seasonal and diurnal behaviour in atmospheric CO₂ concentrations is broadly consistent to both TransCom results and observations, the amplitudes of both these cycles are overestimated at mid and high northern latitude sites using the sharpest scheme. This indicates that the nighttime and winter stable boundary layers are too shallow and that the near-surface mixing is underestimated. The inter-hemispheric difference is also too large using the sharpest scheme, particularly in the northern hemisphere winter, suggesting that the UM has too slow inter-hemispheric mixing, especially at N96 resolution. Switching to the long tail scheme lowered the amplitudes of the seasonal and diurnal cycles, more closely matching the observations. Using the long tail scheme also reduced the inter-hemispheric difference; however, the difference in the winter was still larger than the TransCom range, indicating that despite changing stable boundary layer schemes the UM may still have slow mixing between the hemispheres. The various comparisons indicate that using the long tail scheme comes closest to matching the observations overall.

5. ASSESSING STRATOSPHERIC TRANSPORT IN ACCESS

While atmospheric carbon dioxide (CO₂) concentrations are being widely studied due to their recent rapid increase and global warming potential, methane (CH₄) is also an important greenhouse gas. The radiative efficiency of CH₄ is an order of magnitude larger than that of CO₂ [Ramasuamy et al. 2001], and atmospheric CH₄ concentrations have increased from 715 ppb in 1750 to 1787 ppb in 2008 [Etheridge et al. 1998; Dlugokencky et al. 2009]. The atmospheric growth rate of CH₄ reflects the imbalance between various sources and sinks: CH₄ concentrations increased rapidly in the 1970s and 1980s, slowed significantly in the 1990s, remained relatively stable in the 2000s and have very recently begun increasing again [O'Connor et al. 2010; Blake and Rowland 1988; Dlugokencky et al. 1998, 2003, 2009].

Various studies have analysed the sources and sinks of CH₄. Both natural and anthropogenic emissions increase atmospheric CH₄ concentrations, with wetland emissions being the largest single source [Denman et al. 2007]. The primary removal mechanisms for atmospheric CH₄ are oxidation with the hydroxyl radical (OH), reaction with chlorine (Cl) and oxygen (O¹D) atoms, and biological oxidation in dry soil [O'Connor et al. 2010]. While the total global source is relatively well constrained [Prather et al. 2001; Denman et al. 2007], considerable uncertainty in individual source and sink estimates still exists.

Modelling studies can be used to further quantify CH₄ fluxes; however, they require realistic atmospheric concentrations. In order to simulate the variability in atmospheric CH₄, the spatio-temporal variation in fluxes and the destruction due to OH, Cl and O¹D must be well characterized and the model transport must be accurate. To examine the role of transport, flux distribution, and chemical loss in simulating atmospheric CH₄ concentrations, TransCom is conducting a methane inter-comparison project. The protocol [Patra et al. 2010] for the methane project is similar to previous TransCom activities; however, rather than focusing on CO₂, the main aim of this experiment is to quantify the role of transport, flux distribution and chemical loss in simulating the seasonal cycle, synoptic variations and the diurnal cycle in CH₄ mixing ratios. The individual model simulations are for 1990 through 2007, with six different methane tracers (due to different surface fluxes), as well as methyl chloroform (MCF), radon, and sulphur hexafluoride (SF₆).

Since the methane inter-comparison involves models from a wide variety of institutions, it is important for ACCESS to contribute to the project. Following the project protocol, ACCESS was used to simulate the atmospheric tracers for the requested time period; however, upon analysing the results, it became apparent that there is a problem regarding the transport in the stratosphere, as the top level in the model rapidly decreased in concentration to near zero within two years. This chapter investigates the tracer transport problems using the methane experiment as well as simple test cases.

5.1 TransCom CH₄ model simulation

To participate in the TransCom CH₄ inter-comparison study, ACCESS was setup to simulate the necessary tracers, surface fluxes, and atmospheric chemistry (see section 2.2.3). ACCESS is run at 3.75° longitude by 2.5° latitude (N48) horizontal grid spacing with 38 vertical levels in an AMIP-style configuration. The atmospheric model used is the UM version 7.3, and it is coupled to CABLE. The simulations start in 1988, with the first two years providing spin-up for the atmospheric chemistry. The runs integrate forward for twenty-one years, through 2008.

The TransCom project focuses on six methane tracers with prescribed monthly fluxes at 1° by 1° spatial resolution. To capture the soil sink, prescribed monthly-mean soil fluxes are subtracted from each methane

flux. In addition to methane, the project simulates MCF and SF₆, both with prescribed annual mean fluxes. While the SF₆ emissions have increased, surface fluxes of MCF have rapidly decreased over the last two decades since it is controlled under the Montreal Protocol. Radon is also simulated from constant prescribed land and ocean fluxes. All the surface fluxes are aggregated to the N48 grid, ensuring that the re-gridded global flux remains equal to the prescribed global flux total, except radon which had a slightly different global total due to the different land fraction.

Basic chemistry is included in the model in order to simulate the atmospheric loss of CH₄, MCF, and radon. The dominant loss of CH₄ is reaction with OH. Atmospheric OH concentrations are re-gridded from a prescribed monthly-mean climatological distribution, and the rate constant is set to a temperature-dependent reaction rate. Loss rates from the reaction of CH₄ with Cl and O¹D atoms are also included from a prescribed monthly-mean three-dimensional distribution. For MCF, monthly mean loss rates due to photolysis in the stratosphere and monthly deposition velocities to the ocean surface are provided. The loss of MCF due to its reaction with OH is also simulated, using the prescribed OH distribution and a temperature-dependent rate constant. For radon, the atmospheric concentrations exponentially decay with a half-life of 3.8 days. Since SF₆ does not have any atmospheric loss, the mass is conserved using a mass fixing routine (see Chapter 3).

In order to establish realistic vertical profiles in the stratosphere, the atmospheric CH₄ and MCF tracers are initialized to a distribution representing 1988 conditions, which is based on results from a global chemical transport model that was spun up for five years. These fields have considerable horizontal and vertical gradients. The initial maps are re-gridded to the UM horizontal grid spacing and vertical levels. The radon concentration starts from 0. The SF₆ tracer was initialized uniformly to 1.95 ppt, which corresponds to the mean concentration during January 1988.

5.2 ACCESS CH₄ results

The initial concentration for all six methane tracers has an area-weighted global mean of ~500 ppb in the top model level; however, within two years the methane in the top level of the UM rapidly decreases to near 0 ppb (Fig. 5.1 top, red). Simulating the loss terms in the top model layer depletes the methane in this level, which then mixes down and decreases the concentrations in the neighbouring lower levels.

To determine why the atmospheric CH₄ concentration in the top level (L38) decreases so rapidly, four two-year simulations are performed. These simulations all follow the basic TransCom CH₄ protocol; however, the atmospheric loss in the top level of the atmosphere is altered. The first simulation completely turns off the methane loss in the top level (orange). The second simulation includes loss of CH₄ from its reaction with OH only (green), and the third simulation includes only loss of CH₄ from Cl and O¹D reactions (purple). The final simulation applies the OH distribution and the Cl and O¹D loss rates from the neighbouring lower level (L37) to the concentrations in the top level (blue).

Concentrations in the top three model levels vary significantly depending on the loss of CH₄ in the top level (Fig. 5.1). When atmospheric loss is not included, the methane concentrations in the top level increase due to the mixing in of higher concentrations from below; however, when any loss rate is applied, the methane in the top of the model rapidly decreases, pulling down the concentrations in lower levels of the atmosphere. While there is atmospheric loss in levels 36 and 37, this does not appear to be the major cause of the depletion in these layers, since in the no loss case these levels maintain their initial concentrations, suggesting that the loss is approximately balanced by transport of CH₄ from below.

Methane depletion in the top of the atmosphere is also seen in a recent simulation with the UK Met Office Chemistry-Aerosol-Climate model coupled to the UM (UKCA) (Fig. 5.1 top, black). This simulation, which uses a different version of the UM (7.1) as well as interactive OH and stratospheric loss rates, also has rapidly decreasing methane concentrations in the top level of the atmosphere. While the UKCA case starts with higher concentrations in the top of the model due to different initial conditions, the depletion occurs even faster than using the TransCom setup, with the methane being nearly depleted in only half a year. Since the methane depletion in the top level occurs in two independent simulations performed with two different versions of the model, it indicates that the problem likely involves atmospheric transport rather than model setup.

Changing the methane concentration in the top level of the atmosphere impacts the surface concentrations (Fig. 5.1 bottom). Comparing the original simulation (red) to the no loss case (orange), after only two years the global mean surface concentration differs by more than 7 ppb. The substantial surface differences in only a few months caused by changing methane loss only in the top layer of the atmosphere again indicates a potential problem with atmospheric tracer transport in the top level of the UM.

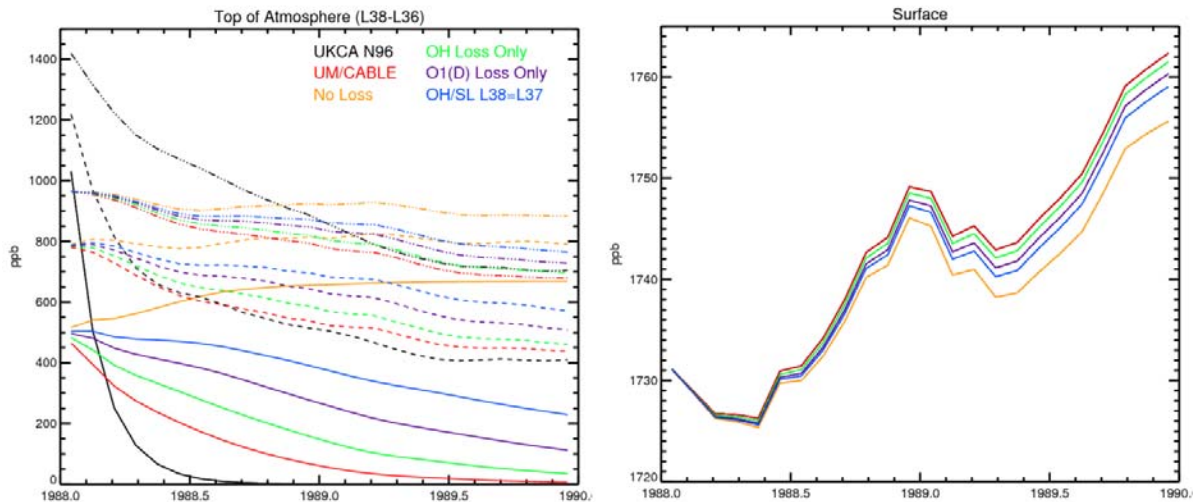


Fig. 5.1 Left) Area-weighted global mean methane concentrations from the top three levels in the model (L38: solid, L37: dashed, L36: dot-dash). Right) Global mean methane concentrations from the bottom model level (nearest the surface).

5.3 Methane test case simulations and results

To further investigate the atmospheric transport in the top level of the UM, we performed a series of one year experiments. Rather than using the full TransCom methane project setup, the runs only simulate a single methane passive tracer with no surface flux and no atmospheric loss, making the initial methane concentration the only difference between each experiment. The first test initializes the tracer to 0 ppb in all levels except the top level, which is initialized to 1700 ppb. Vertical profiles of the zonal mean concentrations for January and December are displayed in Fig. 5.2. The high concentrations in the top level mix down, reducing the gradient in the top of the atmosphere over time, while the concentrations in the lower half of the atmosphere remain constant at 0 ppb. This test reveals that in this case the UM is mixing high concentrations down from the top level.

To investigate mixing into the model top level and the resulting impact on the atmospheric concentrations, we performed seven different tests varying the initial methane concentrations and switching tracer conservation on or off. The tracer conservation scheme referred to here is the conservation scheme included in the UM for advection. None of these tests use the mass fixing scheme described in Chapter 3, which removes any remaining small non-conservation that occurs even when the original UM tracer conservation scheme is used. The initial conditions are either constant values (0 or 1700 ppb depending on the level) or are based on the TransCom initial condition, in some cases averaged in each level to remove any horizontal gradients. The cases are listed in Table 5.1.

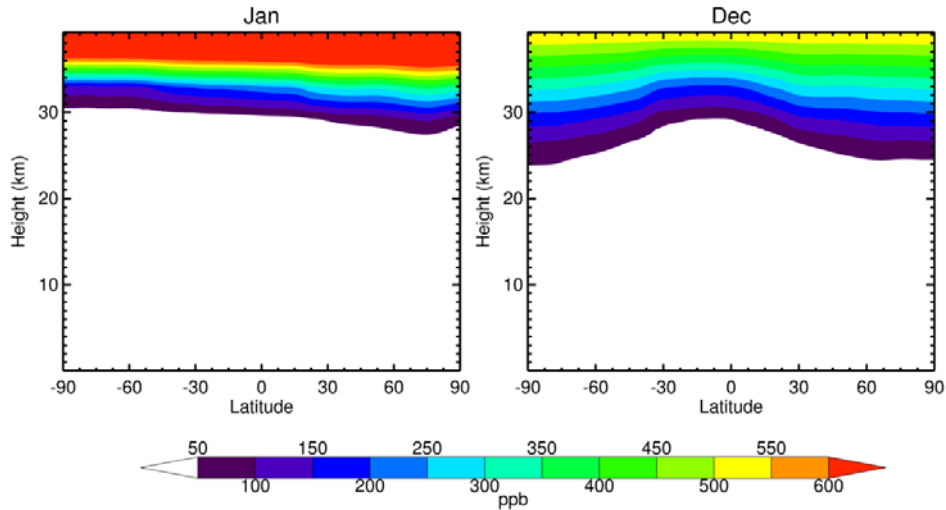


Fig. 5.2 Vertical profile of zonal mean concentrations for January and December from the first test case, with 1700 ppb in the top level only.

Table 5.1 Methane passive tracer tests defined by the initial condition used in level 38, level 37 and the rest of the atmosphere and whether tracer conservation is used. Also given are the label and line colour used in Figs 5.3 and 5.4.

Label	Initial level 38	Initial level 37	Initial level 1-36	Conserve?	Fig colour
L38 0	0 ppb	1700 ppb	1700 ppb	Yes	Black
L38 0 NC	0 ppb	1700 ppb	1700 ppb	No	Red
L37-L38 0	0 ppb	0 ppb	1700 ppb	Yes	Orange
TC VG	TC level mean	TC level mean	TC level mean	Yes	Green
TC	TC	TC	TC	Yes	Blue
TC M38	TC level mean	TC	TC	Yes	Cyan
TC NC	TC	TC	TC	No	Purple

While the mass in the three cases that use the tracer conservation scheme remains constant throughout the entire run, the mass in the two simulations that do not use the tracer conservation scheme decreases substantially in a single year. By December, the test case with 0 ppb in the top levels loses nearly 10 Tg, while the case using the TransCom initial concentrations loses nearly 18 Tg. The sharp decline in the atmospheric methane burden without the tracer conservation scheme indicates that it is important to use this scheme while running atmospheric tracers.

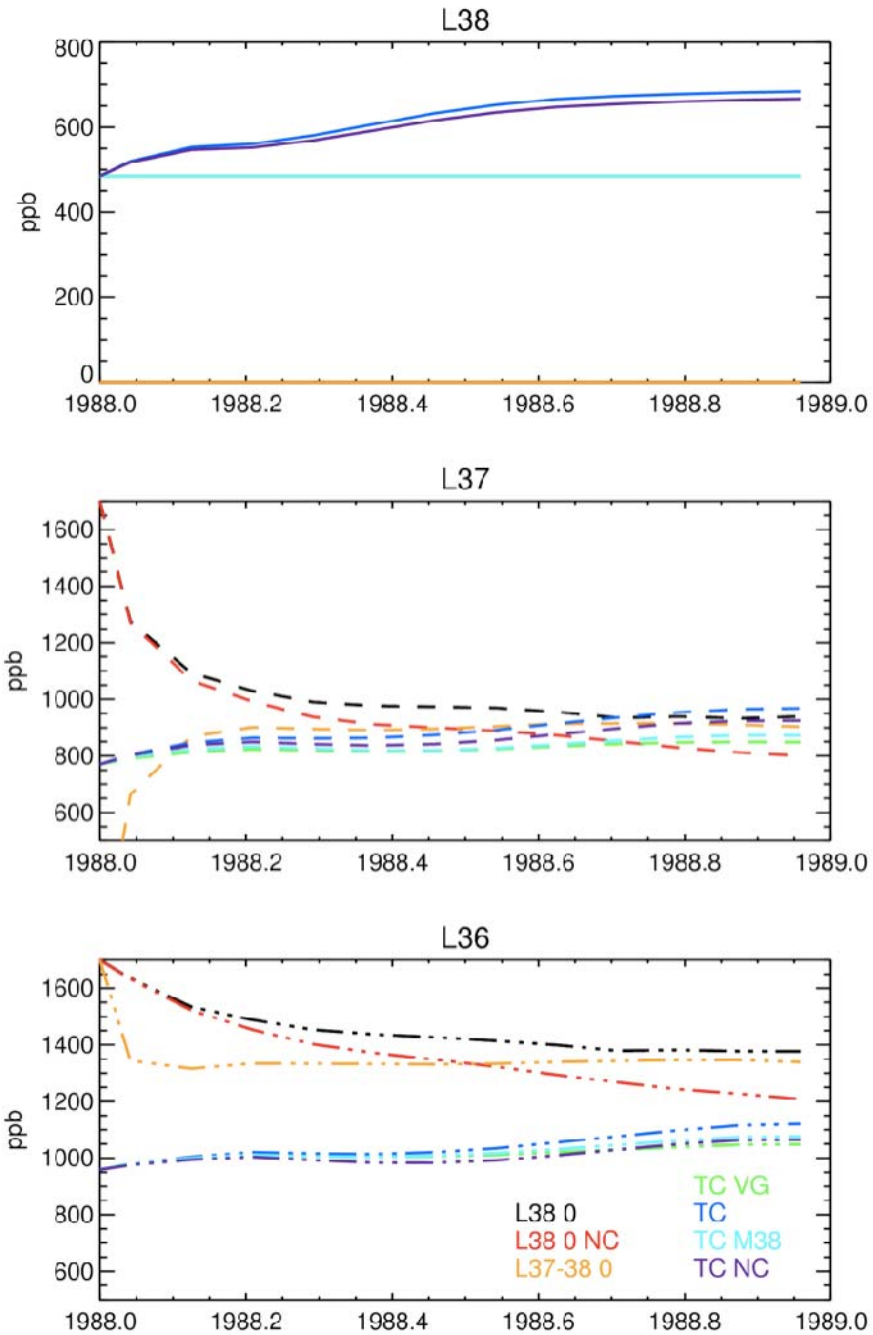


Fig. 5.3 Top of the atmosphere area-weighted global mean concentrations for each of the test simulations for three levels. (Top) L38; (Middle) L37; (Bottom) L36.

For each test case, the atmospheric concentrations from the top three levels (L38, L37, and L36) are displayed in Fig. 5.3. For the two cases with the atmospheric concentration of 0 ppb in L38, the concentrations in this level remain virtually constant throughout the entire year (concentrations of $\sim 1e-7$ occur with potentially realistic spatial structure): essentially no methane is mixed into L38. However, the top level influences multiple lower levels. Due to the low concentration in L38 and the sharp gradient created, concentrations in multiple lower levels decrease. The rate of decline is rapid at first due to the sharp gradient between the top two levels. As the gradient lessens and mixes throughout the atmosphere, the methane decrease in the stratospheric levels slows until the methane concentrations in each level remain relatively constant. In the case where the top two levels are both set to 0 ppb (Fig. 5.3, orange), the top level still remains constant at ~ 0 ppb. Both L37 and L36 adjust rapidly to the initial gradient: the concentration in L36 immediately drops from 1700 ppb to less than 1400 ppb and the concentration in L37 rapidly increases. After only a few months, these levels appear to be in balance and start increasing slightly as the higher concentrations throughout the rest of the atmosphere are slowly mixed into the upper stratosphere. Starting with vertical gradients throughout the entire atmosphere (TC VG; green) also maintains a constant concentration in the top level of the atmosphere (directly under cyan line), despite the lower levels steadily increasing to reduce the gradient between the higher concentrations in the lower levels.

When latitudinal variations in CH_4 are included in the initial conditions, the behaviour in the top level changes. Using the TransCom initial condition, which has higher stratospheric concentrations of methane in the tropics, the global mean concentration in L38 increases. This suggests that including spatial variability in the top level allows mass to enter this level, causing changes in concentrations. In this case, the global mean concentration in L38 increases to reduce the vertical gradient, as the lower levels have higher concentrations. Both L37 and L36 also steadily increase throughout this simulation. Removing the latitudinal gradients in only the top level (TC M38, cyan) caused the concentrations in L38 to remain constant again. Not increasing the concentrations in the top level caused the lower levels to increase less, lowering the concentrations in L37 by nearly 100 ppb after one year. Finally, using the TransCom initial condition but not using the conservation scheme behaves similarly to the TC case, but the concentration increases are less.

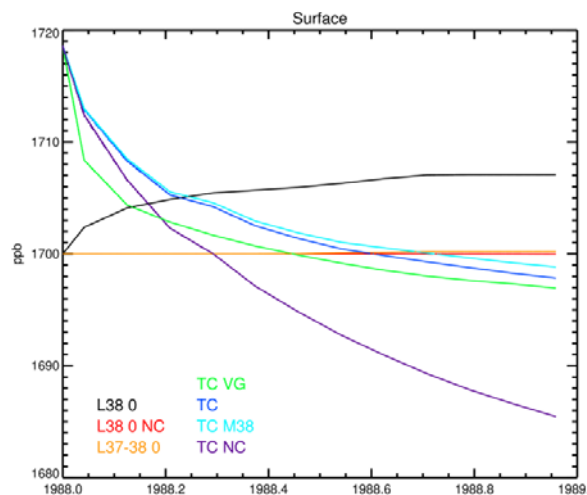


Fig. 5.4 Area-weighted global mean concentrations at the bottom of the atmosphere.

In addition to affecting the behaviour of the top levels in the atmosphere, altering the initial methane distribution has varying impacts near the surface (Fig. 5.4). In the first case, having lower concentrations only in the top level of the atmosphere actually increases the concentrations at the surface, and the near-surface concentrations begin increasing immediately (black). It is likely that the cause for this increase is artificial and is due to the behaviour of the mass conservation scheme: since the concentrations in L36 and L37 decrease without increasing concentrations in the top level, the surface levels are increasing in concentration to compensate. After only a year, the concentrations near the surface have increased by over 6 ppb, and this increase extends throughout the troposphere. When the mass conservation scheme is not used (T38 0, NC; red), the surface concentrations remain constant, as expected; however, significant mass is lost in this simulation. In contrast to the L38=0 only case, setting L37 and L38 to zero at the start of the run minimally impacts the surface concentrations, causing only a very slight increase in the troposphere. This is a curious difference in behaviour that is currently not well understood

For all cases that use the TransCom initial condition, the concentrations near the surface decrease over the year. This is because atmospheric transport is mixing the methane and reducing the vertical gradients in the atmosphere. However, the rate of decline in the methane concentration varies. When the top level is set to a constant value, the concentrations in the surface at the end of the run remain higher than when the top level includes spatial variability. This is again because no mass enters the top level, which perhaps causes the concentrations near the surface to artificially increase to conserve mass. When mass is not conserved, the concentrations in the lower atmosphere decrease substantially.

5.4 Advection scheme tests

The UM has several different options for semi-Lagrangian advection, and the atmospheric tracers use the same advection settings as the moisture fields. Two monotone schemes are available to prevent negative values from being generated: 1) Tri-linear Lagrange interpolation and 2) ECMWF monotone quasi-cubic interpolation. Using a monotone scheme is recommended for moisture. Seven different high order semi-Lagrangian advection schemes are available: 1) cubic Lagrange interpolation, 2) quintic Lagrange interpolation, 3) European Centre for Medium-Range Weather Forecasts (ECMWF) quasi-cubic interpolation, 4) ECMWF monotone quasi-cubic interpolation, 5) bi-cubic Lagrange interpolation in the horizontal and linear interpolation in the vertical, 6) ECMWF quasi-cubic interpolation in the horizontal and quintic in the vertical, and 7) cubic Lagrange interpolation in the horizontal and quintic in the vertical. All the cases discussed in Section 5.3 use monotone scheme 2 with higher-order option 6. Since it is possible the advection scheme may alter the tracer behaviour in the top level of the atmosphere, a series of 1-month simulations using each of the different advection schemes was conducted. The test cases simulate one atmospheric tracer with no flux or loss. Vertical diffusion is off in all cases, the monotone scheme is turned off, and the tracer mass conservation is also turned off. All the test cases are initialized to the same distribution of 1700 ppb in all the atmospheric levels except the top layer, which was set to 0.

Mixing into the top level of the atmosphere is not sensitive to the advection scheme (Fig. 5.5). The top level of the atmosphere remains at 0 ppb throughout the entire month, regardless of the advection scheme. Despite no mass transferring into the top level, all the test cases have decreasing concentrations in the neighbouring lower levels. The rate of decrease is similar for all schemes except scheme 5, which has linear interpolation in the vertical. Using linear interpolation causes L36 and L37 to decrease more than the other options, which is expected due to the large gradient. Setting the top level to 0 causes decreases in thirteen lower levels, down to layer 25. Since the test cases do not use mass conservation, the concentrations near the surface remain at 1700 ppb and considerable mass is lost in the tracer.

The advection tests are repeated using the tracer mass conservation scheme while still turning off the monotone scheme; however, the results are exactly the same. This indicates that the monotone scheme must be on in order to conserve mass in the tracers. The tests are thus repeated again using monotone scheme 1. Using a monotone scheme combined with the conservation scheme does indeed conserve the mass in the tracer; however, the behaviour in the top levels of the atmosphere remains exactly the same as in the non-conserving cases. Rather than altering the concentrations in the top of the atmosphere, to balance the mass lost in the middle and upper levels, the tropospheric concentrations increase by ~10 ppb. All the tests yielding the same concentrations in the top of the atmosphere, with no mass transferring into the top level despite a large vertical gradient, indicates that the mixing problem at the top of the UM is common to all the advection scheme variants.

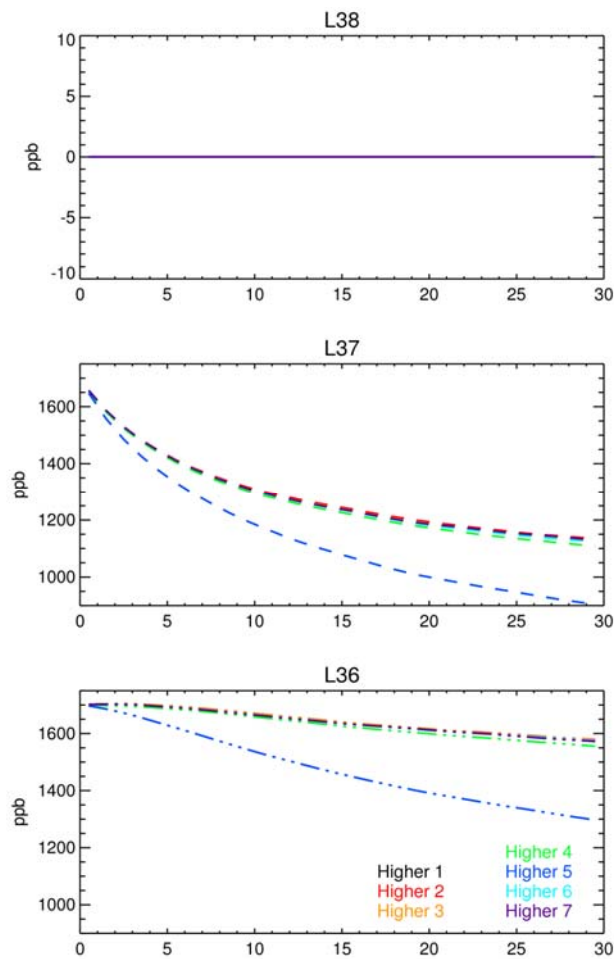


Fig. 5.5 Daily top of the atmosphere area-weighted global mean concentrations from the advection tests: (Higher 1) Cubic Lagrange interpolation, (Higher 2) Quintic Lagrange interpolation, (Higher 3) ECMWF quasi-cubic interpolation, (Higher 4) ECMWF monotone quasi-cubic interpolation, (Higher 5) Bi-cubic Lagrange interpolation in the horizontal and linear interpolation in the vertical, (Higher 6) ECMWF quasi-cubic interpolation in the horizontal and quintic in the vertical, and (Higher 7) Cubic Lagrange interpolation in the horizontal and quintic in the vertical.

5.5 Discussion

The test case experiments help to explain the results seen in the full TransCom methane cases, which include surface fluxes and chemical loss. While the initial condition in the full TransCom case includes horizontal structure in the top layer of the atmosphere, this is rapidly removed in the case including loss in the top level. As the horizontal structure is removed, the mass being added to the top level decreases. It appears that once the top level is relatively well mixed with sufficiently small latitudinal gradients (~ 10 ppb), no tracer is added from below despite higher concentrations in level 37. In the no loss case, horizontal gradients are also mixed out in time, reducing the rate at which the mass increases in the top level. Despite an initial increase in methane concentration in level 38, after only two years the concentration remains primarily constant despite higher concentrations in level 37. Both full methane cases confirm that there appears to be some interaction between horizontal gradients in level 38 and the ability to put tracer into this level. The lack of a horizontal gradient in level 38 apparently stops any tracer taken from level 37 from ‘arriving’ in level 38. The difference in concentration at the surface in the two TransCom methane runs may be due to an interaction between the problems with mixing at the top of the atmosphere and the tracer conservation scheme. Though it is difficult to be certain, we hypothesize that the tropospheric concentrations in the original TransCom case are artificially too high: the lack of mass being added into the top level forces an increase in tropospheric concentrations due to mass conservation.

Since MCF was also simulated and had loss in the atmosphere, the transport in the top levels of the atmosphere can also be investigated for this tracer. Initially, the top level has slightly lower concentrations than the neighbouring lower level, and the top level has a gradient of ~ 20 ppb between maximum concentrations in the tropics and low concentrations over the South Pole. In the original case that includes loss in the top level, MCF decreases rapidly in both level 38 and level 37. In the simulation without loss in level 38, the concentrations in level 37 immediately become lower than in level 38 due to the lack of loss at the top of the model. As long as there are spatial gradients in the top level, it appears that the larger concentrations in the top level are not allowed to mix down into the lower levels, and the vertical gradient between the top two levels increases. In level 38, the concentrations rapidly mix through the northern hemisphere before slowly mixing in the southern hemisphere to create globally constant concentrations. Once the concentration in the top level is completely homogenous and the gradient between the top two levels is large, then the mass in the top level begins to transfer down to the lower levels. Similar to the test case that started with homogenous high concentrations only in level 38, the concentrations in the top level uniformly lower to reduce the vertical gradient. While the test cases of CH_4 suggest that mixing mass into level 38 requires spatial variability in the top level of the atmosphere, the MCF tracer suggests that to mix mass down from level 38 requires this level to be completely homogenous.

Further work investigating the mixing at the top of the atmosphere has been started. A more recent simulation with the UKCA coupled to the UM version 7.3 yielded concentrations in the top level of the atmosphere that remained relatively constant over a year, rather than decreasing sharply as seen with the UM version 7.1. This suggests that the latest version of the UM coupled to the UKCA looks more promising regarding advection in the top of the atmosphere. Rather than quickly removing the spatial variability and then rapidly decreasing the concentrations in the top level, this simulation maintained considerable spatial variability for an entire year, which may have contributed to mixing into the top level and maintaining relatively stable concentrations. Additional analysis of the differences between the model versions and between the specific simulations may further our understanding of the mixing in the top of the model.

To help diagnose the mixing at the top of the UM, the model dynamics have been preliminarily investigated (G. Dietachmayer, M. Dix, and M. Zerroukat, personal communication). The top level for the atmospheric tracers is at the lid of the model, which acts as a fixed lid. A consequence of using a rigid lid approach is that the vertical wind component must be zero, implying that a particle should not enter or leave the top level. This appears inconsistent with the results from our tests cases and may warrant further investigation.

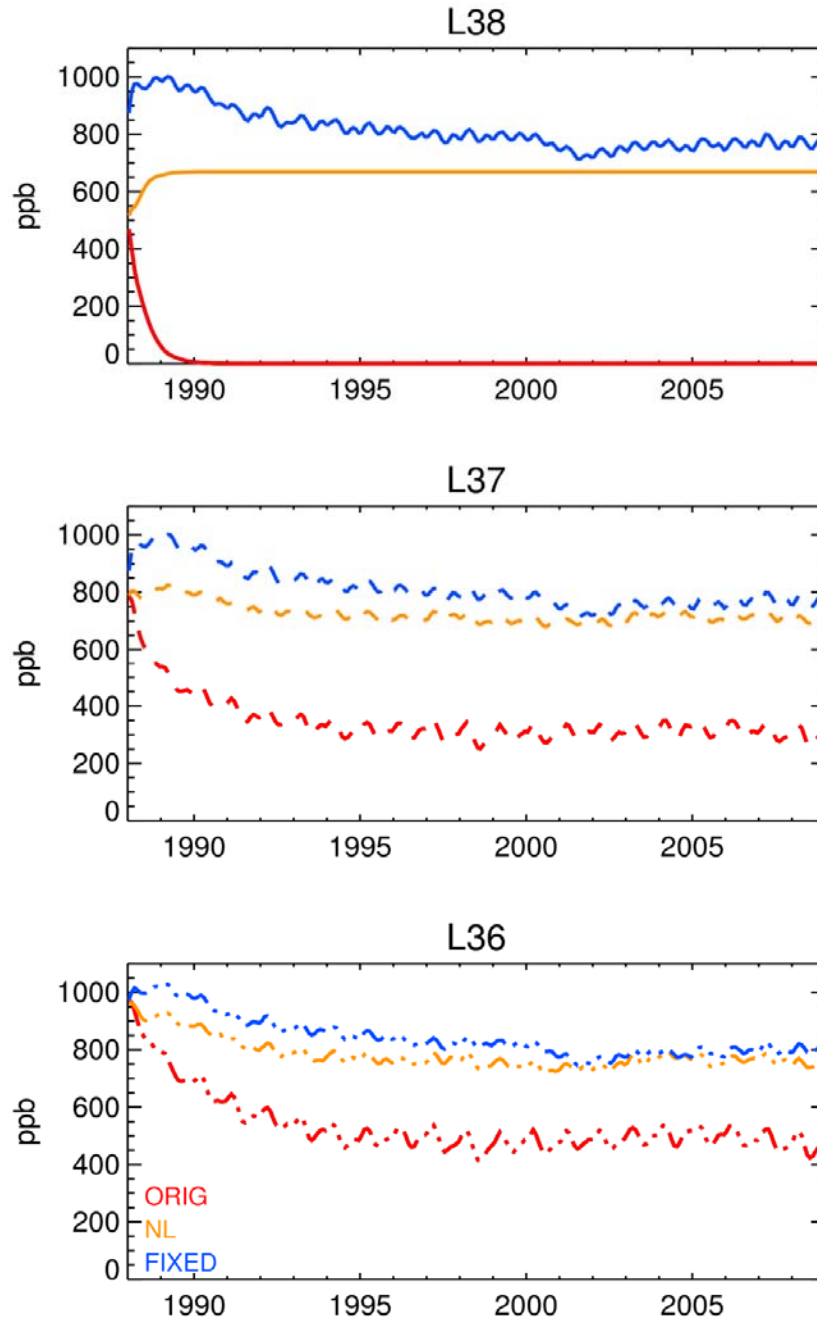


Fig. 5.6 Top of the atmosphere CH₄ concentrations for the CTL tracer from three simulations following the TransCom CH₄ protocol. Red indicates the original set-up, orange shows results from removing the loss from the top level, and blue indicates results from setting the top level equal to the neighbouring lower level.

5.6 Conclusions

Analyses of atmospheric CH₄ and MCF concentrations simulated with the UM indicates a problem involving the atmospheric transport in the top level of the model. Results from test simulations indicate that if the mass is lower in the top of the atmosphere, no mass is mixed into the top layer unless this layer contains spatial gradients. If the concentrations in the top level are horizontally homogeneous, it appears that mass is removed from the level below but is never added to the top level. In contrast, if the mass in the top layer is higher than the lower atmospheric levels, in order to mix the high concentrations down from the top level and relieve the vertical gradient, the top level must not have any spatial variability. This odd mixing behaviour appears to interact with the tracer conservation scheme in ways that are not always predictable, with possible implications throughout the troposphere.

It seems unlikely that this problem with tracer mixing would have any significant consequences for climate only runs. For CO₂, the model is usually initialized with uniform concentrations throughout the stratosphere, so any impact should be minimal. The main issue is for trace gases with significant loss in the stratosphere, such as CH₄ and MCF. Since the mass in the top layer is small, removing the vertical gradients between the top two levels in the atmosphere may be a short-term solution. By not including any loss and setting the top level equal to the neighbouring lower level at every time-step, the atmospheric transport and mass conservation should behave realistically, particularly for tropospheric concentrations. Figures 5.6 and 5.7 show monthly methane concentrations from three TransCom CH₄ simulations. Setting the top level equal to the neighbouring lower level (blue) maintains realistic concentrations in the stratosphere while also producing realistic near-surface concentrations. These results indicate that this temporary solution allows features such as the surface growth rate and seasonal cycle to be compared with observations with reasonable confidence.

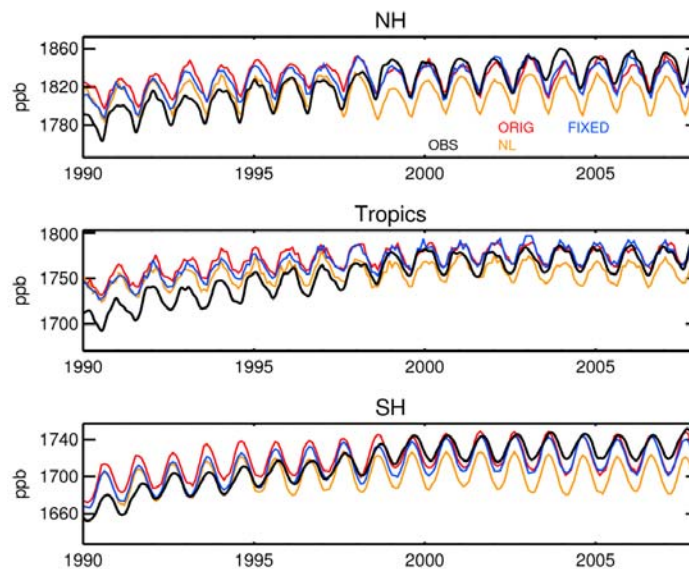


Fig. 5.7 Monthly mean methane concentrations from the three simulations over the northern hemisphere (NH; top), tropics (middle, 20 S through 20 N), and southern hemisphere (SH; bottom). The concentrations are for the CTL tracer and are the mean values from the sites sampled in GLOBALVIEW-CH₄ (GV; 2009), which has weekly temporal resolution. The majority of the sites are located near the surface in the lowest model level. The model is sampled hourly at the grid cell and level that most closely matches the observation location. The black lines indicate the GV results, and the coloured lines show the model results from each of the three simulations in Fig. 5.6.

6. ASSESSING ATMOSPHERIC METHANE IN ACCESS

As discussed in Chapter 5, TransCom is conducting an inter-comparison project focusing on atmospheric methane. ACCESS is participating in this study, simulating six different methane tracers as well as methyl chloroform (MCF), radon, and sulphur hexafluoride (SF₆). Information regarding the fluxes is provided in Table 6.1. ACCESS (UM version 7.3, CABLE land surface model) is run at 3.75° longitude by 2.5° latitude (N48) horizontal grid spacing with 38 vertical levels in an AMIP-style configuration. To realistically simulate concentrations in the stratosphere, the concentrations in the top level of the atmosphere are set every time-step to the concentrations in the next lowest model level. To provide realistic concentrations to easily compare with model output, GLOBALVIEW-CH₄ is a data product that includes over two hundred extended records derived from observations. While extended records are easy to evaluate models with since they fill any missing data with climatological values, the actual time periods with data at an individual site may be quite short. For global and annual means, this is not likely to have a significant impact; however, specific site comparisons may be sensitive to the time period of the actual data. It is also important to note that GLOBALVIEW-CH₄ represents baseline-selected observations, biased towards remote locations. This may improve the comparison with model output since regions with large fluxes are less likely to be sampled. For most of the analysis, the model output has not been baseline-selected. In this section we will compare the model results with weekly concentrations from GLOBALVIEW-CH₄ (2009), sampling the model at the closest grid cell and model level as the observation site, for the time-period between 1990 and 2008.

Table 6.2 List of the six CH₄ tracers simulated in the TransCom-CH₄ inter-comparison project. Fluxes either have interannual variations (IAV) or are annual repeating (CYC).

CH ₄ Tracers	Description	Time Resolution
CTL	Natural emissions from the GISS inventory (Fung et al. 1991) Rice (REAS; Yan et al. 2005) Ocean and mud volcano	Monthly CYC
	Anthropogenic emissions from EDGAR 3.2 FT 2000 (Olivier et al. 2005)	Annual IAV
	Biomass burning and wetlands	Monthly CYC
CTL_E4	Natural emissions (GISS inventory; Fung et al. 1991) Rice (REAS; Yan et al. 2005) Ocean and mud volcano	Monthly CYC
	Anthropogenic emissions from EDGAR 4.0 (van Aardenne et al. 2009)	Annual IAV
	Biomass burning and wetlands	Monthly CYC
BB	CTL	Monthly IAV
	-0.35 Biomass burning	Monthly CYC
	Biomass burning from GFED v. 2 (Randerson et al. 2007)	Monthly IAV (1996-2008) Monthly CYC (1988-1995)
WL_BB	BB	Monthly IAV
	- Wetlands	Monthly CYC
	0.76 Wetlands from ORCHIDEE (Ringeval et al. 2010)	Monthly IAV (1994-2000) Monthly CYC (1988-1993) (2001-2008)
INV	IPSL optimized flux (Bousquet et al. 2006)	Monthly IAV (1988-2005)
		Monthly CYC (2006-2008)
EXTRA	BB	Monthly IAV
	- Wetlands	Monthly CYC
	- Rice	Monthly CYC
	VISIT model simulated wetland and rice (Inatomi and Ito, 2008)	Monthly IAV

6.1 Global spatial and vertical methane distributions

To provide an overview of atmospheric methane concentrations, mean near-surface global distributions of simulated methane from the control flux (CTL) are displayed in Fig. 6.1 (left). In January, atmospheric CH₄ concentrations are low in the southern hemisphere (< 1700 ppb) and high in the northern hemisphere (> 1925 ppb). The concentrations are higher over land than over the ocean, where the dominant sources are located. The highest concentrations occur in Asia, with regions of concentrations exceeding 2000 ppb also occurring over Europe, central South America, and eastern North America. In July, the concentrations in the southern hemisphere are higher, weakening the north-south gradient. High regional concentrations occur in southern South America as well as in eastern Australia. In the northern hemisphere, the concentrations are lower both over the ocean as well as over land.

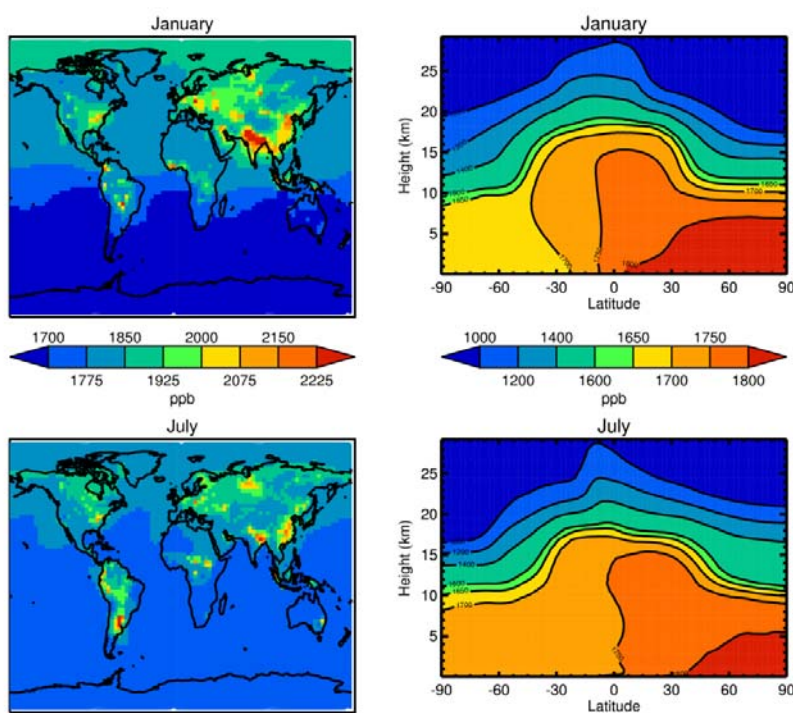


Fig. 6.1 Top left) Mean near-surface January methane concentrations. Bottom left) Mean near-surface July methane concentrations. Top right) Mean zonally averaged vertical profile for January. Bottom right) Mean zonally averaged vertical profile for July.

To see methane concentrations higher in the atmosphere, vertical profiles of zonal mean methane concentrations are displayed in Fig. 6.1 (right), extending up to 30 km. The figure clearly shows the north-south gradient near the surface, which extends up to approximately 5 km. The concentrations are always higher in the northern hemisphere, where the sources dominate, with the highest concentrations and largest inter-hemispheric gradient during the northern hemisphere winter. The methane concentrations are relatively well mixed in the troposphere, up to approximately 10 km in the high latitudes and approximately 15 km in the tropics. Above the troposphere the methane concentrations rapidly decrease with height, with a sharp gradient near the tropopause. The simulated concentrations in the stratosphere are significantly lower than the tropospheric values, with concentrations less than 1000 ppb above 20 km.

6.2 Simulated vs. GLOBALVIEW CH₄ concentrations

To assess ACCESS, time-series of mean atmospheric CH₄ over the northern hemisphere (NH), tropics, and southern hemisphere (SH) are displayed in Fig. 6.2. As seen in the concentration maps, the concentrations are highest in the NH and lowest in the SH. The amplitude of the seasonal cycle is also largest in the NH, with higher concentrations during the winter. Overall, ACCESS does a reasonable job at matching the magnitude of the atmospheric concentrations during the second half of the simulation; however, the model overestimates the concentrations at the beginning of the simulation for the first five years in all three regions. The concentrations from four of the fluxes (CTL, BB, WL_BB, EXTRA) all behave similarly. The concentrations from the INV flux severely overestimate the concentrations in the early 1990s and then underestimate the concentrations in the late 90s and early 2000s despite these fluxes being optimised to match concentrations. Presumably the atmospheric loss in our simulation is rather different from that used in the inversion that produced the fluxes. The concentrations resulting from the emissions including EGDAR 4.0 (CTL_E4) increase rapidly at the end of the simulation, resulting in overestimates of more than 30 ppb from 2005 through 2008, suggesting that these emissions are unrealistically large. In both the NH and the tropics, ACCESS matches the observed concentrations relatively well from the late 1990s. In the SH, the model most closely matches the observations in the mid-1990s and then underestimates the concentrations from 2000.

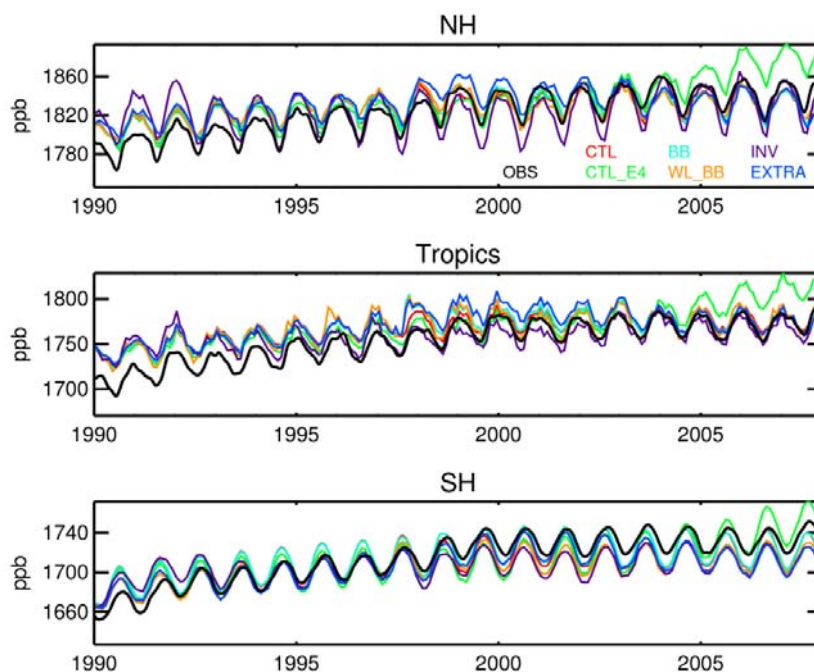


Fig. 6.2 Monthly mean methane concentrations in the northern hemisphere (NH; top), tropics (middle, 20° S through 20° N), and southern hemisphere (SH; bottom). The concentrations are the mean values from the sites sampled in GLOBALVIEW-CH₄ (GV; 2009), which has weekly temporal resolution. The model is sampled hourly at the grid cell and level that most closely matches the observation location. The black lines indicate the GV results, and the coloured lines show the model results from each of the six different methane tracers.

To investigate the seasonality in the model, the mean seasonal cycle of CH₄ is displayed in Fig. 6.3. Overall, the model does a reasonable job at simulating both the timing and magnitude of the mean seasonal cycle in all three regions. In the NH, the concentrations during the summer are slightly too high and reach their minimal values slightly later than observed. In the fall, the observed concentrations rapidly increase in September, which is not seen in the model. Using the inverse fluxes results in the largest seasonal cycle amplitude and the fluxes with wetlands and biomass burning yield the smallest seasonal cycle. In the tropics, all the tracers behave very similarly, matching the observed seasonal cycle quite well. In the SH, ACCESS underestimates summer (DJF) concentrations and overestimates the winter (JJA) concentrations, shifting the timing of the maximum concentrations in the seasonal cycle earlier than observed.

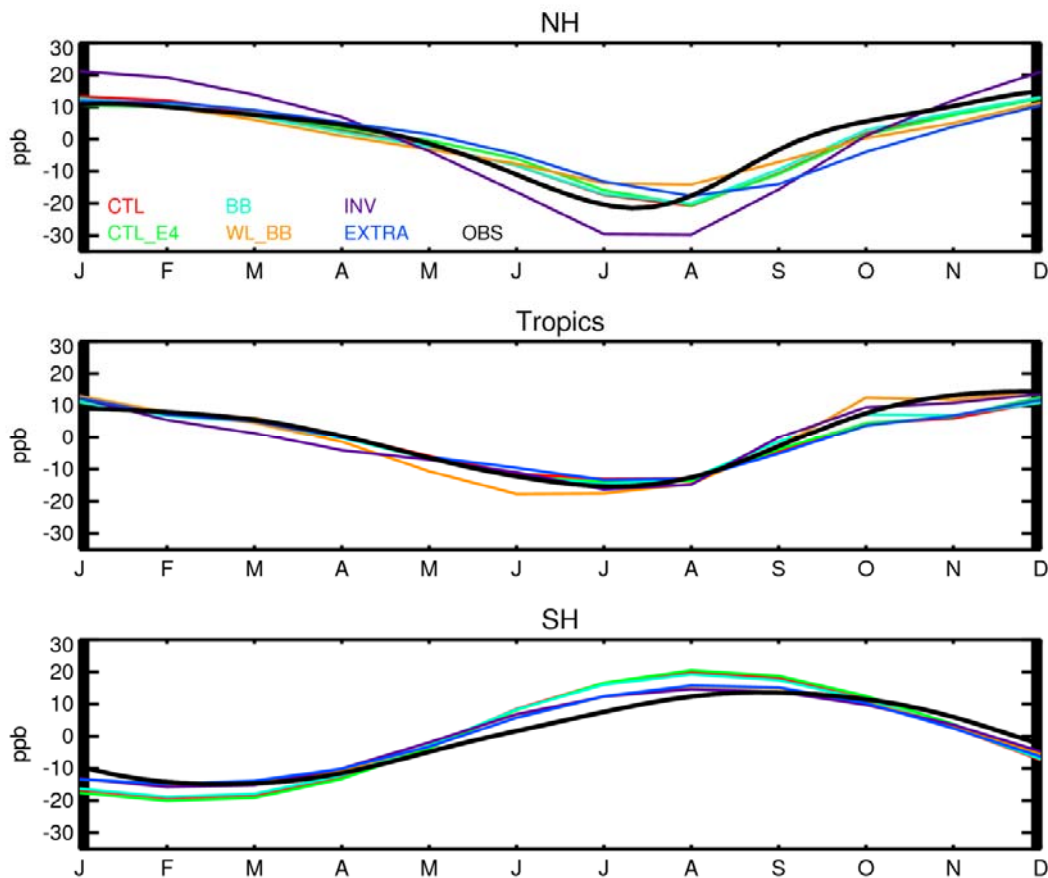


Fig. 6.3 Methane mean seasonal cycle for sites in the NH (top), tropics (middle), and SH (bottom). Black lines show the GV results and coloured lines indicate the model results.

Focusing on the inter-hemispheric difference, Fig. 6.4 shows both the annual mean differences between the SH and the NH and the monthly mean differences. Both the GV data and the models show an overall decrease in the inter-hemispheric difference over time, with the minimum difference occurring around the turn of the century. There is considerable spread between the different methane tracers; however, all the tracers have a large inter-hemispheric difference in 1998. This sudden increase in the north-south difference is also seen in the observations; however, the magnitude is overestimated in all the modelled tracers. The hemispheric difference resulting from the CTL_E4 flux increases during the last eight years, consistent with the suggestion that these emissions are too large in the NH. During the final six years of the run, both the

tracers resulting from the biomass burning (BB) flux and from the control flux (CTL) match the difference in GV quite well.

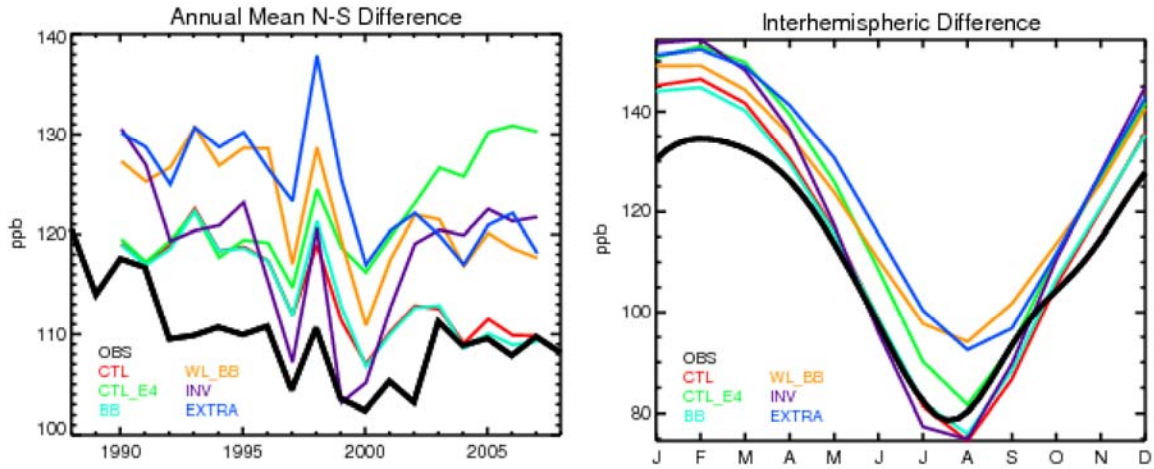


Fig. 6.4 Left) Annual mean methane inter-hemispheric differences, calculated by subtracting the monthly mean SH concentrations from the NH concentrations. Right) Methane monthly mean inter-hemispheric difference.

Looking at the monthly mean inter-hemispheric differences, the inter-hemispheric difference is the largest in DJF and smallest in JJA. While ACCESS captures the correct seasonality in the inter-hemispheric difference, it overestimates the gradient during the NH winter. Two of the tracers (WL_BB and EXTRA) also overestimate the difference during the NH summer; however, the amplitude of the seasonal cycle in the inter-hemispheric difference is captured well. The remaining four tracers more closely match the observed gradient during JJA; however, they overestimate the amplitude of the seasonal cycle in the inter-hemispheric difference.

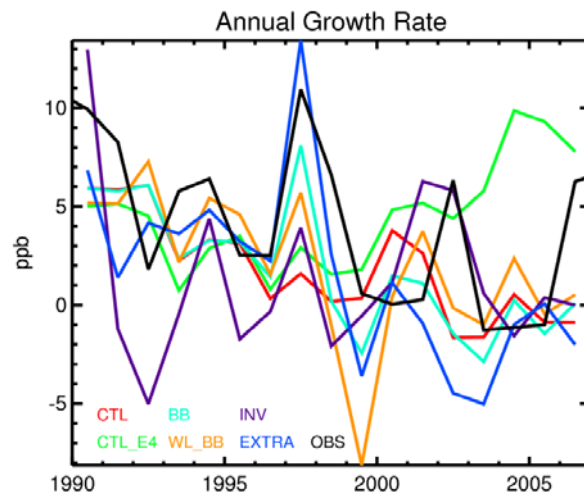


Fig. 6.5 The annual growth rate of methane for both the GV dataset (black) and the UM (colours), calculated by subtracting the annual mean concentrations.

The annual growth rate is shown in Fig. 6.5. All of the tracers have difficulty in matching the observed annual growth rate, and it varies relatively significantly between each of the different tracers. Near the beginning of the time period, the inverse fluxes capture the sharp decrease in the growth rate between 1992 and 1993; however, the magnitude of the decrease is severely overestimated. Nearly all of the CH₄ tracers capture the rapid increase during 1997 especially when inter-annually varying biomass burning fluxes are included; however, the majority of the fluxes underestimate the magnitude of the atmospheric growth. As expected, the fluxes with EDGAR 4.0 overestimate the growth rate during the last five years, resulting in the high concentrations seen earlier.

6.3 Simulated vs. GLOBALVIEW CH₄ vertical distributions

To investigate the model performance throughout the troposphere, Fig. 6.6 shows vertical profiles of monthly mean CH₄ concentrations at the five locations in GV sampled by aircraft. The model captures the magnitude of the concentrations reasonably well at three sites, but ACCESS underestimates the concentrations at PFA and RTA. In general, the concentrations remain relatively constant with height or decrease slightly with height in the NH but in the SH the concentrations increase slightly with height. The model does a reasonable job of capturing this behaviour in all the tracers, despite a large difference in the magnitude of the tracer concentrations. In the NH, the concentrations in January are higher than the July concentrations, while the opposite occurs in the SH. All of the different tracers tend to have more similar profiles in January than in July, and the INV fluxes tend to produce the lowest concentrations for both January and July.

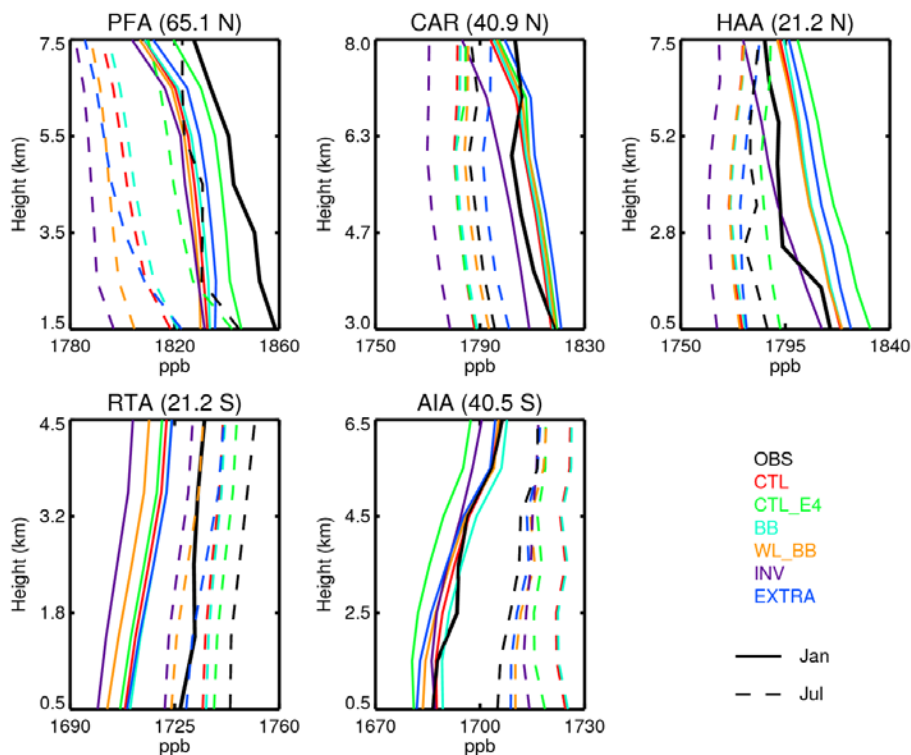


Fig. 6.6 Vertical profiles of monthly mean methane concentrations at the five GV sites sampled by aircraft. Rather than using the full extended record, the comparisons only include times when there are actual data. Solid lines show the profiles in January, and dashed lines show the profiles in July. The sites are ordered by decreasing latitude.

Vertical profiles of the seasonal cycle amplitude are shown in Fig. 6.7. The amplitude of the observed seasonal cycle decreases slightly with height at all the locations. While Fig. 6.3 showed that the model does a reasonable job at capturing the amplitude of the seasonal cycle averaged across all NH GV sites, at the three NH sites with vertical profile information shown here, ACCESS overestimates the amplitude of the seasonal cycle. In the high and mid latitude NH sites (PFA and CAR), the model overestimates the amplitude at ~5 km, putting the maximum amplitudes at this mid-tropospheric level. At HAA, the model captures the shape of the profile, with the largest seasonal cycle near the surface and a minimal seasonal cycle at ~5 km. In the SH, the results from the modelled tracers span the amplitude of the seasonal cycle and capture the decrease in the amplitude of the seasonal cycle with height seen in the GV dataset.

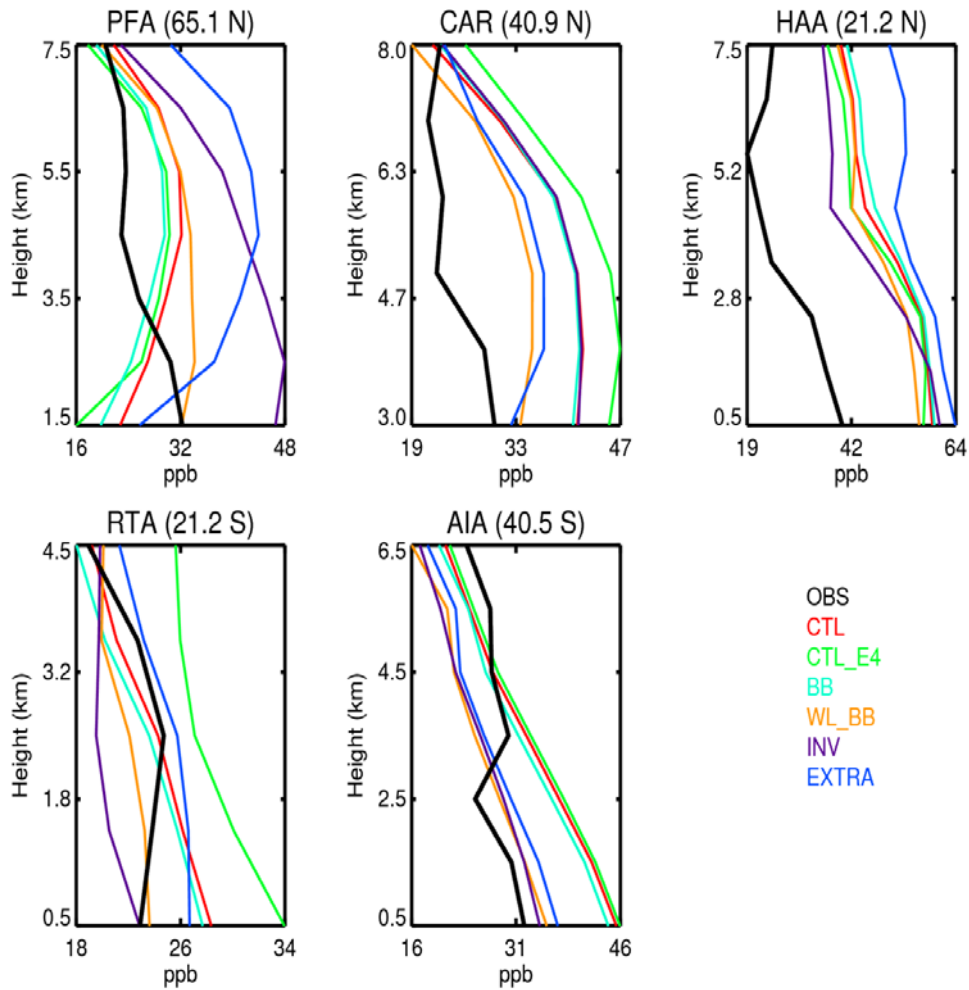


Fig. 6.7 Vertical profiles of monthly mean methane concentrations at the five GV sites sampled by aircraft. Rather than using the full extended record, the comparisons only include times when there are actual data. Solid lines show the profiles in January, and dashed lines show the profiles in July. The sites are ordered by decreasing latitude.

6.4 Conclusions

With simple atmospheric chemistry, ACCESS can be used to simulate atmospheric methane concentrations. Over a twenty-year time-period, the model captures the magnitude of tropospheric concentrations in the northern hemisphere and the tropics well during the second half of the simulation; however, during the last ten years the concentrations in the southern hemisphere are too low. The underestimated SH concentrations combined with an offset in the timing of the seasonal cycle yield inter-hemispheric differences that are a little larger than observed. This result supports the earlier conclusion that the inter-hemispheric mixing in ACCESS may be too slow, but preliminary results from the TransCom experiment suggests that ACCESS is giving similar inter-hemispheric differences to most other participating models. Overall the model realistically simulates atmospheric methane concentrations, and future analysis into the concentrations at Cape Grim will yield further understanding of the CH₄ fluxes over Australia.

7. FUTURE WORK

This study highlights several ongoing issues in ACCESS that should be addressed in the future. Since it is essential to conserve mass for both atmospheric CO₂ concentrations and atmospheric tracers, a more sophisticated mass fixing routine may be useful. While the simple mass fixer added did not significantly alter the near-surface concentration distribution, it applies a mass adjustment factor uniformly over the globe, which may overestimate the changes in locations with large surface fluxes.

The simulations in this report reveal several issues in atmospheric transport. The studies into the impact of various stable boundary layer parameterizations showed that the long tail scheme more closely matches observations than the sharpest scheme, which underestimates the nighttime and winter vertical mixing; however, even with the long tail scheme, the north-south gradient was overestimated. The slow inter-hemispheric transport was also noted in studies by UK colleagues (Fiona O'Connor, pers. comm.) and needs more investigation. It is unclear what contribution cross-hemisphere transport has versus the impact from underestimated boundary layer mixing in higher latitudes. In the stratosphere, using atmospheric concentrations in the top model level equal to the nearest lower level produces realistic results; but further investigation should be conducted regarding the mixing at the top of the model.

Since CABLE simulates photosynthesis and respiration, ACCESS can be used to evaluate the CABLE carbon fluxes using both surface fluxes as well as the atmospheric CO₂ tracer. Once CABLE realistically simulates current carbon fluxes, ACCESS can be used to investigate the impact of land cover change on the carbon cycle. In addition, current work is being done to improve the carbon cycle and to include the nitrogen and phosphorous cycle, and simulations with ACCESS with the enhanced CABLE version will be useful for a variety of applications.

One limitation for using ACCESS is the inability to accurately simulate real weather and synoptic variability. Modelled variables cannot be compared with observations on synoptic time-scales since the model currently uses a 360-day year with the climate driven solely by sea surface temperatures. A high priority should be to use a full calendar year and to have the capability to nudge to weather data.

ACKNOWLEDGMENTS

We acknowledge use of the Met Office Unified Model™ (UK) and appreciate the help of staff at the Met Office, particularly Chris Jones and Fiona O'Connor, who shared their expertise with us.

We sincerely thank Martin Dix for his tremendous help in setting up and running ACCESS. We wish to thank Eva Kowalczyk for all her hard work in coupling CABLE to the UM. We thank Jhan Srbinovsky for setting up the current configuration of vegetation and soil types in CABLE, and we thank Ying-Ping Wang and Bernard Pak for all their expertise with CABLE.

This work has been undertaken as part of the Australian Climate Change Science Program, funded jointly by the Department of Climate Change, the Bureau of Meteorology and CSIRO.

This research was undertaken on the NCI National Facility in Canberra, Australia, which is supported by the Australian Commonwealth Government.

The TransCom-continuous model simulations were provided by AM2/AM2t (S. Fan, S.-J. Lin), CCAM (R. M. Law), CCSR_NIES (P. Patra, M. Takigawa), CDTM (T. Maki), CHIMERE (C. Aulagnier, L. Rivier, R. Vautard), COMET (G. Pieterse, A. T. Vermeulen), DEHM (C. Geels, J. Brandt, J. H. Christensen), IFS (S. Serrar), IMPACT (D. J. Bergmann, P. J. Cameron-Smith), LMDZ/LMDZ_THERM (P. Bousquet, F. Delage), NICAM (Y. Niwa, R. Imasu, M. Satoh), NIES05 (S. Maksyutov, R. Onishi), PCTM.CSU (R. Lokupitiya, A. S. Denning, N. Parazoo, J. Kleist), PCTM.GSFC (S. R. Kawa, Z. Zhu), REMO (U. Karstens), STAG/STAGN (S. Taguchi), TM3_fg/TM3_vfg (C. Rödenbeck), TM5_glb3x2/TM5_nam1x1 (W. Peters, L. Bruhwiler), TM5_eur1x1 (M. C. Krol, S. Houweling).

REFERENCES

- Baker, D.F., Law, R.M., Gurney, K.R., Rayner, P., Peylin, P., Denning, A. S., Bousquet, P., Bruhwiler, L., Chen, Y.-H., Ciais, P., Fung, I.Y., Heimann, M., John, J., Maki, T., Maksyutov, S., Masarie, K., Prather, M., Pak, B., Taguchi, S. and Zhu, Z. 2006. TransCom 3 inversion inter-comparison: Impact of transport model errors on the interannual variability of regional CO₂ fluxes, 1988–2003. *Global Biogeochem. Cycles*, 20 (GB1002), doi:10.1029/2004GB002439.
- Bakwin, P.S., Tans, P.P., Hurst, D.F. and Zhao, C. 1998. Measurements of carbon dioxide on very tall towers: Results of the NOAA/CMDL program. *Tellus, Ser. B*, 50, 401–415.
- Barnes, R. 2008. Unified Model Documentation Paper C4: The Storage Handling and Diagnostic System (STASH). *Technical Report C4*, Met Office, U. K.
- Bergamaschi, P., Frankenberg, C., Meirink, J.F., Krol, M., Villani, M.G., Houweling, S., Dentener, F., Dlugokencky, E.J., Miller, J.B., Gatti, L.V., Engel, A. and Levin, I. 2009. Inverse modelling of global and regional CH₄ emissions using SCIAMACHY satellite retrievals. *J. Geophys. Res.*, 114 (D22301), doi:10.1029/2009JD012287.
- Biraud, S., Ciais, P., Ramonet, M., Simmonds, P., Kazan, V., Monfray, P., O’Doherty, S., Spain, G. and Jennings, S.G. 2002. Quantification of carbon dioxide, methane, nitrous oxide and chloroform emissions over Ireland from atmospheric observations at Mace Head. *Tellus, Ser. B*, 54, 41–60.
- Blake, D.R. and Rowland, F.S. 1988. Continuing worldwide increase in tropospheric methane, 1978 to 1987. *Science*, 239, 1129–1131.
- Bousquet, P., Ciais, P., Miller, J.B., Dlugokencky, E.J., Hauglustaine, D.A., Prigent, C., van der Werf, G.R., Peylin, P., Brunke, E.-G., Carouge, C., Langenfelds, R.L., Lathiere, J., Papa, F., Ramonet, M., Schmidt, M., Steele, L.P., Tyler, S.C. and White, J. 2006. Contribution of anthropogenic and natural sources to atmospheric methane variability. *Nature*, 443, 439–443, doi:10.1038/nature05132.
- Bowman, K.P. and Erukhimova, T. 2004. Comparison of global-scale Lagrangian transport properties of the NCEP reanalysis and CCM3. *J. Clim.*, 17, 1134–1146.
- Bratseth, A.M. 2003. Zonal-mean transport characteristics of ECMWF re-analysis data. *Q. J. R. Meteorol. Soc.*, 129, 2331–2346.
- Collins, W.J., Bellouin, N., Doutriaux-Boucher, M., Gedney, N., Hinton, T., Jones, C.D., Liddicoat, S., Martin, G., O’Connor, F., Rai, J., Senior, C., Totterdell, I., Woodward, S., Reichler, T., Kim, J. and Halloran, P. 2008. Evaluation of the HadGEM2 model. *Technical Report 74*, Hadley Centre, Met Office, U. K.
- Cox, P. 2001. Description on the TRIFFID dynamic global vegetation model. *Technical Report 24*, Hadley Centre, Met Office, U. K.
- Denman, K., Brasseur, G., Chidthaisong, A., Ciais, P., Cox, P.M., Dickinson, R.E., Hauglustaine, D., Heinze, C., Holland, E., Jacob, D., Lohmann, U., Ramachandran, S., da Silva Dias, P.L., Wofsy, S.C. and Zhang, X. 2007. Coupling between changes in the climate system and biogeochemistry. In *Climate Change 2007: The Physical Science Basis. Contribution of Working Group I to the Fourth Assessment Report of the Intergovernmental Panel on Climate Change*, edited by S. Solomon et al. pp. 499–587,

REFERENCES

Cambridge University Press, U.K.,

Denning, A.S., Holzer, M., Gurney, K.R., Heimann, M., Law, R.M., Rayner, P.J., Fung, I.Y., Fan, S.-M., Taguchi, S., Friedlingstein, P., Balkanski, Y., Taylor, J., Maiss, M. and Levin, I. 1999. Three-Dimensional Transport and Concentration of SF₆: A Model Inter-comparison Study (TransCom 2). *Tellus*, 51B, 266-297.

Dlugokencky, E.J., Masarie, K.A., Lang, P.M. and Tans, P.P. 1998. Continuing decline in the growth rate of the atmospheric methane burden. *Nature*, 393, 447-450.

Dlugokencky, E.J., Houweling, S., Bruhwiler, L., Masarie, K.A., Lang, P.M., Miller, J.B. and Tans, P.P. 2003. Atmospheric methane levels off: Temporary pause or a new steady-state? *Geophys. Res. Lett.*, 30 (19), doi:10.1029/2003GL018126.

Dlugokencky, E.J., Bruhwiler, L., White, J.W.C., Emmons, L.K., Novelli, P.C., Montzka, S.A., Masarie, K.A., Lang, P. M., Crotwell, A.M., Miller, J.B. and Gatti, L.V. 2009. Observational constraints on recent increases in the atmospheric CH₄ burden. *Geophys. Res. Lett.*, 36 (L18803), doi:10.1029/2009GL039780.

Dunn, A.L., Barford, C.C., Wofsy, S.C., Goulden, M.L. and Daube, B.C. 2007. A long-term record of carbon exchange in a boreal black spruce forest: Means, responses to interannual variability, and decadal trends. *Global Change Biol.*, 13, 577–590, doi:10.1111/j.1365-2486.2006.01221.x.

Etheridge, D.M., Steele, L.P., Francey, R.J. and Langenfelds, R.L. 1998. Atmospheric methane between 1000 A.D. and present: Evidence of anthropogenic emissions and climatic variability. *J. Geophys. Res.*, 103 (D13), 15979-15993.

Friedlingstein, P., Cox, P., Betts, R., Bopp, L., Von Bloh, W., Brovkin, V., Cadule, P., Doney, S., Eby, M., Fung, I., Bala, G., John, J., Jones, C., Joos, F., Kato, T., Kawamitya, M., Knorr, W., Lindsay, K., Matthews, H.D., Raddatz, T., Rayner, P., Reick, C., Roeckner, E., Schnitzler, K.-G., Schnur, R., Strassmann, K., Weaver, A.J., Yoshikawa, C. and Zeng, N. 2006. Climate-carbon cycle feedback analysis: Results from the C⁴MIP model inter-comparison. *J. Climate*, 19, 3337-3353.

Fung, I., John, J., Lerner, J., Matthews, E., Prather, M., Steele, L.P. and Fraser, P.J. 1991. Three-dimensional model synthesis of the global methane cycle. *J. Geophys. Res.*, 96, 13033-13065.

GLOBALVIEW-CH₄, 2009. Cooperative Atmospheric Data Integration Project – Methane. CD-ROM, NOAA ESRL, Boulder Colorado. [Also available on Internet via anonymous FTP to ftp.cmdl.noaa.gov, Path: ccg/ch4/GLOBALVIEW].

GLOBALVIEW-CO₂. 2009. Cooperative Atmospheric Data Integration Project - Carbon Dioxide. CD-ROM, NOAA CMDL, Boulder, Colorado. [Also available on Internet via anonymous FTP to ftp.cmdl.noaa.gov, Path: ccg/co2/GLOBALVIEW].

Gurney, K.R., Law, R.M., Denning, A.S., Rayner, P.J., Baker, D., Bousquet, P., Bruhwiler, L., Chen, Y.H., Ciais, P., Fan, S., Fung, I.Y., Gloor, M., Heimann, M., Higuruchi, K., John, J., Maki, T., Maksyutov, S., Masarie, K., Peylin, P., Prather, M., Pak, B.C., Randerson, J., Sarmiento, J., Taguchi, S., Takahashi, T. and Yuen, C.W. 2002. Towards robust regional estimates of CO₂ sources and sinks using atmospheric transport models. *Nature*, 415, 626-630.

Gurney, K.R., Law, R.M., Denning, A.S., Rayner, P.J., Pak, B.C., Baker, D., Bousquet, P., Bruhwiler, L., Chen, Y.-H., Ciais, P., Fung, I.Y., Heimann, M., John, J., Maki, T., Maksyutov, S., Peylin, P., Prather, M. and Taguchi, S. 2004. TransCom 3 inversion inter-comparison: Model mean results for the estimation of seasonal carbon sources and sinks. *Global Biogeochem. Cycles*, 18 (GB1010), doi:10.1029/2003GB002111.

Haszpra, L. 2006. Atmospheric CO₂ hourly concentration data, Hegyhatsal, in World Data Centre for Greenhouse Gases, Japan Meteorol. Agency, Tokyo. (Available at <http://gaw.kishou.go.jp/wdcgg.html>)

Hatakka, J. 2006. Atmospheric CO₂ hourly concentration data, Pallas, in World Data Centre for Greenhouse Gases, Japan Meteorol. Agency, Tokyo. (Available at <http://gaw.kishou.go.jp/wdcgg.html>).

Heald, C.L., Jacob, D.J., Jones, D.B.A., Palmer, P.I., Logan, J.A., Streets, D.G., Sachse, G.W., Gille, J.C., Hoffman, R.N. and Nehrkorn, T. 2004. Comparative inverse analysis of satellite (MOPITT) and aircraft (TRACE-P) observations to estimate Asian sources of carbon monoxide. *J. Geophys. Res.*, 109 (D23306), doi:10.1029/2004JD005185.

Hess, P.G. 2005. A comparison of two paradigms: The relative global roles of moist convective versus non-convective transport. *J. Geophys. Res.*, 110 (D20302), doi:10.1029/2004JD005456.

Higuchi, K., Worthy, D.E.J., Chan, D. and Shashkov, A. 2003. Regional source/sink impact on the diurnal, seasonal and inter-annual variations in atmospheric CO₂ at a boreal forest site in Canada, *Tellus, Ser., B*, 55, 115–125.

Hutyra, L., Munger, J.W., Saleska, S.R., Gottlieb, E.W., Daube, B.C., Dunn, A.L., Amaral, D.F., de Camargo, P.B. and Wofsy, S.C. 2007. Seasonal controls on the exchange of carbon and water in an Amazonian rainforest. *J. Geophys. Res.*, 112 (G03008), doi:10.1029/2006JG000365.

Inatomi, M. and Ito, A. 2008. Estimation for global terrestrial methane budget using a coupled carbon and nitrogen cycles model VISIT. *EOS Trans, AGU*, 90(52), Fall Meet. Suppl., Abstract B33B-0429.

Iwata, S. 2006. Atmospheric CO₂ hourly concentration data, Mikawa-Ichinomiya, in World Data Centre for Greenhouse Gases, Japan Meteorol. Agency, Tokyo. (Available at <http://gaw.kishou.go.jp/wdcgg.html>).

Kawa, S.R., Erickson III, D.J., Pawson, S. and Zhu, Z. 2004. Global CO₂ transport simulations using meteorological data from the NASA data assimilation system. *J. Geophys. Res.*, 109 (D18312), doi:10.1029/2004JD004554.

Kopacz, M., Jacob, D.J., Henze, D.K., Heald, C.L., Streets, D.G. and Zhang, Z. 2009. Comparison of adjoint and analytical Bayesian inversion methods for constraining Asian sources of carbon monoxide using satellite (MOPITT) measurements of CO columns. *J. Geophys. Res.*, 114 (D04305), doi:10.1029/2007JD009264.

Kim, J.-S. and Park, K.-J. 2006. Atmospheric CO₂ hourly concentration data, Anmyeon-do, in World Data Centre for Greenhouse Gases, Japan Meteorol. Agency, Tokyo. (Available at <http://gaw.kishou.go.jp/wdcgg.html>)

REFERENCES

- Law, R.M. et al. 1996. Variations in modelled atmospheric transport of carbon dioxide and the consequences for CO₂ inversions. *Global Biogeochem. Cycles*, 10, 783-796.
- Law, R.M. et al. 2008. TransCom model simulations of hourly atmospheric CO₂: Experimental overview and diurnal cycle results for 2002. *Global Biogeochem. Cycles*, 22 (GB3009), doi:10.1029/2007GB003050.
- Law, R.M. and Corbin, K.D. 2010. Simulating the atmospheric transport of CO₂ and SF₆ using the UK Met Office Unified Model. *CAWCR Research Letters*, 2, 18-24.
- Lintner, B.R., Buermann, W., Koven, C.D. and Fung, I.Y. 2006. Seasonal circulation and Mauna Loa CO₂ variability. *J. Geophys. Res.*, 111 (D13104), doi:10.1029/2005JD006535.
- Lueker, T.J., Walker, S.J., Vollmer, M.K., Keeling, R.F., Nevison, C.D., Weiss, R.F. and Garcia, H.E. 2003. Coastal upwelling air-sea fluxes revealed in atmospheric observations of O₂/N₂, CO₂ and N₂O. *Geophys. Res. Lett.*, 30(6), 1292, doi:10.1029/2002GL016615.
- Miyazaki, K., Patra, P.K., Takigawa, M., Iwasaki, T. and Nakazawa, T. 2008. Global-scale transport of carbon dioxide in the troposphere. *J. Geophys. Res.*, 113 (D15301), doi:10.1029/2007JD009557.
- Miyazaki, K., Machida, T., Patra, P.K., Iwasaki, T., Sawa, Y., Matsueda, H. and Nakazawa, T. 2009. Formation mechanisms of latitudinal CO₂ gradients in the upper troposphere over the subtropics and tropics. *J. Geophys. Res.*, 114 (D03306), doi:10.1029/2008JD010545.
- Morgenstern, O., Braesicke, P., O'Connor, F.M., Bushell, A.D., Johnson, C.E., Osprey, S.M. and Pyle, J.A. 2009. Evaluation of the new UKCA climate-composition model – Part I: The stratosphere. *Geosci. Model Dev.*, 2, 43-57.
- Muto, Y. 2006. Atmospheric CO₂ hourly concentration data, Kisai, Mt. Dodaira, in World Data Centre for Greenhouse Gases, Japan Meteorol. Agency, Tokyo. (Available at <http://gaw.kishou.go.jp/wdceg.html>)
- O'Connor, F.M., Boucher, O., Gedney, N., Jones, C.D., Folberth, G.A., Coppel, R., Friedlingstein, P., Collins, W.J., Chappallaz, J., Ridley, J. and Johnson, C.E. 2010. Possible role of wetlands, permafrost and methane hydrates in the methane cycle under future climate change: A review. *Rev. Geophys.*, 48, RG4005, doi:10.1029/2010RG000326.
- Olivier, J.G.J., Van Aardenne, J.A., Dentener, F., Pagliari, V., Ganzeveld, L.N. and Peters, J.A.H.W. 2005. Recent trends in global greenhouse gas emissions: regional trends 1970-2000 and spatial distribution of key sources in 2000. *Env. Sc.*, 2 (2-3), 81-99, doi: 10.1088/15693430500400345.
- Palmer, P.I., Jacob, D.J., Jones, D.B.A., Heald, C.L., Yantosea, R.M., Logan, J.A., Sachse, G.W. and Streets, D.G. 2003. Inverting for emissions of carbon monoxide from Asia using aircraft observations over the western Pacific. *J. Geophys. Res.*, 108 (D218828), doi:10.1029/2003JD003397.
- Patra, P.K., Law, R.M., Peters, W., Rödenbeck, C., Takigawa, M., Aulagnier, C., Baker, I., Bergmann, D.J., Bousquet, P., Brandt, J., Bruhwiler, L., Cameron-Smith, P.J., Christensen, J.H., Delage, F., Denning, A.S., Fan, S., Geels, C., Houweling, S., Imasu, R., Karstens, U., Kawa, S.R., Kleist, J., Krol, M.C., Lin, S.-J., Lokupitiya, R., Maki, T., Maksyutov, S., Niwa, Y., Onishi, R., Parazoo, N., Pieterse, G., Rivier, L., Satoh, M., Serrar, S., Taguchi, S., Vautard, R., Vermeulen, A.T.

- and Zhu, Z. 2008. TransCom model simulations of hourly atmospheric CO₂ : Analysis of synoptic-scale variations for the period 2002–2003. *Global Biogeochem. Cycles*, 22 (GB4013), doi:10.1029/2007GB003081.
- Patra, P. K., Houweling, S., Krol, M., Bousquet, P., Bruhwiler, L. and Jacob, D. 2010, Protocol for TransCom CH₄ intercomparison, Version 7, April.
(available online at www.jamstec.go.jp/frcgc/research/d4/prabir/papers/TC_CH4protocol_v7.pdf).
- Plumb, R.A. and Mahlman, J.D. 1987. The zonally averaged transport characteristics of the GFDL general circulation/tracer model. *J. Atmos. Sci.*, 44, 298-327.
- Prather, M.J., Ehhalt, D., Dentener, F., Derwent, R.G., Dlugokencky, E., Holland, E., Isaksen, I.S.A., Katima, J., Kirchhoff, V., Matson, P., Midgley, P.M. and Wang, M. 2001. Atmospheric chemistry and greenhouse gases. In *Climate Change 2001: The Scientific Basis. Contributions of Working Group I to the Third Assessment Report of the IPCC*, edited by J. T. Houghton et al. pp. 239-287, Cambridge University Press, New York.
- Ramaswamy, V., Boucher, O., Haigh, J., Hauglustaine, D., Haywood, J., Myhre, G., Nakajima, T., Shi, G.Y. and Solomon, S. 2001. Radiative forcing of climate change. In *Climate Change 2001: The Scientific Basis. Contributions of Working Group I to the Third Assessment Report of the IPCC*, edited by J. T. Houghton et al. pp. 239-287, Cambridge University Press, New York.
- Randerson, J.T., van der Werf, G.R., Giglio, L., Collatz, G.J. and Kasibhatla, P.S. 2007. Global fire emissions database, version 2 (GFEDv2.1). Data set. Available on-line [<http://daac.ornl.gov/>] from Oak Ridge National Laboratory Distributed Active Archive Center, Oak Ridge, Tennessee, U.S.A., doi: 10.3334/ORNLDAAAC/849.
- Rayner, P.J. and Law, R.M. 1995. A comparison of modelled responses to prescribed CO₂ Sources. CSIRO Division of Atmospheric Research. *Technical Paper No. 36*.
- Ringeval, B., de Noblet-Ducoudre, N., Ciais, P., Bousquet, P., Prigent, C., Papa, F. and Rossow, W. 2010. An attempt to quantify the impact of changes in wetland extent on methane emissions on the seasonal and interannual time scales. *Global Biogeochem. Cycles*, 24 (GB2003), doi:10.1029/2008GB003354.
- Rödenbeck, C., Houweling, S., Gloor, M. and Heimann, M. 2003. CO₂ flux history 1982-2001 inferred from atmospheric data using a global inversion of atmospheric transport. *Atmos. Chem. Phys.*, 3, 1919-1964.
- Sasaki, H. 2006. Atmospheric CO₂ hourly concentration data, Ryori, in World Data Centre for Greenhouse Gases, Japan Meteorol. Agency, Tokyo.
(Available at <http://gaw.kishou.go.jp/wdcgg.html>).
- Strahan, S.E., Douglass, A.R., Nielsen, J.E. and Boering, K.A. 1998. The CO₂ seasonal cycle as a tracer of transport. *J. Geophys. Res.*, 103, 13,729-13,741.
- Tiwari, Y.K., Gloorm, M., Engelen, R.J., Chevallier, F., Rodenbeck, C., Korner, S., Peylin, P., Braswell, B.H. and Heimann, M. 2006. Comparing CO₂ retrieved from Atmospheric Infrared Sounder with model predictions: Implications for constraining surface fluxes and lower-to-upper tropospheric transport. *J. Geophys. Res.*, 111 (D17106), doi:10.1029/2005JD006681.

REFERENCES

- Tohjima, Y., Mukai, H., Machida, T., Fujinuma, Y. and Katsumoto, M. 2006. Atmospheric CO₂ hourly concentration data, Cape Ochi-ishi, in World Data Centre for Greenhouse Gases, Japan Meteorol. Agency, Tokyo. (Available at <http://gaw.kishou.go.jp/wdcgg.html>)
- Uhse, K. and Meinhardt, F. 2006. Atmospheric CO₂ hourly concentration data, Deuselbach, Neuglobsow, Schauinsland, Westerland, Zingst, Zugspitze/ Schneefernerhaus, in World Data Centre for Greenhouse Gases, Japan Meteorol. Agency, Tokyo. (Available at <http://gaw.kishou.go.jp/wdcgg.html>)
- Urbanski, S., Barford, C., Wofsy, S., Kucharik, C., Pyle, E., Budney, J., McKain, K., Fitzjarrald, D., Czikowsky, M. and Munger, J.W. 2007. Factors controlling CO₂ exchange on timescales from hourly to decadal at Harvard Forest. *J. Geophys. Res.*, 112 (G02020), doi:10.1029/2006JG000293.
- Van Aardenne, J., Monni, S., Olivier, J., Doering, U., Pagliari, V., Peters, J., SanMartin, F., Orlandini, L. and Maenhout, G. 2009. EDGAR v 4.0: A global perspective on emissions in developed and developing countries. Global Emissions Inventory Activity (GEIA), *Emissions of Gases and Aerosols Progress and Modeling Needs Conference*, Oslo, Norway, 228 October.
- Villani, M.G., Bergamaschi, P., Krol, M., Meirink, J.F. and Dentener, F. 2010. Inverse modelling of European CH₄ emissions: sensitivity to the observational network. *Atmos. Chem. Phys.*, 10, 1249-1267.
- Wilson, D.R. and Bushell, A.C. 2007. The PC2 cloud scheme. *Unified Model documentation paper 29*, available from the UK Met Office.
- Wilson, D.R., Bushell, A.C., Kerr-Munslow, A.M., Price, D. and Morcrette, C. 2008. PC2: A prognostic cloud fraction and condensation scheme. Part I: Scheme description. *Q. J. R. Meteorol. Soc.*, 134 (637), 2093-2107, doi:10.1002/qj.333.
- Yan, X., Yagi, K., Akiyama, H. and Akimoto, H. 2005. Statistical analysis of the major variables controlling methane emission from rice fields. *Global Change Biology*, 11, 1131-1141.

APPENDIX A – MODIFIED ROUTINES IN ACCESS

Atmosphere Routines

Boundary_Layer

Bl_tracer_intctl.F90

- Added tracer fluxes into call to bl_trmix_dd.

Bl_trmix_dd.F90

- Added tracer fluxes into surface level of atmospheric tracers.
- Commented code that copied diagnostic information into tracer fluxes.
- Uncommented code to add CABLE fluxes into CO₂ array.

Short_Wave_Radiation

Glue_rad-rad_ctl3c.F90

- Added L_CO2_RADIATION in call to subroutine.
- Set L_CO2_3D to the switch L_CO2_RADIATION, which is specified in the CNTLATM scrip file.

Ni_rad_ctl.F90

- Added L_CO2_RADIATION in call to this subroutine.
- Added L_CO2_RADIATION in call to glue_rad subroutine.

Tracer_advection

Sl_tracer2-sltrac2_2a.F90

- Commented out calls to q_pos_ctl, allowing tracers to be negative.

Tracer_mass.F90

- Modified routine for calculating tracer mass.

Control Routines

Ancillaries

Inancila-inanca1a.F90

- In D1 references, switched to using stash SI array to allow any sections to be used for the tracer fluxes, which are in section three.
- Changed the filename variable for ancillary files to include user-specified names in the setup script UPANCA (set FINPUT=1 and FNAME='filename' for each UPANCA field), rather than using environmental variables only.

Replanca-rpanca1a.F90

- Added tracer fluxes to be copied from saved ancillary data into the main D1 storage array.

Top Level

Addres.F90

- Added boundary layer section to looping of prognostic variables for STASH information and array allocation.

Atm_fields_mod.F90

- Added tracer flux variables to store the data for reference, rather than having to use the D1 array.

Atm_step.F90:

- Added L_CO2_RADIATION switch in call to atmos_physics1.
- Added tracer flux variables in call to atmos_physics2 in order to pass variables along to surface routine, where they will be added into the atmosphere.
- Put in the call to the tracer mass fixer routine.
- Put in calls to atmospheric loss for methane, MCF, and radon.

Atmos_physics1.F90

- Added L_CO2_RADIATION in call.
- Added L_CO2_RADIATION in call to ni_rad_ctl.

Atmos_physics2.F90

- Added tracer fluxes and global CO₂ emissions in call.
- Added tracer fluxes and global CO₂ emissions in call to ni_imp_ctl.

Glue_rad-rad_ctl2.F90

- Added switch L_CO2_RADIATION to control 3-D CO₂ interaction with radiation.

Inancctl.F90

- Added SI array and three other diagnostics into INANCILA call.

Ni_imp_ctl.F90

- Added tracer flux variables in sub-routine call.
- Added tracer flux variables in call to bl_tracer_intctl.
- Added call to tracer_fluxemit to calculate global CO₂ emissions.

Scm_main.F90

- Added tracer flux variables to atmos_physics2 call.

Set_atm_fields.F90

- Set tracer flux variables to data stored in D1 array, which allows the fluxes to be called by simple tracer_flux names.

Set_atm_pointers.F90

- Set pointers for the flux variables.

Include Routines

Argument

Arg_atm_fields.h

- Added tracer fluxes.

Common

Cancila.h

- Added variables to store ancillary file names.

Cntlratm.h

- Added various control switches:
 - CABLE (L_CABLE)
 - CO₂ radiation interaction (L_CO2_RADIATION)
 - CO₂ mass fixer (L_CO2_MASS)
 - Tracer mass fixer (L_TRACER_MASS)
 - Methane atmospheric loss (L_METHANE_LOSS)
 - MCF atmospheric loss (L_MCF_LOSS)
 - Radon decay (L_RADON_DECAY)
- Added various integer values to store user settings:
 - Number of tracer to start mass fixer (I_TRACERMASS_START)
 - Number of methane tracers (I_METHANE_TRACERS)
 - Number of the radon tracer (I_RADON_TRACERNUMBER)
 - Number of the MCF tracer (I_MCF_TRACERNUMBER)
- Added variables to store CO₂ emissions mass (CO2EMITMASS)
- Added variable to store CO₂ and tracer mass (TMASS(21))

S_mainn.h

- Added tracer fluxes.

Typ_atm_fields.h

- Declared/added tracer fluxes.

Typptr.h

- Added integer pointers for tracer fluxes.

Constant**Cancmaxa.h**

- Increased maximum number of ancillary fields.

Canctita.h

- Added title names for tracer flux variables.

Declaration**S_maina.h**

- Added tracer fluxes.

Other**Canclsta.h**

- Added tracer fluxes to cross-reference list of ancillary fields.

Cancftna.h

- Added file unit numbers for tracer fluxes.

Utility Routines**Qxreconf****Calc_nlookups_mod.F90**

- Modified the file name containing ancillary files from an environmental variable to a local saved name in order to include user files. The tracer fluxes are currently specified as user fields using user files for initialization and updating. For initialization, the files containing the flux fields are specified in the RECONA script, under the ITEMS section, with USER_PROG Ancil_File. For updating, the files containing the flux fields are specified in the CNTLATM script, under the UPANCA section, in the FNAME field.

Inancila-rcf_inancila.F90

- Modified the file name containing ancillary files from an environmental variable to a local saved name in order to include user files. If reading the filename from an environmental variable fails, then try to find a filename for the ancillary field that needs updating from the specified filename in the CNTLATM script, under the UPANCA section, in the FNAME field.

Rcf_address_mod.F90

- Added the boundary layer section to be included with prognostic variables for the reconfiguration.

Rcf_ancil_atmos_mod.F90

- Added user ancillary fields and files lists to be processed in the reconfiguration for the tracer fluxes.

Rcf_aux_file_mod.F90

- Commented out reading of tracers line to avoid duplication.

Rcf_create_dump_mod.F90

- Replaced reading the tracer initialization file from an environmental variable to the file specified in RECONA, under the ITEMS section, with USER_PROG Ancil_File.

Rcf_set_data_source_mod.F90

- Added boundary layer initialization to prognostic variable initialization, setting the fields to zero.

Rcf_stashcodes_mod.F90: Added stascode_bl_sec parameter, which is the section including the tracer flux variables.

Replanca-rcf_replanca.F90

- Modified the file name containing ancillary files for initialization from an environmental variable to a local saved name. The file names for the necessary field are specified in the RECONA script, under the ITEMS section, with USER_PROG Ancil_File.

APPENDIX B – NEW ROUTINES IN ACCESS

Atmosphere Routines

Tracer_advection

Tracer_methaneloss.F90

- Calculates loss of methane in atmospheric tracers due to OH and stratospheric Cl and O¹D reactions.

Tracer_fluxemit.F90

- Calculates global surface emissions total for mass conservation routine.

Tracer_massfix.F90

- Adjusts atmospheric tracer concentrations to conserve mass.

Tracer_massinit.F90

- Calculates the initial values for conserving tracer mass.

Tracer_massprint.F90

- Prints atmospheric tracer mass and emissions into the standard output.

Tracer_mcfloss.F90

- Calculates the atmospheric loss of MCF from ocean deposition, OH reactions, and stratospheric photolysis loss.

Tracer_radondecay.F90

- Calculates the decay rate of radon.

APPENDIX C – MASS CONSERVATION SUBROUTINE

This appendix includes the code for the simple mass fix routine. The routine is called from the main control routine for each atmospheric time-step, `ATM_STEP.F90`. As inputs, the routine requires a number of basic atmospheric variables from the UM, in addition to the CO₂ and tracer fields, the mass of the surface emissions for the CO₂ tracer, the surface fluxes for the atmospheric tracers, and the previous atmospheric mass for CO₂ and the tracers. Two flags, one for the CO₂ tracer (`L_CO2_MASS`) and one for atmospheric tracers (`L_TRACER_MASS`), are also passed to the subroutine to determine whether to alter the mass.

If `L_CO2_MASS` is set to true, the routine alters the mass of the CO₂ tracer by forcing the model atmospheric mass in the current time-step to equal the CO₂ mass from the previous time-step plus the specified mass of the surface emissions. To calculate the global CO₂ atmospheric mass for the current time-step, the subroutine calls a routine already included in the UM to calculate the global atmospheric mass for the CO₂ tracer and the dry mass of the atmosphere. The mass of the CO₂ surface emissions is calculated in `NI_IMP_CTL.F90` using the total CO₂ flux, which is calculated in the `BL_TRMIX_DD.F90` subroutine. The total CO₂ flux currently includes the land fluxes and the emissions provided by the user in the `CO2_EMITS` file. Once the current CO₂ mass is calculated, the atmospheric mass and input mass of the surface fluxes are divided by the dry mass of the atmosphere, to conserve the mixing ratio in attempt to remove changes in the dry mass of the atmosphere. The surface emissions are added to the CO₂ mass from the previous time-step, and the factor required to conserve mass is calculated by dividing the calculated mass from the previous time-step added to the emissions by the CO₂ mass from the current time-step. The subroutine then alters the CO₂ concentrations by multiplying by the factor necessary to adjust the concentrations to conserve mass. Following the calculation, the previous mass variable is updated to the current mass for the next time-step.

If `L_TRACER_MASS` is set to true, the routine alters the mass of the free atmospheric tracers. Since many different species can be used in the free tracers, the routine only conserves mass for the tracers above a specified tracer number, `I_TRACERMASS_START`. This allows the user to only conserve mass for a select number of tracers, rather than requiring all tracers to conserve mass. The `I_TRACERMASS_START` variable is set in the `CNTLATM` script via a hand edit. The procedure to conserve mass for the free atmospheric tracers is the same as for the CO₂ tracer. For any tracers defined about the specified value, the routine calculates the atmospheric mass as well as the mass of the surface emissions provided in the tracer flux input variables. The masses are converted to mixing ratios, a new mass is calculated by adding the mass of the tracer from the previous time-step to the emissions, and a fixing factor is calculated by dividing the new mass calculated from the previous time-step by the current mass. The fix factor is then multiplied to the tracer array to scale the concentrations to match the conserved value, and the mass stored for the previous time-step is updated to the current mass.

```

SUBROUTINE TRACER_MASSFIX( &
&   row_length, rows, model_levels & !Array sizes
&   ,tr_levels, tr_vars, min_tracer & !Tracer info
&   ,halo_i, halo_j, offx, offy, mype & !UM info
&   ,timestep,timestep_number & !Timestep info
&   ,r_theta_levels, r_rho_levels & !Vars for mass calc
&   ,exner_theta_levels & !Var for mass calc
&   ,FV_cos_theta_latitude, delta_lambda, delta_phi & !Area info
&   ,RHO, q, qcl, qcf & !Moisture variables
&   ,L_CO2_MASS, L_TRACER_MASS & !CO2 and Tracer Flags
&   ,CO2, tracer & !CO2 and tracer 3-D fields
&   ,co2emitmass & !CO2 flux mass
&   ,tracer_flux1,tracer_flux2,tracer_flux3 & !Tracer fluxes
&   ,tracer_flux4,tracer_flux5,tracer_flux6 &
&   ,tracer_flux7,tracer_flux8,tracer_flux9 &
&   ,tracer_flux10,tracer_flux11,tracer_flux12 &
&   ,tracer_flux13,tracer_flux14,tracer_flux15,tracer_flux16 &
&   ,tracer_flux17,tracer_flux18,tracer_flux19,tracer_flux20 &
&   ,prevco2mass,prevtmass & !Previous CO2 and tracer mass
&   )

```

IMPLICIT NONE

```

!-----
!INPUT variables
!-----

```

```

INTEGER :: row_length, rows, model_levels
INTEGER :: tr_levels, tr_vars, min_tracer
INTEGER :: halo_i, halo_j, offx, offy, mype, timestep_number
REAL    :: delta_lambda,delta_phi,timestep
REAL    :: prevco2mass,prevtmass(20)
LOGICAL :: L_CO2_MASS, L_TRACER_MASS

```

```

REAL
&   R_THETA_LEVELS(1-halo_i:row_length+halo_i, &
&   1-halo_j:rows+halo_j,0:model_levels) &
&   R_RHO_LEVELS(1-halo_i:row_length+halo_i, &
&   1-halo_j:rows+halo_j,0:model_levels) &
&   EXNER_THETA_LEVELS(1-offx:row_length+offx, &
&   1-offy:rows+offy,model_levels) &
&   FV_cos_theta_latitude(1-offx:row_length+offx, &
&   1-offy:rows+offy) &
&   RHO(1-offx:row_length+offx,1-offy:rows+offy, &
&   model_levels) &
&   q(1-halo_i:row_length+halo_i,1-halo_j:rows+halo_j, &
&   model_levels) &
&   qcl(1-halo_i:row_length+halo_i, &
&   1-halo_j:rows+halo_j,model_levels) &
&   qcf(1-halo_i:row_length+halo_i, &
&   1-halo_j:rows+halo_j,model_levels) &
&   CO2(1-offx:row_length+offx, &
&   1-offy:rows+offy,model_levels) &
&   tracer(1-offx:row_length+offx,1-offy:rows+offy, &
&   tr_levels,tr_vars)

```

```

REAL                                &
& co2emitmass                        &
&, tracer_flux1(row_length,rows), tracer_flux2(row_length,rows) &
&, tracer_flux3(row_length,rows), tracer_flux4(row_length,rows) &
&, tracer_flux5(row_length,rows), tracer_flux6(row_length,rows) &
&, tracer_flux7(row_length,rows), tracer_flux8(row_length,rows) &
&, tracer_flux9(row_length,rows), tracer_flux10(row_length,rows) &
&, tracer_flux11(row_length,rows), tracer_flux12(row_length,rows) &
&, tracer_flux13(row_length,rows), tracer_flux14(row_length,rows) &
&, tracer_flux15(row_length,rows), tracer_flux16(row_length,rows) &
&, tracer_flux17(row_length,rows), tracer_flux18(row_length,rows) &
&, tracer_flux19(row_length,rows), tracer_flux20(row_length,rows)

!-----
!LOCAL variables
!-----
REAL :: tempracer(row_length+2*offx,rows+2*offy,model_levels)
REAL :: tempflux(row_length,rows)
REAL :: traceremitval,co2emitppm
REAL :: field1mass,field2mass,field3mass,drymass
REAL :: badco2mass,newco2mass,co2fixfactor
REAL :: temitppm(tr_vars)
REAL :: badtmass(tr_vars),newtmass(tr_vars),tfixfactor(tr_vars)
INTEGER, parameter :: flux_vars=20
INTEGER :: i,n_tr
CHARACTER*2 :: tnumber

!-----
!Fix CO2 Mass
!-----
IF (L_CO2_MASS) THEN

!Calculate tracer mass and dry atmospheric mass
!DEPENDS ON: tracer_mass
call tracer_mass(      &
  halo_i, halo_j, offx, offy, &
  offx, offy, 1, &
  row_length, rows, rows, &
  model_levels,model_levels,model_levels, &
  r_theta_levels,r_rho_levels, &
  FV_cos_theta_latitude,delta_lambda,delta_phi, &
  rho, q, qcl, qcf, &
  CO2,CO2,CO2, &
  exner_theta_levels,"Tracer_Mass: Fixing Mass ", &
  timestep_number,-99, &
  field1mass,field2mass,field3mass,drymass)

!Convert to ppm
badco2mass=field1mass/drymass
co2emitppm=co2emitmass/drymass
newco2mass=prevco2mass+co2emitppm

```

APPENDIX C – MASS CONSERVATION SUBROUTINE

```

!Calculate fix factor
  co2fixfactor=newco2mass/badco2mass

!Change CO2 concentrations:
  CO2(:, :, :) = CO2(:, :, :) * co2fixfactor

!Write out results to output file
if (mype == 0) then
  write(6,*) "
  write(6,*) 'TRACER_MASSFIX: Re-setting CO2 mass'
  write(6,*) 'Prev CO2 Mass: ', prevco2mass, ' CO2 emit: ', co2emitppm
  write(6,*) 'Bad CO2 Mass: ', badco2mass, ' New CO2 Mass: ', newco2mass
  write(6,*) 'CO2 Fix Factor: ', co2fixfactor
endif

!Update previous mass
  prevco2mass = prevco2mass + co2emitppm
ENDIF

!-----
!Fix Tracer Mass
!-----
if (L_TRACER_MASS) then
if (tr_vars .gt. flux_vars) then
  write(6,*) 'ERROR FIXING TRACER MASS: Too many tracers'
  write(6,*) ' Only fixing mass for ', flux_vars, ' tracers'
  n_tr = flux_vars
else
  n_tr = tr_vars
endif
do i = min_tracer, n_tr

  Select Case (i)
  Case (1)
    !Tracer Flux 1
    tempflux(:, :) = TRACER_FLUX1(:, :)

    . (Fluxes for tracers 1-20 are specified from individual arrays)
    .
    .

  Case (20)
    !Tracer Flux 20
    tempflux(:, :) = TRACER_FLUX20(:, :)

  End Select

  tempracer(:, :, :) = tracer(:, :, 1:model_levels, i)

!Calculate tracer mass and dry atmospheric mass
!DEPENDS ON: tracer_mass

```

```

call tracer_mass(      &
  halo_i, halo_j, offx, offy, &
  offx, offy, 1,      &
  row_length, rows, rows, &
  model_levels,model_levels,model_levels, &
  r_theta_levels,r_rho_levels, &
  FV_cos_theta_latitude,delta_lambda,delta_phi, &
  rho, q, qcl, qcf, &
  temptracer,temptracer,temptracer, &
  exner_theta_levels,"Tracer_Mass: Fixing Mass  ", &
  timestep_number,-99, &
  field1mass,field2mass,field3mass,drymass)

!Calculate global emissions
!DEPENDS ON: tracer_fluxemit
call tracer_fluxemit(row_length, rows, mype, timestep, &
  tempflux,offx,offy, &
  FV_cos_theta_latitude, delta_lambda, delta_phi, traceremitval)

!Check to make sure tracer is being used and mass is not 0
If (traceremitval .ne. 0.) Then
  !Convert to ppm
  badtmass(i)=field1mass/drymass
  temitppm(i)=traceremitval/drymass
  newtmass(i)=prevtmass(i)+temitppm(i)

  !Calculate fix factor
  tfixfactor(i)=newtmass(i)/badtmass(i)

  !Change tracer concentrations:
  tracer(:, :, 1:model_levels, i)=temptracer(:, :, :)*tfixfactor(i)

  !Write out results to output file
  if (mype == 0) then
    write(tnumber,989) i
    write(6,*) "
    write(6,*) 'TRACER_MASSFIX: Re-setting tracer ',tnumber,' mass'
    write(6,*) ' Prev: ',prevtmass(i),' Emit: ', temitppm(i)
    write(6,*) ' Bad Mass: ',badtmass(i),' New: ',newtmass(i)
    write(6,*) ' Fix Factor: ',tfixfactor(i)
  endif
  989 format(i2.2)

  !Update previous mass
  prevtmass(i) = prevtmass(i)+temitppm(i)
  Endif !emitval ne 0.
enddo !loop over tracers
endif !l_tracer_mass
RETURN
END SUBROUTINE TRACER_MASSFIX

```

APPENDIX D – METHODOLOGY TO UTILIZE THE ATMOSPHERIC CO₂ TRACER

D.1 UMUI checklist to turn on the atmospheric CO₂ tracer

In Input/Output -> User hand edit files, add the co2.ed hand edit file (provided below).

The hand edit file sets up the UM to use atmospheric concentrations by adding the following commands to the UM job scripts:

- Turns on interactive CO₂ (L_CO2_INTERACTIVE=.TRUE.)
- Sets short-wave radiation scheme to constant CO₂ concentration (L_CO2_RADIATION=.FALSE.)
- Turns on the mass fix routine to conserve the atmospheric CO₂ mass
- Initializes the CO₂ flux from a file to 0 (ITEM=251,SOURCE=3)
 - Required regardless if using emissions from a file, as this variable is automatically allocated if the CO₂ interactive scheme is turned on
- Initializes the CO₂ concentrations 380 ppm (ITEM=252, SOURCE=6, USER_PROG_RCONST=5.766e-04)

Note: If the model application requires CO₂ fluxes specified from a file to be added into the land surface fluxes from CABLE for inclusion in the CO₂ atmospheric tracer, then add the co2_emits.ed hand edit file to the list of hand edit files (provided below). This hand edit performs the following commands:

- Turns on the CO₂ emissions flag to combine the fluxes from a file with the land surface fluxes from CABLE into the total carbon flux that is to be contributed to the atmospheric CO₂ concentration (L_CO2_EMITS=.TRUE.)
- Specifies the name of the file containing the CO₂ emissions (CO2EMITS)
- Initializes the CO₂ fluxes to the emissions specified in the file (ITEM=251, SOURCE=2)
- Adds the CO₂ flux to the list of variables to be updated throughout the run, with hourly updates (UPANCA ANC_REF_NO=78, PERIOD=4, INTERVAL=1)
 - For the timing, PERIOD=4 -> hour; 3-> day; 2 -> month
 - If the fluxes are constant, the changes to the UPANCA section can be removed

In Atmosphere ->-Scientific Parameters and Sections -> General Physics Constants

- Make sure the specification of CO₂ absorption is set to the simple method
- Set the CO₂ mass mixing ratio to use for the radiation scheme
 - 5.766e-04 is 380 ppm
 - If L_CO2_RADIATION=.TRUE., then this value is ignored

In Atmosphere -> STASH -> STASH

- Add the atmospheric CO₂ concentrations (section 0, item 252) to the model output
 - Units of mass mixing ratio (kg kg⁻¹)
 - Multiply by 10⁶ * (29/44) to convert to ppm
- Add the total CO₂ flux (section 3, item 327) to the model output
 - Flux units of kg CO₂ m⁻² s⁻¹
 - Multiply by 10⁹/44 to convert to μmol m⁻² s⁻¹
- If CO₂ emissions from a file are being included into the CO₂ tracer, add these fluxes to the model output (section 0, item 251)

D.2 CO₂ concentration hand edit file (CO2.ed)

```

#!/bin/ksh
#
#Hand edit file for CO2 concentrations.
#Turns on interactive CO2, but not 3-D radiation interaction
#Turns on CO2 mass fix
#Initializes CO2 field to 380 ppm

ed CNTLATM <<\EOF
/L_CO2_INTERACTIVE/
a
L_CO2_INTERACTIVE=.TRUE.,
L_CO2_RADIATION=.FALSE.,
L_CO2_MASS=.TRUE.
.
w
q
EOF

ed CONTCNTL <<\EOF
/L_CO2_INTERACTIVE/
a
L_CO2_INTERACTIVE=.TRUE.,
.
w
q
EOF

ed RECONA <<\EOF
/L_CO2_INTERACTIVE/
a
L_CO2_INTERACTIVE=.TRUE.,
.
/!!! Atmos user-prognostic fields !!!/
c
&ITEMS SECTION=0, ITEM=251, DOMAIN=1, SOURCE=3, /
&ITEMS SECTION=0, ITEM=252, DOMAIN=1, SOURCE=6,
USER_PROG_RCONST=5.766e-04, /
.
w
q
EOF

```

D.3 CO₂ flux hand edit file (CO₂_emits.ed)

```

#!/bin/ksh
#Hand edit file for CO2 fluxes in CO2_EMITS.
#Turns on CO2_EMITS variable and sets CO2_EMITS filename
#Initializes to CO2_EMITS file values
# For initialization, SOURCE=2 -> ancillary file, 3 -> zero
#Sets CO2_EMITS to update every hour
# For timing, PERIOD=4 -> hour; 3 -> day; 2 -> monthly

ed CONTCNTL <<\EOF
/L_CO2_EMITS/
a
L_CO2_EMITS= .TRUE.,
.
w
q
EOF

ed INITHIS <<\EOF
/CO2EMITS= 'CO2EMITS : '/
c
CO2EMITS= 'CO2EMITS : /short/p66/kxc599/ancil-files/CASA3hr_N48.anc',
.
w
q
EOF

ed RECONA <<\EOF
/L_CO2_EMITS/
a
L_CO2_EMITS= .TRUE.
.
/ITEMS/
a
&ITEMS ITEM=251, DOMAIN=1, SOURCE=2, /
.
w
q
EOF

ed CNTLATM <<\EOF
/L_CO2_EMITS/
a
L_CO2_EMITS= .TRUE.,
.
/UPANCA/
a
&UPANCA ANC_REF_NO=78, PERIOD=4, INTERVAL=1 /
.
w
q
EOF

```

APPENDIX E – METHODOLOGY TO UTILIZE ATMOSPHERIC TRACERS

E.1 UMUI checklist to use atmospheric tracers with prescribed CO₂/SF₆ fluxes

In Input/Output -> User hand edit files, add the co2_tracers.ed file (sample in Appendix F.3).

The hand edit file sets up the UM to use atmospheric tracers of CO₂ and SF₆ by adding the following commands to the UM job scripts:

- Turns on the mass fixing routine for atmospheric tracers
- Initializes the tracer concentrations to zero
- Initializes the tracer fluxes from files
- Adds the tracer fluxes to the ancillary files list to be updated throughout the run, with hourly and daily updates
 - For the timing, PERIOD=4 -> hour; 3 -> day; 2 -> month
- Adds the tracer fluxes to the user-defined ancillary field file
- Adds the tracer flux files to the user-defined ancillary file

In Atmosphere -> Model Configuration -> Atmospheric Tracers

- Turn on tracers in the atmosphere
- Make sure the mass conservation is selected
- Set the value in the select column to 2 for the tracers being used
- Turn on boundary layer mixing of tracers

In Atmosphere -> STASH -> User-STASHmaster files

- Add the tracer flux stash file (tracer_fluxes.stash, provided below)

In Atmosphere -> STASH -> STASH

- Add the atmospheric tracers (section 33, items 1-20)
- Add the tracer fluxes (section 3, items 100-119)

E.2 UMUI checklist to use atmospheric tracers with prescribed fluxes of CH₄, MCF, Radon and SF₆

In Input/Output -> User hand edit files, add the all_tracers.ed file (sample in Appendix F.4).

The hand edit file sets up the UM to use two atmospheric tracers of CH₄ and single tracers representing MCF, Radon, and SF₆ by adding the following commands to the UM job scripts:

- Turns on the mass fixing routine for atmospheric tracers, but does not use the fixer for the first four tracers
- Calculate the loss of CH₄ in the atmosphere for the first two tracers
- Calculates the loss of MCF in the atmosphere for the third tracer
- Calculates the decay of Radon in the atmosphere for the fourth tracer
- Sets the filename for the OH/Cl and O¹D/photolysis/deposition (CHEMOXID) ancillary file
- Initializes the tracers (section 33, items 1-5)
 - First three tracers set to distribution from file
 - Fourth tracer, Radon, initialized to 0
 - Fifth tracer, SF₆, initialized to a constant value equivalent to 1.95 ppt of SF₆
- Initializes the tracer fluxes (section 3, items 100-104) from files
- Adds the OH field, the Cl and O¹D loss rates, the photolysis rates and the ocean deposition rates to the list of variables to be updated throughout the run, with daily updates
- Adds the tracer fluxes to the list of variables to be updated throughout the run, with hourly updates
- Adds the tracer fluxes to the user-defined ancillary field file
- Adds the tracer flux files to the user-defined ancillary file

In Atmosphere -> Model Configuration -> Atmospheric Tracers

- Turn on tracers in the atmosphere
- Make sure the mass conservation is selected
- Set the value in the select column to 2 for the tracers being used
- Turn on boundary layer mixing of tracers

In Atmosphere -> STASH -> User STASH-master files

- Add the user STASH-master file for tracer fluxes (tracer_fluxes.stash, Appendix F.5)
- Add the user STASH-master file for OH, O¹D and Cl loss rates, MCF photolysis rates, and MCF ocean deposition rates (methane_loss.stash, Appendix F.6)

In Atmosphere -> STASH -> Initialisation of User Prognostics

- Initialize the OH, Cl and O¹D loss rates, MCF loss rates, and MCF ocean deposition rates to a file by setting all four variables to option 2
 - Note: the filename is specified in the hand edit

In Atmosphere -> STASH -> STASH

- Add the necessary tracers (section 33, items 1-20)
- Add the necessary tracer fluxes (section 3, items 100-119)
- Add the OH, Cl and O¹D loss rates, MCF photolysis rates, and MCF ocean deposition rates (section 0, items 122-125)

E.3 CO₂ tracer hand edit file (CO2_tracers.ed)

Below is a sample hand edit file to use two atmospheric tracers with associated surface fluxes specified from files. Note that the UAFLDS_A and UAFILES_A sections only contain sample entries, rather than the list for all twenty fluxes. In order to use the file, the filenames for the tracer fluxes need to be specified and the UAFLDS_A and UAFILES_A entries need to be filled in.

```
#!/bin/ksh
#
#Hand edit file for two tracers.
#Turns on tracer mass fixer for tracers.
#Initializes tracers to zero.
#Initializes tracer fluxes from files.
#Adds tracer fluxes to ancillary files list to be updated every hour.
#Adds tracer fluxes to user-defined ancillary fields.
#Adds tracer fluxes to user-defined ancillary files.

ed CNTLATM <<\EOF
/L_CO2_EMITS/
a
  L_TRACER_MASS=.TRUE.,
.
w
q
EOF

ed RECONA <<\EOF
/!!! Tracer fields !!!
c
.
/ &ITEMS SECTION=33, ITEM=1, DOMAIN=1, SOURCE=5, /
c
  &ITEMS SECTION=33, ITEM=1, DOMAIN=1, SOURCE=3, /
  &ITEMS SECTION=3, ITEM=100, DOMAIN=1, SOURCE=2,
  USER_PROG Ancil_FILE="/directory/filename1"
.
/ &ITEMS SECTION=33, ITEM=2, DOMAIN=1, SOURCE=5, /
c
  &ITEMS SECTION=33, ITEM=2, DOMAIN=1, SOURCE=3, /
  &ITEMS SECTION=3, ITEM=101, DOMAIN=1, SOURCE=2,
  USER_PROG Ancil_FILE="/directory/filename2"
.
w
q
EOF

ed CNTLATM <<\EOF
```

APPENDIX E – METHODOLOGY TO UTILIZE ATMOSPHERIC TRACERS

/UPANCA/

a

&UPANCA ANC_REF_NO=188, PERIOD=4, INTERVAL=1, FINPUT=1,
FNAME="/directory/filename1" /

&UPANCA ANC_REF_NO=189, PERIOD=3, INTERVAL=1, FINPUT=1,
FNAME="/directory/filename2" /

.

w

q

EOF

ed UAFLDS_A <<\EOF

/H4| TYPE=ANCIL_FIELDS/

a

#

#|Ref No|Model | Sect | Item |Name |

#|File N|

#

=====

#

1| 188 | 1 | 3 | 100 |Flux of Tracer 1 |

2| 48 |

#

=====

#

1| 189 | 1 | 3 | 101 |Flux of Tracer 2 |

2| 49 |

#

=====

.

.

.

=====

#

1| 207 | 1 | 3 | 119 |Flux of Tracer 20 |

2| 67 |

#

=====

.

w

q

EOF

ed UAFILES_A <<\EOF

```

/H4| TYPE=ANCIL_FILES/
a
#
#|FILE N|Model|Env Vr | Title           |
#
#=====
#
1| 48 | 1 |TFLUX1 |Flux of Tracer 1           |
#
#=====
#
1| 49 | 1 |TFLUX2 |Flux of Tracer 2           |
#
#=====
#
.
.
.
#=====
#
1| 67 | 1 |TFLUX20 |Flux of Tracer 20        |
#
#=====
.
w
q
EOF

```

E.4 CH₄, MCF, and Radon hand edit file (all_tracers.ed)

Below is a sample hand edit file to use five atmospheric tracers with associated surface fluxes specified from files. Note that the UAFLDS_A and UAFILES_A sections only contain sample entries, rather than the list for all twenty fluxes. In order to use the file, the filenames need to be specified and the UAFLDS_A and UAFILES_A entries need to be filled in.

```
#!/bin/ksh
#
# Sample hand edit file for two CH4 tracers, MCF, Radon, and SF6.

#Turns on methane atmospheric loss
#Sets number of methane tracers to 2
#Turns on MCF loss and sets the tracer number for MCF
#Turns on radon decay and sets the tracer number for radon
ed CNTLATM <<\EOF
/L_CO2_EMITS/
a
L_TRACER_MASS=.TRUE.,
I_TRACERMASS_START=5,
L_METHANE_LOSS=.TRUE.,
I_METHANE_TRACERS=2,
L_MCF_LOSS=.TRUE.,
I_MCF_TRACERNUMBER=3,
L_RADON_DECA Y=.TRUE.,
I_RADON_TRACERNUMBER=4,
.
w
q
EOF

#Set filename for OH/Stratospheric Loss/Photolysis/Ocean Deposition data
ed INITHIS <<\EOF
/CHEMOXID/
c
CHEMOXID= 'CHEMOXID : /directory/filename',
.
w
q
EOF
```

```

#Initializes the tracers and tracer fluxes
# For zero initialization, use SOURCE=3
# For constant initialization, use SOURCE=6, USER_PROG_RCONST=
# For file initialization, use SOURCE=5, USER_PROG Ancil_FILE="filename"
# For flux file, use SOURCE=2, USER_PROG Ancil_FILE="flux_filename"
ed RECONA <<\EOF
/!!! Tracer fields !!!/
c
.
/ &ITEMS SECTION=33, ITEM=1, DOMAIN=1, SOURCE=5, /
c
  &ITEMS SECTION=33, ITEM=1, DOMAIN=1, SOURCE=5,
  USER_PROG Ancil_FILE="/directory/filename1" /
  &ITEMS SECTION=3, ITEM=100, DOMAIN=1, SOURCE=2,
  USER_PROG Ancil_FILE="/directory/flux_filename1" /
.
/ &ITEMS SECTION=33, ITEM=2, DOMAIN=1, SOURCE=5, /
c
  &ITEMS SECTION=33, ITEM=2, DOMAIN=1, SOURCE=5,
  USER_PROG Ancil_FILE="/directory/filename2" /
  &ITEMS SECTION=3, ITEM=101, DOMAIN=1, SOURCE=2,
  USER_PROG Ancil_FILE="/directory/flux_filename2" /
.
/ &ITEMS SECTION=33, ITEM=3, DOMAIN=1, SOURCE=5, /
c
  &ITEMS SECTION=33, ITEM=3, DOMAIN=1, SOURCE=5,
  USER_PROG Ancil_FILE="/directory/filename3" /
  &ITEMS SECTION=3, ITEM=102, DOMAIN=1, SOURCE=2,
  USER_PROG Ancil_FILE="/directory/flux_filename3" /
.
/ &ITEMS SECTION=33, ITEM=4, DOMAIN=1, SOURCE=5, /
c
  &ITEMS SECTION=33, ITEM=4, DOMAIN=1, SOURCE=3, /
  &ITEMS SECTION=3, ITEM=103, DOMAIN=1, SOURCE=2,
  USER_PROG Ancil_FILE="/directory/flux_filename4" /
.
/ &ITEMS SECTION=33, ITEM=5, DOMAIN=1, SOURCE=5, /
c
  &ITEMS SECTION=33, ITEM=5, DOMAIN=1, SOURCE=6,
  USER_PROG_RCONST=9.81724e-12 /
  &ITEMS SECTION=3, ITEM=104, DOMAIN=1, SOURCE=2,
  USER_PROG Ancil_FILE="/directory/flux_filename5" /
.
w
q
EOF

```

APPENDIX E – METHODOLOGY TO UTILIZE ATMOSPHERIC TRACERS

```

#Adds OH, CH4 stratospheric loss rates, MCF photolysis rates, and
#MCF ocean sink rates to ancillary files list to be updated during run,
#all with daily updates
#
#Adds tracer fluxes to ancillary files list to be updated during run,
#all with hourly updates
#
#For timing: PERIOD=4 -> hour; 3 -> day; 2 -> month
ed CNTLATM <<EOF
/UPANCA/
a
&UPANCA ANC_REF_NO=73, PERIOD=3, INTERVAL=1 /
&UPANCA ANC_REF_NO=74, PERIOD=3, INTERVAL=1 /
&UPANCA ANC_REF_NO=75, PERIOD=3, INTERVAL=1 /
&UPANCA ANC_REF_NO=76, PERIOD=3, INTERVAL=1 /
&UPANCA ANC_REF_NO=188, PERIOD=4, INTERVAL=1, FINPUT=1,
FNAME="/directory/flux_filename1" /
&UPANCA ANC_REF_NO=189, PERIOD=4, INTERVAL=1, FINPUT=1,
FNAME="/directory/flux_filename2" /
&UPANCA ANC_REF_NO=190, PERIOD=4, INTERVAL=1, FINPUT=1,
FNAME="/directory/flux_filename3" /
&UPANCA ANC_REF_NO=191, PERIOD=4, INTERVAL=1, FINPUT=1,
FNAME="/directory/flux_filename4" /
&UPANCA ANC_REF_NO=192, PERIOD=4, INTERVAL=1, FINPUT=1,
FNAME="/directory/flux_filename5" /
.
w
q
EOF

```

#Sets tracer fluxes as user ancillary fields

```

ed UAFLDS_A <<\EOF
/H4| TYPE=ANCIL_FIELDS/

```

```

a
#
#|Ref No|Model | Sect | Item |Name           |
#|File N|
#
#=====
#
1| 188 | 1 | 3 | 100 |Flux of Tracer 1      |
2| 48 |
#
#=====
#
.
.

```

```

.
#=====
#
1| 207 | 1 | 3 | 119 |Flux of Tracer 20      |
2| 67 |
#
#=====
.
w
q
EOF

#Sets tracer fluxes as user ancillary files
ed UAFILES_A <<\EOF
/H4| TYPE=ANCIL_FILES/
a
#
#|FILE N|Model|Env Vr | Title              |
#
#=====
=====
#
1| 48 | 1 |TFLUX1 |Flux of Tracer 1      |
#
#=====
.
.
.
#=====
#
1| 67 | 1 |TFLUX20 |Flux of Tracer 20      |
#
#=====
.
w
q
EOF

```

E.5 Tracer flux STASH-master file (tracer_fluxes.stash)

Below is a sample STASH-master file for atmospheric tracers. To use the file, the entries for tracer fluxes 101-118 need to be filled in.

```

H1| SUBMODEL_NUMBER=1
H2| SUBMODEL_NAME=ATMOS
H3| UM_VERSION=6.3
#
#|Model |Sectn | Item |Name          |
#|Space |Point | Time | Grid |LevelT|LevelF|LevelL|PseudT|PseudF|PseudL|LevCom|
#| Option Codes          | Version Mask      | Halo |
#|DataT |DumpP | PC1 PC2 PC3 PC4 PC5 PC6 PC7 PC8 PC9 PCA |
#|Rotate| PPF | USER | LBVC | BLEV | TLEV |RBLEVV| CFLL | CFFF |
#=====
#
1| 1| 3| 100|FLUX OF TRACER 1 IN BL  KG/M**2/S|
2| 2| 0| 1| 1| 5| -1| -1| 0| 0| 0| 0|
3| 00000000000000000000000000000000| 0000000000011100000 | 3|
4| 1| 2| -99 -99 -99 -99 -99 -99 -99 -99 -99 -99 |
5| 0| 1389| 0| 129| 0| 0| 0| 0| 0|
#=====
.
.
.
#=====
#
1| 1| 3| 119|FLUX OF TRACER 20 IN BL  KG/M**2/S|
2| 2| 0| 1| 1| 5| -1| -1| 0| 0| 0| 0|
3| 00000000000000000000000000000000| 0000000000011100000 | 3|
4| 1| 2| -99 -99 -99 -99 -99 -99 -99 -99 -99 -99 |
5| 0| 1389| 0| 129| 0| 0| 0| 0| 0|
#=====
#
1| -1| -1| -1|END OF FILE MARK          |
2| 0| 0| 0| 0| 0| 0| 0| 0| 0| 0| 0|
3| 00000000000000000000000000000000| 00000000000000000000 | 0|
4| 0| 0| -99 -99 -99 -99 -30 -99 -99 -99 -99 |
5| 0| 0| 0| 0| 0| 0| 0| 0| 0|
#

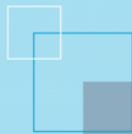
```

E.6 OH, Cl and O¹D, photolysis and ocean deposition STASH-master file (methane_loss.stash)

```

H1| SUBMODEL_NUMBER=1
H2| SUBMODEL_NAME=ATMOS
H3| UM_VERSION=6.3
#
#|Model|Sectn|Item|Name|
#|Space|Point|Time|Grid|LevelT|LevelF|LevelL|PseudT|PseudF|PseudL|LevCom|
#|Option Codes|Version Mask|Halo|
#|DataT|DumpP|PC1|PC2|PC3|PC4|PC5|PC6|PC7|PC8|PC9|PCA|
#|Rotat|PPF|USER|LBVC|BLEV|TLEV|RBLEV|CFL|CFFF|
#=====
#
1| 1| 0| 122|3D OH CONCENTRATIONS IN MCULES/CC|
2| 2| 0| 1| 1| 2| 1| 2| 0| 0| 0| 0|
3| 00000000000000000000000000000000| 00000000000000000001| 3|
4| 1| 0|-99|-99|-99|-99|-99|-99|-99|-99|-99|
5| 0| 580| 0| 65| 0| 0| 0| 9999| 0|
#=====
#
1| 1| 0| 123|3D O1D AND CL LOSS RATES IN S-1|
2| 2| 0| 1| 1| 2| 1| 2| 0| 0| 0| 0|
3| 00000000000000000000000000000000| 00000000000000000001| 3|
4| 1| 0|-99|-99|-99|-99|-99|-99|-99|-99|-99|
5| 0| 580| 0| 65| 0| 0| 0| 9999| 0|
#=====
#
1| 1| 0| 124|3D MCF J LOSS RATES IN S-1|
2| 2| 0| 1| 1| 2| 1| 2| 0| 0| 0| 0|
3| 00000000000000000000000000000000| 00000000000000000001| 3|
4| 1| 0|-99|-99|-99|-99|-99|-99|-99|-99|-99|
5| 0| 580| 0| 65| 0| 0| 0| 9999| 0|
#=====
#
1| 1| 0| 125|3D MCF Ocean Sink Loss Rates IN M/S|
2| 2| 0| 1| 1| 2| 1| 2| 0| 0| 0| 0|
3| 00000000000000000000000000000000| 00000000000000000001| 3|
4| 1| 0|-99|-99|-99|-99|-99|-99|-99|-99|-99|
5| 0| 580| 0| 65| 0| 0| 0| 9999| 0|
#=====
#
1| -1| -1| -1|END OF FILE MARK|
2| 0| 0| 0| 0| 0| 0| 0| 0| 0| 0| 0|
3| 00000000000000000000000000000000| 00000000000000000000| 0|
4| 0| 0|-99|-99|-99|-99|-30|-99|-99|-99|-99|
5| 0| 0| 0| 0| 0| 0| 0| 0| 0| 0|
#

```

The Centre for Australian Weather and
Climate Research is a partnership between
CSIRO and the Bureau of Meteorology.